

NASA Contract Report 185135

An Investigation of Counterrotating Tip Vortex Interaction

R.K. Majjigi, K. Uenishi, and P.R. Gliebe

GE Aircraft Engines
Advanced Engineering Technologies Department
Cincinnati, Ohio 45215

October 1989

Prepared for

Lewis Research Center
Under Contract NAS3-24080



National Aeronautics and
Space Administration

(NASA-CR-185135) AN INVESTIGATION OF
COUNTERROTATING TIP VORTEX INTERACTION (GE)
124 p

CSCL 20A

N90-11549

Unclassified
G3/71 0234874



Summary

A tip vortex interaction model that was originally developed for compressors has been extended and adapted for use with counterrotating open rotors. This report documents the analytical modeling, model evaluation with limited experimental data, and certain key parametric studies pertaining to the tip vortex as a noise-source mechanism for the unsteady loading noise of counterrotating propfan propulsors. The existing, simple, basic model can be extended toward establishing a more sophisticated, complete model in the future. Particularly, the empirical constants used in the model can be further modified and improved once detailed tip vortex aerodynamics and acoustic data become available through controlled experimental studies.



Table of Contents

Section		Page
1.0	Introduction	1
	1.1 Statement of the Problem and Method of Approach	1
	1.2 Literature Survey	2
2.0	Counterrotating Blade Tip Vortex Model	3
	2.1 Mathematical Description	3
	2.2 Empirical Relationships	8
3.0	Model Evaluation	17
	3.1 Parametric Studies	17
	3.1.1 Influence of Tip Vortex Strength and Drag Coefficient	19
	3.1.2 Influence of Tangential Location of Tip Vortex	26
	3.1.3 Influence of Tip Vortex Trajectory	29
	3.1.4 Influence of Decay Rate of Tip Vortex	33
	3.1.5 Influence of Progressive Clipping of Aft Rotor	33
	3.2 Data - Predictions Evaluation	38
4.0	Conclusions and Recommendations	52
	4.1 Conclusions	52
	4.2 Recommendations	52
5.0	References	54
6.0	Nomenclature	56
	Appendix A	59

List of Illustrations

Figure		Page
1.	The Combined Forced (Within the Core) and Free (Outside the Core) Vortex Model for the Tip Vortex.	4
2.	Nature of the Tip Vortex Flow Model for a Ducted Rotor.	5
3.	Comparison of Gust Harmonic Spectra at Three Spanwise Locations for Increasing Values of Tip Clearance and for No Tip Vortex Case.	7
4.	Correlation and Data for the Streamwise Variation of Normalized ($V\theta$)_{max} of the Tip Vortex.	10
5.	Correlation and Data for the Streamwise Variation of Normalized Radius of the Tip Vortex Core.	10
6.	Representative Correlation and Data for the Streamwise Variation of Normalized ($V\theta$)_{max}, Radius, and Circulation of the Tip Vortex.	11
7.	Streamwise Variation of Normalized Circulation of the Tip Vortex for Three Different Power Law Decay Rates.	12
8.	Spanwise Variation of the Local Section Lift Coefficient for Takeoff and Cruise Conditions for F-7 Blades.	14
9.	Spanwise Variation of the Chord for the F-7 Blade Design.	14
10.	Correlation and Data for the Trajectory of the Tip Vortex.	15
11.	Planform of the F-7/A-7 Unducted Fan Blade Design, Showing the Extent of Clipping on the Aft Rotor.	18
12.	Schematic of a Narrowband Acoustic Spectrum of a 9 × 8 Blade Number Configuration.	20
13.	Predicted Effect of Tip Vortex Strength on Gust Harmonic Spectra with Three Different C_d Values at the Streamline of 100% Span from the Hub.	21
14.	Predicted Effect of the Tip Vortex Strength on Gust Harmonic Spectra with Three Different C_d Values at the Streamline of 70.7% Span from the Hub.	22
15.	Predicted Effect of Tip Vortex Strength on Gust Harmonic Spectra with Three Different C_d Values at the Streamline Location of 45.4% Span from the Hub.	23

List of Illustrations(Continued)

Figure		Page
16.	The Predicted Effect of the Tip Vortex Strength on Interaction Tone SPL Sum with $C_d = 0.005$.	24
17.	Predicted Effect of the Drag Coefficients on the Interaction Tone SPL Sum with $C_i = 2.0$.	24
18.	Predicted Tip Vortex Effect of the Drag Coefficients (0.03, 0.02, and 0.005) on Interaction Tone SPL Sum with $C_i = 2.0$.	25
19.	Predicted Tangential Distribution of Gust Velocity at Three Radial Locations for Various Tangential Locations of Tip Vortex, and for the Case of No Tip Vortex.	27
20.	Predicted Effect of Tangential Location of Tip Vortex on Gust Harmonic Spectra at Three Radial Locations.	28
21.	A Comparison of the Predicted and Measured Individual Interaction Tones.	29
22.	Sensitivity of the Tone SPL Sum of Interaction Noise to the Tangential Location of Tip Vortex.	30
23.	Predicted Influence of the Tip Vortex Trajectory on Gust Harmonic Spectra at Three Streamlines in the Tip Region.	31
24.	Predicted Influence of Tip Vortex Trajectory on Each Interaction Tone at Observer Angle of 91°.	32
25.	Predicted Influence of Tip Vortex Trajectory on Interaction Noise Tone SPL Sum.	32
26.	Predicted Gust Harmonic Spectra at Two Rotor-to-Rotor Spacings for the Tip Vortex at Different Decaying Rates and for the Case of No Tip Vortex at Two Streamline Locations.	34
27.	Assumed Performance of the Progressively Clipped Aft Rotor.	35
28.	Predicted Effect of Progressive Clipping of the Aft Rotor on the Steady Loading and Thickness Noise.	35
29.	Predicted Effect of Progressive Clipping of the Aft Rotor on the Wake/Tip Vortex Interaction Noise.	36

List of Illustrations (Concluded)

Figure		Page
30.	The Predicted Effect of Progressive Clipping of the Aft Rotor on the OASPL Directivity.	37
31.	Comparison of the Measured and Predicted Effect of Clipping of the Aft Rotor on Steady Loading and Thickness Noise.	39
32.	Comparison of the Measured and Predicted Steady Loading and Thickness Tones for Standard and Clipped Aft Rotor at 105° Observer Angle.	39
33.	Comparison of the Measured and Predicted Effect of Clipping of the Aft Rotor on Interaction Tone SPL Sum With and Without the Tip Vortex Model ($C_d = 0.02$, $C_i = 2$, $K_{vtx} = 2.0$, $bt/S = 0.5$).	40
34.	Comparison of the Effect (Measured and Predicted) of Clipping of the Aft Rotor on Interaction Tone SPL Sum with and without the Tip Vortex Model ($C_d = 0.005$, $C_i = 2$, $K_{vtx} = 2.0$, $bt/S = 0.5$).	41
35.	A Comparison of the Measured and Predicted Effect of the Clipping of the Aft Rotor on Interaction Tone Sum With and Without the Tip Vortex Model ($C_d = 0.005$, $C_i = 1$, $K_{vtx} = 2.0$, $bt/S = 0.5$).	42
36.	A Measured and Predicted Effect Comparison of Clipping of the Aft Rotor on Interaction Tone Sum, With and Without the Tip Vortex Model ($C_d = 0.005$, $C_i = 3$, $K_{vtx} = 2.0$, $bt/S = 0.5$).	43
37.	Comparison of the Measured and Predicted Effect of Clipping of the Aft Rotor on Individual Interaction Tones, With and Without the Tip Vortex Model ($C_d = 0.005$, $C_i = 3$, $K_{vtx} = 1.0$, $bt/S = 0.5$).	45
38.	The Predicted Spanwise Variation of Normalized Streamwise Distance, Wake Centerline Defect, and Semiwake Width.	47
39.	Comparison of the Measured and Predicted Effect of Clipping of the Aft Rotor on Steady Loading and Thickness Noise for 80% rpm.	49
40.	Measured and Predicted Effect of Clipping of the Aft Rotor on Interaction Tone SPL Sum With and Without the Tip Vortex Model ($C_d = 0.005$, $C_i = 3$, $K_{vtx} = 1.0$, $bt/S = 0.5$).	49
41.	Comparison of the Measured and Predicted Effect of Clipping of the Aft Rotor on Individual Interaction Tones with and without the Tip Vortex Model ($C_d = 0.005$, $C_i = 3$, $K_{vtx} = 1$, $bt/S = 0.5$).	50

1.0 Introduction

In recent times, the high speed swept-propfan concept has attracted considerable attention from the aircraft industry (Reference 1). This is due to the higher propulsion efficiencies and a correspondingly lower sfc (specific fuel consumption) at high cruise Mach numbers (typically $M_\infty \approx 0.8$), compared to the modern high bypass turbofan engines. Application of two counter-rotating, swept propellers to extract the swirl energy that would be lost in the case of a single propeller is expected to yield even higher levels of propulsion efficiency. The development of acoustic technology to understand the noise characteristics of this new propulsion concept is an important aspect in the design phase; hence GEAE (GE Aircraft Engines), in cooperation with NASA, has undertaken an extensive scale model program to investigate the influence of various geometric and aerodynamic parameters on the performance and noise characteristics of swept, counterrotating propellers.

1.1 Statement of the Problem and Method of Approach

The acoustic signature of a counterrotating propeller is rich in tonal content which can be ascribed to various noise-generating mechanisms at work. The analytical modeling of these mechanisms will enable a better physical understanding which, in turn, will help in evolving a methodology for low noise designs. The principal noise mechanisms associated with the tonal spectrum of a counterrotating propeller are:

- Steady loading and thickness noise of each rotor
- Unsteady loading noise generated by the aft rotor due to an interaction with the wake shed by the forward rotor
- Unsteady loading noise generated by the aft rotor due to an interaction with the tip vortex of the forward rotor
- Unsteady loading noise (generated by either rotor) due to the presence of a rotating potential field of the other rotor.

This report documents work performed on the analytical modeling of the unsteady loading noise due to the tip vortex interaction. The physical process involved in the generation of the tip vortex of these propulsors is similar to that of fixed wings; that is, a static pressure differential between the pressure and suction sides of the airfoil in the tip region of the wing results in a flow from the pressure to the suction side, which ultimately rolls up into a tip vortex. This physical process can be explained using finite wing theory; that is, the effect of a reduction in the wingspan from infinity to a finite length may be viewed as the effect of a removal of tip vortices extending indefinitely in the direction of the span and a replacement of these vortices by trailing vortices connected at the downstream ends by starting vortices (Reference 2).

The analytical modeling of the upwash field (gust) created by the tip vortex of the forward propulsor at the leading edge (or one-fourth chord) of the aft propulsor is based on an approach previously implemented for fan tone noise (References 3 and 4). This approach

consists of modeling the tip vortex as a free vortex (that is, $r = \text{constant}$, $V_\theta \propto 1/r$) with a forced vortex core (that is, within the core, $V_\theta \propto r$), the strength, size, and streamwise development of which are empirically modeled. The gust field of the tip vortex at the aft rotor determines the unsteady lift response of the aft rotor blade and, hence, the additional unsteady loading noise due to the tip vortex.

1.2 Literature Survey

A survey of existing literature on tip vortices of open-tipped wings (for instance, fixed wings, helicopter rotors) was conducted to aid in understanding the characteristics of such tip vortices (namely, size, strength, trajectory, and decay rate), so that certain empirical relationships could be developed for application to the tip vortex model for an unducted rotor. Unfortunately, very little information could be found in the open literature on tip vortices of highly swept propfans. The literature survey was conducted with the objective of finding experimental information about the following:

- Tip vortex trajectory
- Tip vortex strength such as, circulation or $(V_\theta)_{\max}$ and size of the core
- Growth/decay of tip vortex with streamwise distance.

Experimental information on the tip vortex trajectory contained in References 5 and 6 relates to helicopter rotors in hover mode. The experimental data was essentially the spanwise coordinate of the tip vortex at different axial stations. The rotors were typical helicopter rotors with large aspect ratio ($4.5 \leq AR \leq 18$) and low hub/tip ratio ($HTR \approx 0.1$).

Wind tunnel measurements of a tip vortex shed from a fixed wing at low subsonic speeds (from References 7 and 8) provided the information for developing empirical relationships for the size and strength of the tip vortex. The experimental information on the streamwise development of the tip vortex contained in Reference 8 was used to model the growth/decay of the tip vortex with streamwise distance.

2.0 Counterrotating Blade Tip Vortex Model

This section briefly describes the aerodynamic model developed for predicting the gust field at the aft rotor due to the tip vortex of the forward rotor. This data is used to evaluate the fluctuating lift and the associated unsteady loading or interaction noise of the counterrotating propellers. The quasi-3D (quasi-three-dimensional) aerodynamic model of the forward rotor exit flow field employs a streamline-by-streamline approach (References 3 and 4 provide a detailed description). The velocity field induced by the tip vortex of the forward rotor at the aft rotor is computed first for a coordinate system rotating with the forward rotor. A coordinate transformation of this velocity field relative to the aft rotor is performed; this yields the upwash velocity perturbations from the freestream value for the aft rotor. The upwash velocity perturbations exhibit a periodicity coinciding with that of the forward rotor. Fourier analysis of the upwash waveform yields the upwash gust harmonics distribution. The twist of the forward rotor blade from hub to tip causes a time/phase lag between the flow field from the hub and tip regions impinging on the aft rotor blade. This spanwise distortion and clocking of the rotor wake/vortex "sheet" as it convects downstream results in a spanwise phase variation of the wake/vortex field. The analysis for predicting this phase lag due to the twist of the rotor blades was developed under a previous GE IR&D (Independent Research and Development) project and is described in Reference 3. The spanwise distribution of the gust harmonics, along with the above-described aerodynamic phase, gives a complete description of the gust field impinging on the aft rotor.

Computation of the fluctuating lift force on the aft rotor due to the upwash gust is performed next by using the classical (incompressible) unsteady lift response theory of Sears (Reference 9), modified to take compressibility effects into account according to a procedure developed by Amiet (Reference 10). The fluctuating lift force forms the right-hand side of the wave equation, whose formulation and method of solution are beyond the scope of this report. Developed under a GE IR&D project, the acoustic model used in this report is formulated in the frequency domain and computes the tone noise generated by the steady loading and thickness sources of the rotor rows, together with the tone noise resulting from the unsteady loading due to fluctuating lift forces. The fundamental formulation of the model can be found in Reference 11. Subsection 2.1 briefly describes the tip vortex model development, and Sub-section 2.2 describes the procedure followed in establishing certain empirical relationships associated with the tip vortex model.

2.1 Mathematical Description

The tip vortex model has evolved from a similar model for computing secondary flow vortices (in and behind a ducted rotor blade passage) which are dominated by the tip clearance leakage flow (References 12 and 13). The tip vortex model assumes the existence of a core that contains all of the shed vorticity, so that the motion outside is irrotational. Figure 1 is a sketch of the radial variation of tangential velocity (V_θ) induced by the tip vortex and the associated circulation of the vortex. Obviously, even at large distances from the vortex center, sufficiently large swirl velocities exist, in terms of $V_\theta/(V_\theta)_{\max}$. It should be noted that the current

tip vortex model does not include an effect of an axial velocity component of the tip vortex; however, this will be included in future work, as detailed data become available.

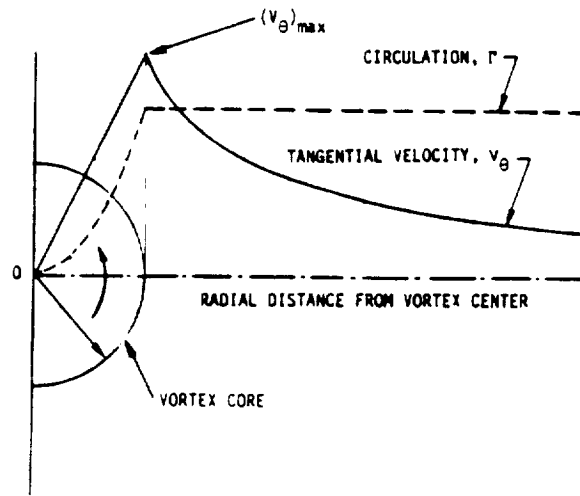


Figure 1. The Combined Forced (Within the Core) and Free (Outside the Core) Vortex Model for the Tip Vortex.

For the tangential velocity W_t

$$w_t = -\frac{\Gamma_{vtx}}{2S} \left[\frac{\sinh M}{\cosh M - \cos p} - \frac{\sinh N}{\cosh N - \cos p} \right] \quad (1)$$

and for the radial velocity W_r

$$w_r = -\frac{\Gamma_{vtx}}{2S} \left[\frac{\sin p}{\cosh M - \cos p} - \frac{\sin p}{\cosh N - \cos p} \right] \quad (2)$$

where

$$M = \frac{2\pi}{S} (y - b_r - \tau) \quad (3)$$

$$N = \frac{2\pi}{S} (y + b_r - \tau) \quad (4)$$

and

$$P = \frac{2\pi}{S} (x - b_t) \quad (5)$$

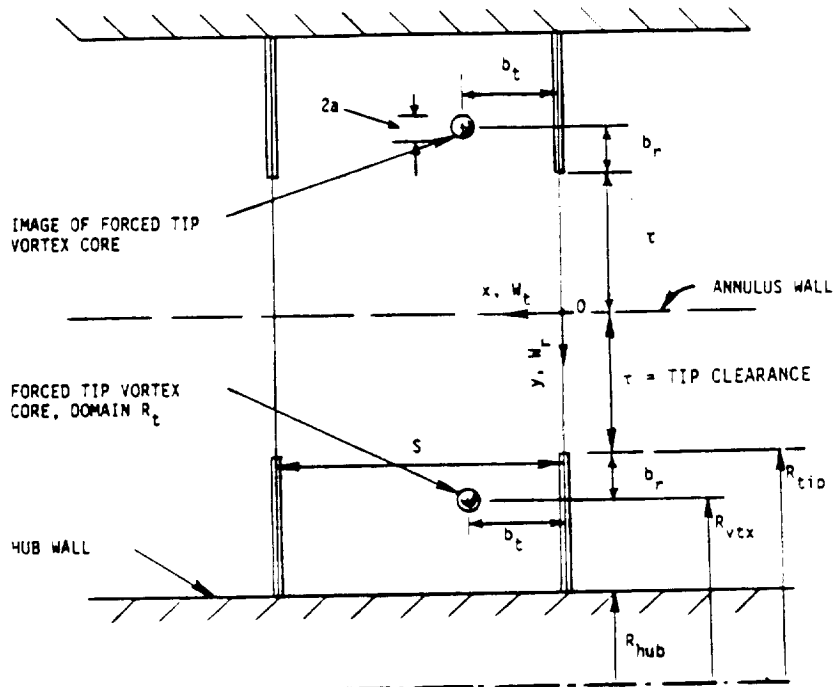


Figure 2. Nature of the Tip Vortex Flow Model for a Ducted Rotor.

The parameters "x" and "y" are coordinates of the unwrapped annulus (the annulus is unrolled). It can be seen that at $y = 0$ (that is, at the annulus wall), Equation 1 reduces to:

$$w_t \Big|_{y=0} = \frac{r_{vtx}}{s} \left[\frac{\sinh(b_r + \tau)}{\cosh(b_r + \tau) - \cos p} \right] \quad (6)$$

and Equation 2 reduces to:

$$w_r \Big|_{y=0} = 0 \quad (7)$$

For a given value of $(b_r + \tau)$, as y increases, $\sinh M \rightarrow \sinh N$ and $\cosh M \rightarrow \cosh N$, and the expressions for tangential and radial velocities created due to the tip vortex approach zero (Equations 1 and 2); thus, implying that as one approaches the hub wall, the tangential and radial velocities created due to the tip vortex vanish, which is physically realistic.

The region within the domain R_t behaves as a forced vortex (like a solid body of revolution); the domain R_t is given by:

$$(x - b_t)^2 + (y - b_r - \tau)^2 \leq a^2 \quad (8)$$

where "a" is the radius of the vortex core.

The angular velocity of the tip vortex can be related to the circulation of the tip vortex by:

$$\omega = \frac{\Gamma_{vtx}}{2 \pi a^2} \quad (9)$$

For a point P(x,y) within the domain R_t , the tangential component of the velocity induced by the tip vortex is given by:

$$w_t = -\omega r \sin \alpha \quad (10)$$

and the radial component by

$$w_r = \omega r \cos \alpha \quad (11)$$

where

$$r = \left\{ (x - b_t)^2 + (y - b_r - \tau)^2 \right\}^{1/2}$$

and

$$\alpha = \tan^{-1} \left[\frac{y - b_r - \tau}{x - b_t} \right]$$

Equations 1 through 11 specify the induced velocity field in a radial plane behind the blade trailing edge due to the presence of the tip vortex.

For the unducted fan, the annulus wall does not exist. This is mathematically modeled by increasing the value of the tip clearance to a large value, so that the effect of the image vortex is made negligible. Figure 3 compares the gust spectra at three spanwise locations for increasing values of tip clearance. The nondimensional tip clearance shown in Figure 2 is tip clearance divided by the forward rotor chord at the tip. Typical values of τ for ducted fan rotors are ≈ 0.01 . It is seen that when τ is increased by a factor of 1000, the solution has converged so that even an increase in τ does not alter the results. For the sake of completeness, gust harmonic spectra for the case of no tip vortex (that is, wake alone) are also presented (Figure 3).

Although the tip vortex is seen to have considerable influence on the gust harmonic spectra at the tip streamline and at the streamline which is 89% of the span from hub; the gust harmonic spectra at the hub are not affected by the tip vortex. Also note that the gust spectral levels without the tip vortex (that is, wake alone) in the tip region are much lower in amplitude, compared to the hub region. This is because the smaller spacing and larger chord at the hub yield smaller values of streamwise distance/chord ratio which, in turn, makes the wakes stronger at the hub (compared to the tip).

The gust spectra (with the tip vortex) at the tip streamline and the streamline 89% of the span from hub demonstrate a different character. Based on the tip vortex trajectory model, the 89% streamline is very close to the region of impact of tip vortex on the aft rotor. (This aspect will be discussed further in Subsections 2.2 and 3.1.3). The gust spectral levels at the

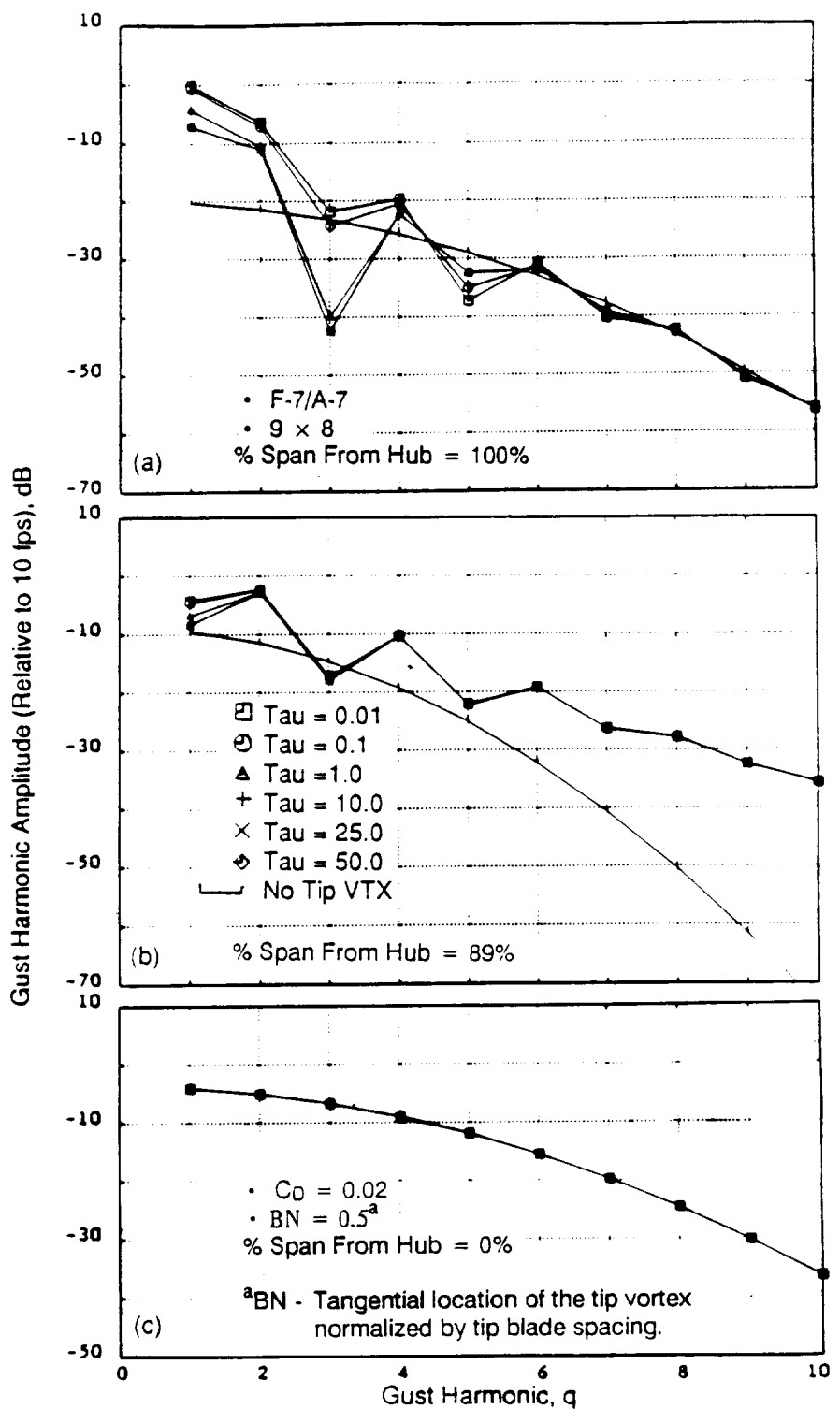


Figure 3. Comparison of Gust Harmonic Spectra at Three Spanwise Locations for Increasing Values of Tip Clearance and for No Tip Vortex Case.

89% streamline are seen to be higher than for the tip streamline. The gust harmonic falloff for increasing values of the gust harmonic "q" is also lower for the 89% streamline (compared to the tip streamline), indicating a sharp profile for the gust waveform near the point of impact of the tip vortex.

2.2 Empirical Relationships

As discussed in Subsection 2.1, computation of the flow field created due to the tip vortex can be performed if one knows both the:

- Circulation of tip vortex at the axial station of interest (Γ_{vtx})
- Radial and tangential coordinates of the tip vortex (b_r and b_t).

The experimental data reported in Reference 8 contained information on the variation of $(V\theta)_{max}$ and radius of the vortex core of a uniform NACA-0012 airfoil (with an aspect ratio of 6), set at an angle-of-attack of 7.5°, at two freestream velocities, 70- and 100-fps (feet per second). Vortex measurements were made with a yawhead pressure probe from 10 to 30 chord lengths downstream of the trailing edge. The experimental data chosen from Reference 7 were obtained on a NACA-0012 airfoil of an aspect ratio of 6 at a freestream velocity of 110-fps. The variation of tip vortex radius with angle-of-attack was measured at approximately six chord lengths downstream of the trailing edge using a vorticity meter. The applicability of the data (based on the wing configuration) to the significantly swept UDF®* blade geometry should be verified once experimental tip vortex data can be obtained from these UDF® blade configurations.

Empirical corrections for $(V\theta)_{max}/(V_\infty \sqrt{C_L})$ and $a/(c \sqrt{C_L})$ were developed by employing a linear rational function of the type (Reference 3):

$$y = \frac{dx + e}{fx + 1} \quad (12)$$

where d, e, and f are empirically determined constants, and y could be $(V\theta)_{max}/(V_\infty \sqrt{C_L})$ or $a/(c \sqrt{C_L})$, and $x = s/c$.

Constants d, e, and f in Equation 12 were determined through an iteration scheme aimed at minimizing the standard deviation (Reference 3 provides more details). The following correlations yielded minimum standard deviation:

$$\frac{(V\theta)_{max}}{V_\infty \sqrt{C_L}} = \frac{0.024 \text{ (s/c)} + 0.5586}{0.0504 \text{ (s/c)} + 1.0} = Y(s/c) \quad (13)$$

* UDF® is a registered trademark of the General Electric Company, U.S.A.

ORIGINAL PAGE IS
OF POOR QUALITY

where:

$(V_\theta)_{\max}$ = maximum tangential velocity of the tip vortex

V_∞ = freestream velocity

C_L = local section lift coefficient

s = streamwise distance

c = chord

and

$$\frac{a}{c \sqrt{C_L}} = \frac{0.01584 (s/c) + 0.0014}{0.184 (s/c) + 1.0} = Z(s/c) \quad (14)$$

Figures 4 and 5 demonstrate these correlations, along with the data for:

$$\frac{(V_\theta)_{\max}}{V_\infty \sqrt{C_L}} \text{ and } \frac{a}{c \sqrt{C_L}},$$

respectively. The empirical corrections provided in Equations 13 and 14 can be improved by adjusting the constants d, e, and f when more detailed experimental data for the UDF® blades become available.

By definition, the circulation of the tip vortex is:

$$\begin{aligned} (\Gamma)_{vtx} &= \int_{\theta=0}^{2\pi} (V_\theta)_{\max} a \, d\theta \\ &= \int_{\theta=0}^{2\pi} V_\infty \sqrt{C_L} Y(s/c) c \sqrt{C_L} Z(s/c) \, d\theta \\ &= 2\pi (V_\theta)_{\max} a \end{aligned} \quad (15)$$

Figure 6 shows the correlations given by Equations 13 and 14 and the computed circulation (Equation 15), along with the data. It is seen that the maximum tangential velocity decreases with s/c ; whereas, the radius of the vortex core increases with s/c , and the tip vortex circulation initially rises and then shows almost no decay over 10 to 30 chord lengths. The absence of a decay in the circulation of the tip vortex noted in the above set of data has been confirmed on full-scale aircraft tip vortex measurements for up to 1,000 chord lengths downstream of the aircraft (Reference 15). The linear-rational-function correlations employed for $(V_\theta)_{\max}$ and

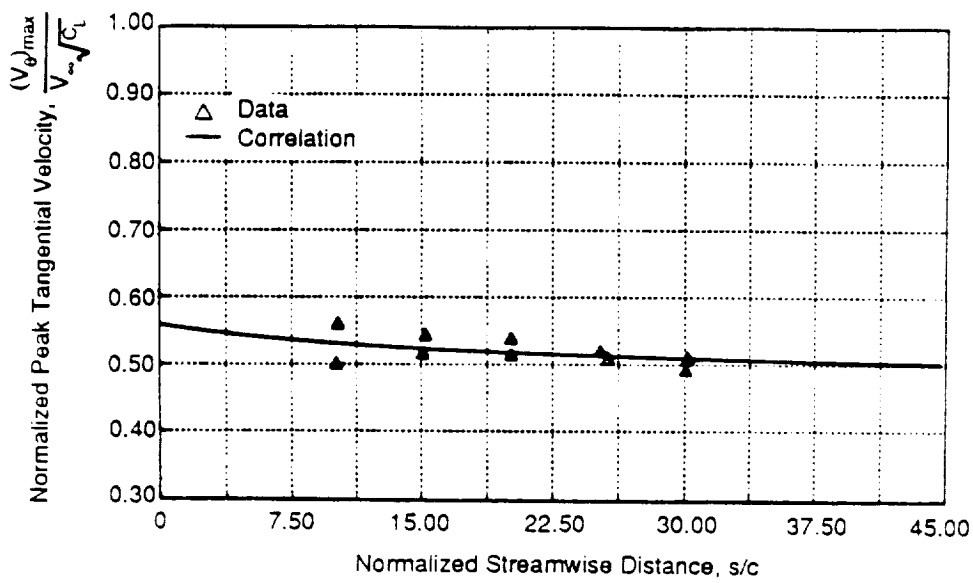


Figure 4. Correlation and Data for the Streamwise Variation of Normalized(V_θ)_{max} of the Tip Vortex.

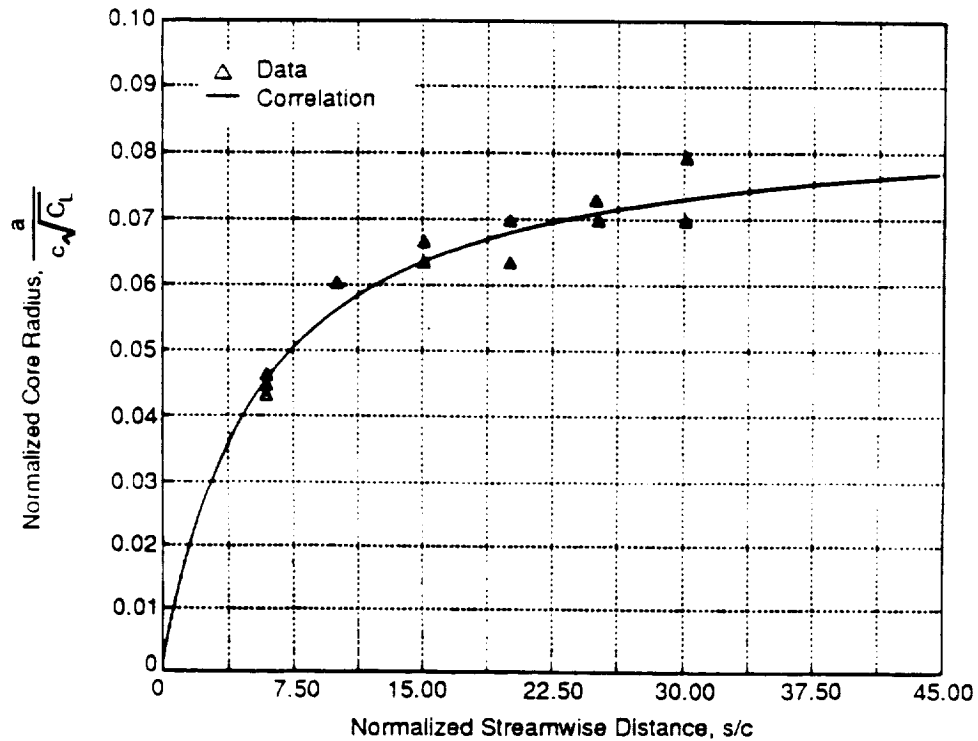


Figure 5. Correlation and Data for the Streamwise Variation of Normalized Radius of the Tip Vortex Core.

ORIGINAL PAGE IS
OF POOR QUALITY

radius of the vortex core simulate this behavior of the tip vortex very well. Certain limiting forms of $(\Gamma)_{vtx}$ are examined next. For example:

(16)

$$\text{At } (s/c) = 0 \quad (\Gamma)_{vtx} = 2\pi V_\infty c C_L (0.5586 \times 0.0014)$$

or

$$\frac{(\Gamma)_{vtx}}{2\pi V_\infty c} = 0.000782$$

For large values of s/c :

$$\lim_{(s/c) \rightarrow \infty} \left[\frac{(\Gamma)_{vtx}}{2\pi V_\infty c C_L} \right] = \left(\frac{0.024}{0.0504} \right) \left(\frac{0.01584}{0.184} \right) = 0.040994 \quad (17)$$

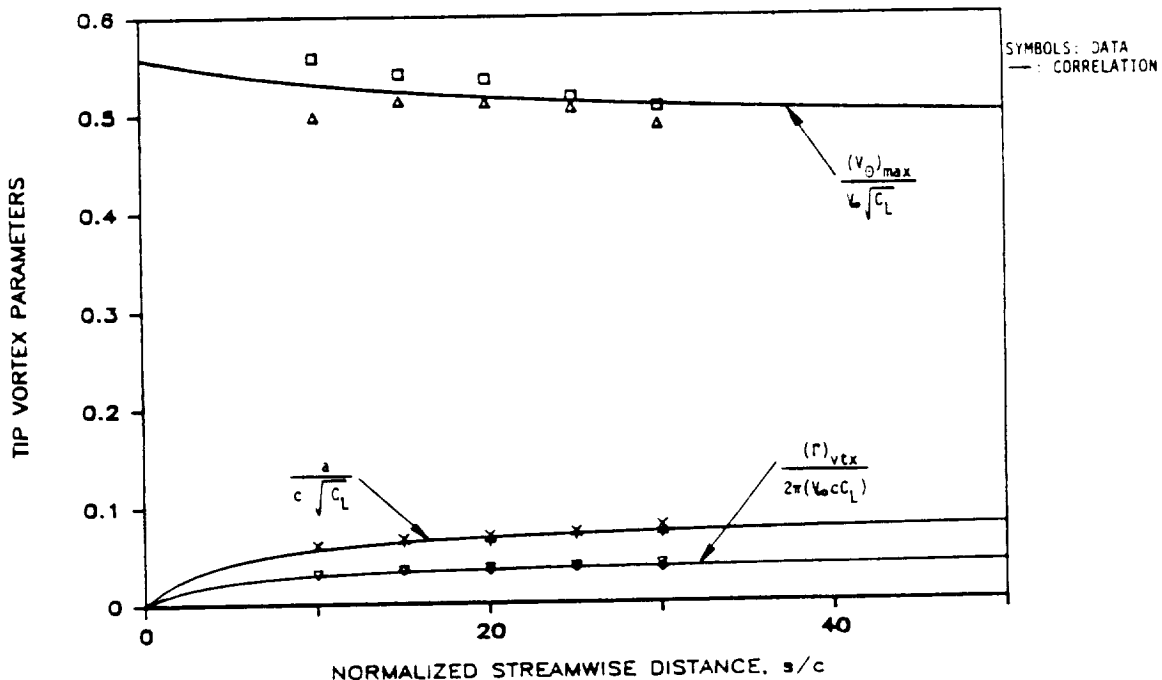


Figure 6. Representative Correlation and Data for the Streamwise Variation of Normalized $(V_\theta)_{\max}$, Radius, and Circulation of the Tip Vortex.

Hence, for large values of s/c , the circulation of the vortex reaches an asymptotic value which is higher than the value at the trailing edge. The initial rise in tip vortex circulation (as indicated by these correlations) may be viewed as a result of the initial roll-up of the shed spanwise vorticity into a well-defined tip vortex. Thus, the correlations seem to represent some of the physical features exhibited by the wing tip vortices. Unfortunately however, for the UDF®

configurations, the range of the s/c value (that is, spacing between the forward and aft rotors) is less than 5.0; within this range, there is a lack of data, as evidenced by Figures 4 through 6.

Flow-field visualization studies conducted on helicopter rotors (Reference 5) show that the shed tip vortices for rotating blade rows diffuse within one to two revolutions, and the distinction of the tip vortices is lost. However, no quantitative information exists regarding the circulation of $(V\theta)_{max}$ or radius of such rotating tip vortices for use in modeling the decay of rotating tip vortices. The more rapid decay of rotating tip vortices (compared to translating tip vortices) may be due to the relatively larger turbulence and more efficient mixing processes prevalent in the near field of a rotating blade row, compared to a wing in translation wherein the decay could be due predominantly to viscous dissipation. In the absence of applicable information regarding the decay of the tip vortex for an unducted rotor, different power law decay rates are proposed for the current model:

$$(\Gamma)_{vtx} \propto \frac{1}{(1 + s/c)^\eta} \quad (18)$$

Figure 7 demonstrates streamwise variations of normalized tip vortex circulation for three decay rates (that is, $\eta = 0, 1/4$, and $1/2$); the exponential value that was used for tip vortices of the ducted fan rotor was $1/2$ (Reference 3). The presence of the annulus wall and the large number of blades of a ducted fan rotor would cause a faster diffusion of tip vortex, compared

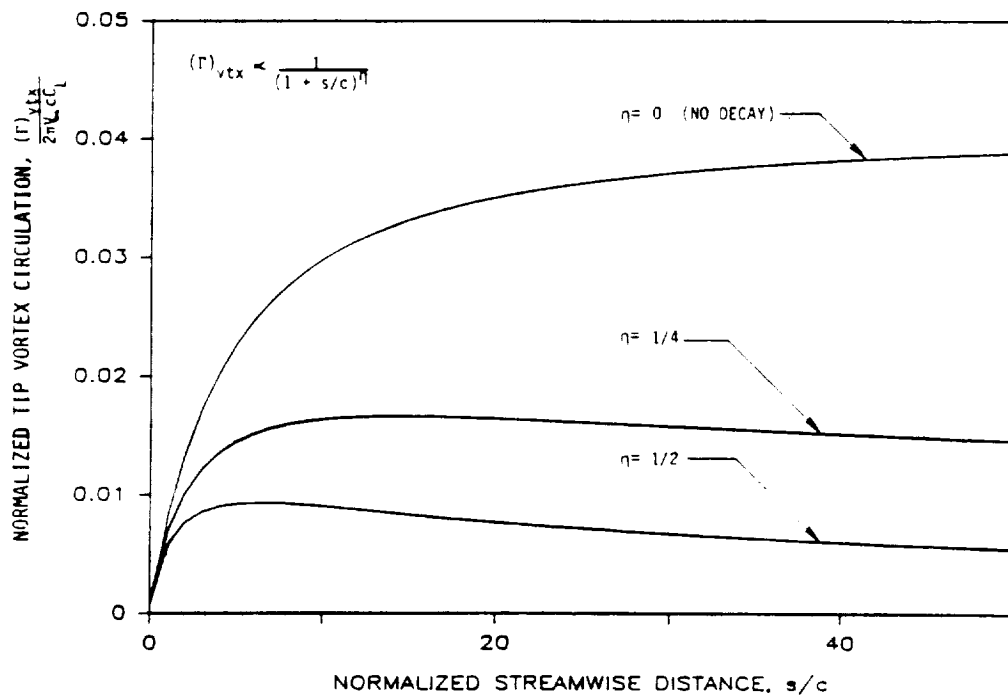


Figure 7. Streamwise Variation of Normalized Circulation of the Tip Vortex for Three Different Power Law Decay Rates.

to the unducted fan rotor; hence, $\eta = 1/4$ is proposed as the exponent for the tip vortex decay rate of an unducted fan. The influence of the decay rate on the acoustic predictions of unducted rotors will be examined through parametric studies in Subsection 3.1.4.

Since the correlations for $(V_\theta)_{\max}$ and radius of the tip vortex core (Equations 13 and 14) were developed using the data of wings of constant cross sections without any twist, the local section lift coefficient (C_L) and chord distribution along the span did not vary; however, such is not the case for an unducted fan rotor. To determine what value of local section lift coefficient and chord must be used for computing $(V_\theta)_{\max}$ and radius of the tip vortex core in this case, we resorted to published literature on helicopter tip vortices for some guidelines. The measurements and predictions of Donaldson, et al. (Reference 16) indicate that, for helicopter blades, the loading in only the outboard 30% span of the blade contributes to the tip vortex structure. The above criterion has been used as a guide in the selection of C_L and "c" for the tip vortex of unducted rotors. Figure 8 shows the spanwise variation of local section lift coefficient for typical takeoff and cruise conditions for a typical unducted fan forward rotor blade design (such as, the F-7 blade). Figure 9 depicts the spanwise variation of chord for the F-7 blade. In accordance with Reference 16, the average values of lift coefficient and chord are computed using their distribution over the outboard 30% span. These average values, $(C_L)_{av}$ and $(c)_{av}$, are used as the parameters characterizing the tip vortex in computing $(V_\theta)_{\max}$ and radius of the tip vortex core (Equations 13 and 14). This averaging procedure takes into account the spanwise variation of the blades and yields an "equivalent" blade of uniform section, in a very rough sense.

Due to a lack of detailed UDF® blade tip vortex experimental data, there is some uncertainty as to applicability of the value of $(V_\theta)_{\max}$ and radius of the tip vortex core (see Equations 13 and 14), as these are based on the configuration of the wing, rather than of the UDF® blade. Therefore, an empirical factor known as the circulation index (C_i) was introduced to modulate the circulation of the tip vortex, which is defined as:

(19)

$$(\Gamma)_{VTX} = C_i \{2\pi (V_\theta)_{\max} a\}$$

A value of $C_i = 1$ reproduces the circulation given by Equation 15. The value of $C_i > 1$ means that the tip vortex structure includes the influence of loading in more than the outboard 30% span of the blade. Conversely, the value of $C_i < 1$ provides less circulation strength than is provided by Equation 15. Improvements to this simple procedure may be adopted when more information is available on characteristics of the tip vortices of the UDF® blades. A sensitivity of the circulation index on the unsteady noise is studied and discussed in Subsection 3.1.1.

Next, an empirical relationship is developed for the trajectory of the tip vortices employing the flow visualization data (References 5 and 6) which were obtained for helicopter blades in a typical hover mode. All of these data indicated that tip vortices move radially inward for increasing axial distance, which is ascribable to the stream tube contraction (Figure 10).

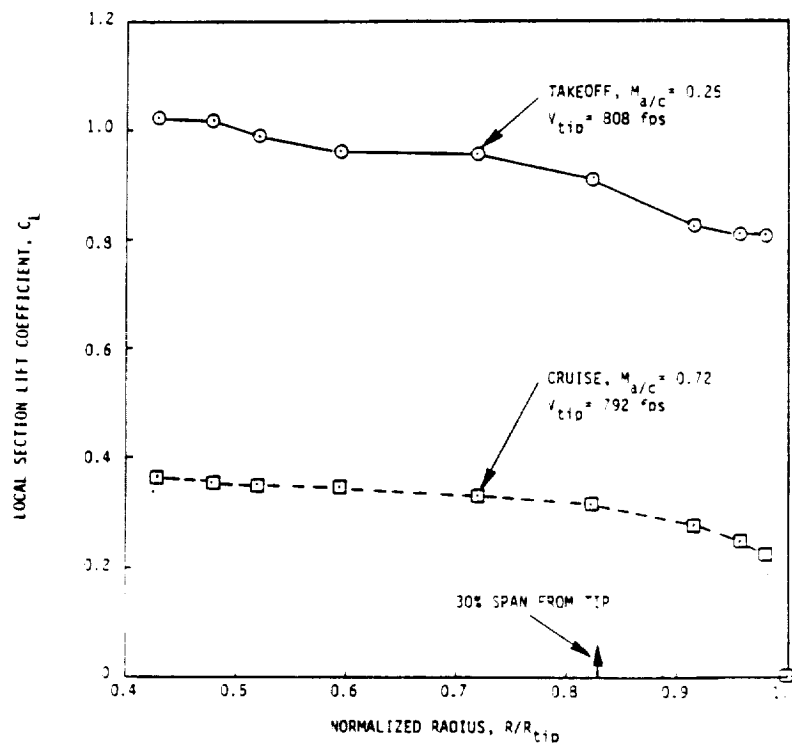


Figure 8. Spanwise Variation of the Local Section Lift Coefficient for Takeoff and Cruise Conditions for F-7 Blades.

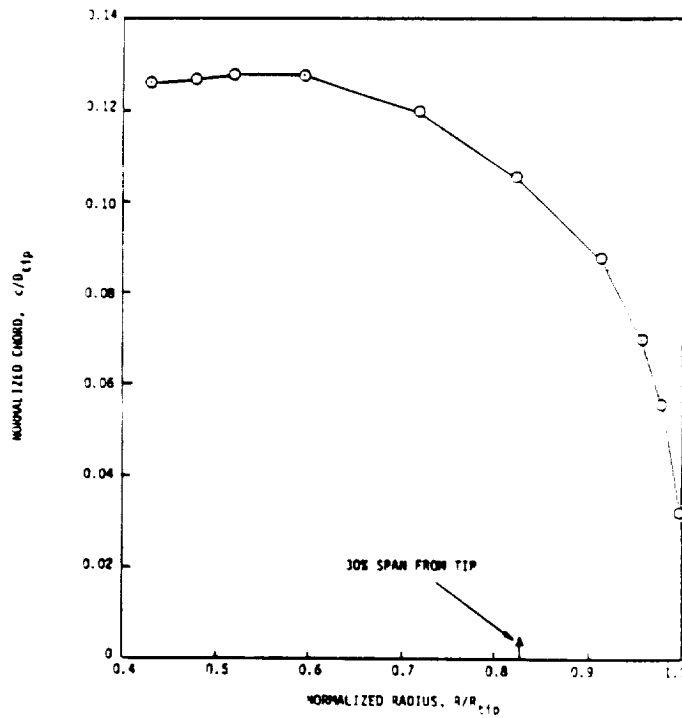


Figure 9. Spanwise Variation of the Chord for the F-7 Blade Design.

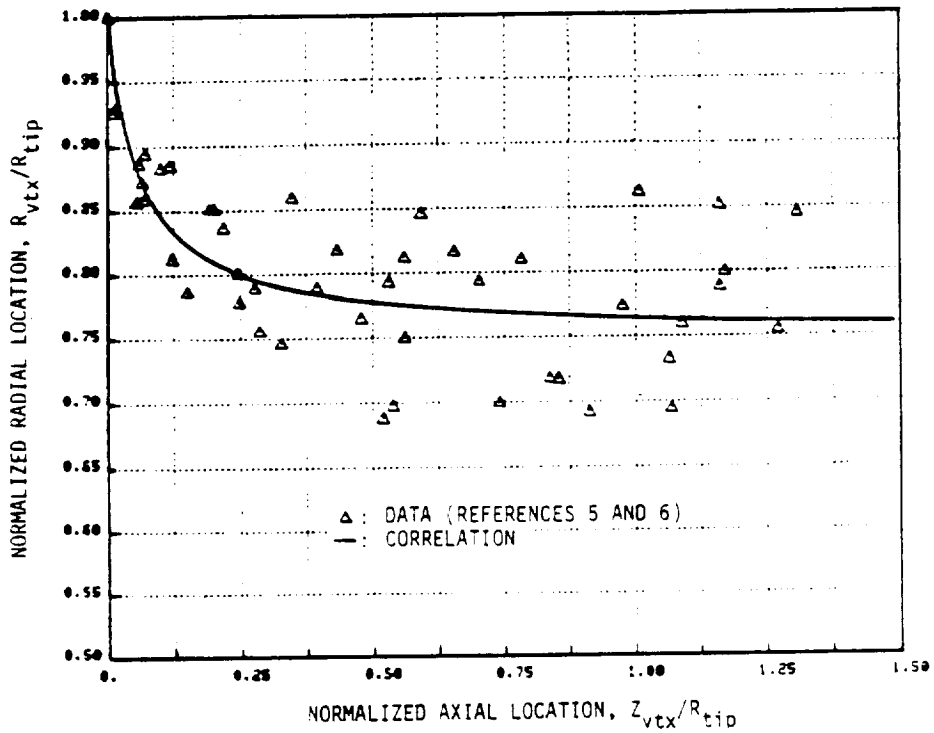


Figure 10. Correlation and Data for the Trajectory of the Tip Vortex.

Linear-rational-function correlation methods (Reference 3) were used again to develop an empirical relation for the trajectory of the tip vortex. Linear-rational functions are applicable if the dependent variable shows a monotonic trend with the independent variable. Since the radial movement of the tip vortex with axial distance is monotonic, approaching an asymptotic value, linear-rational function was chosen. The empirical relationship which yielded minimum standard deviation is:

$$\frac{R_{vtx}}{R_{tip}} = \frac{12 (Z_{vtx})/R_{tip} + 1.0}{16 (Z_{vtx})/R_{tip} + 1.0} \quad (20)$$

where

R_{vtx} : radial location of core of tip vortex

Z_{vtx} : axial location of core of tip vortex.

Since the formulation for tip vortex discussed in Subsection 2.1 uses $b_r = R_{tip} - R_{vtx}$, Equation 20 is written in terms of b (see Figure 2 also):

$$\frac{b_r}{R_{tip}} = 1 - \frac{R_{vtx}}{R_{tip}} = \frac{4 (Z_{vtx})/R_{tip}}{16 (Z_{vtx})/R_{tip} + 1.0} \quad (21)$$

There is a lot of scatter in the data for large values of Z/R_{tip} ; this, mainly, is a result of the uncertainty in defining the tip vortex at large values of Z/R_{tip} due to the diffusion of the tip vortex.

The development of Equation 21 is based on the data base for helicopter rotors. The HTR for helicopter rotors is approximately less than 0.1; however, the HTR for the UDF® blades is approximately 0.4. This introduces some amount of uncertainty regarding the applicability of the tip vortex trajectory correlation of Equation 21 to the UDF® configuration. Due to the lack of a data base for the higher values of HTR, the general form of the tip vortex trajectory for UDF® blades is assumed from Equation 18 as follows:

$$\frac{b_r}{R_{tip}} = \frac{K_{vtx} (Z_{vtx})/R_{tip}}{16 (Z_{vtx})/R_{tip} + 1.0} \quad (22)$$

where K_{vtx} is an adjustable constant.

For a given HTR, the tip vortex trajectory can be expressed in terms of a blade span percent of the tip by: $(b_r/R_{tip})/(1-HTR)$. For example, the value of $b_r/R_{tip} = 0.1$ translates to about a 17% span from the tip, with $HTR = 0.4$. On the other hand, the value of $b_r/R_{tip} = 0.1$ approximates K_{vtx} to be 2 for $Z_{vtx}/R_{tip} = 0.3$. Thus, the value of K_{vtx} for the UDF® blades should be chosen with consideration of blade geometries, forward and aft rotor spacing, aeroperformance, etc., which would affect the tip vortex trajectories. The value of K_{vtx} was assumed to be between 0.5 and 2.0, based on a flow-field computation performed using GE's in-house codes. The parametric evaluation of the tip vortex trajectory on the unsteady noise due to the tip vortex is reported in Subsection 3.1.3. Again, a detailed experimental data base will be required to obtain the proper value of K_{vtx} for the UDF® blade configurations.

3.0 Model Evaluation

The aerodynamic model for the tip vortex of counterrotating propulsors (described in Section 2.0) is evaluated in this section by:

1. Parametrically evaluating the effect certain key parameters (such as: tip vortex strength, drag coefficient, tip vortex trajectory, decay rate, tangential location of the tip vortex, and extent of clipping of the aft rotor) have on the acoustic characteristics of the counterrotating UDF® propulsors.
2. Comparing selective acoustic data and predictions of the counterrotating UDF® propulsors, aimed at evaluating the tip vortex model.

Due to the relatively low values of solidity over most of the span, UDF® propulsors may be viewed as isolated airfoils in computing the gust harmonic spectra resulting from impingement of the forward rotor wake and the tip vortex on the aft rotor. Hence, the unsteady gust model developed by Kemp and Sears (Reference 17) was selected for predicting the gust harmonic spectra of unsteady loadings induced by the tip vortex and the rotor wakes.

In the rotor wake model, the resultant aft rotor unsteady lift is strongly influenced by the forward rotor exit wake profile. As discussed in References 3 and 4, this wake profile modeling has been significantly affected by the drag coefficient of the local blade section. However, due to a lack of detailed UDF® aerodynamic data, there are large uncertainties to determine the accurate local section drag coefficient. The drag coefficients used in the present study were obtained based on GE's in-house analytical method, along with the aeroperformance of the scale model test of the UDF® configuration. The following section describes the sensitivity study of the drag coefficient on gust spectra and interaction noise levels.

3.1 Parametric Studies

The studies described in this section parametrically evaluate the effect of certain geometric and aerodynamic parameters (described in Section 2.2) of the tip vortex on the acoustic characteristics of a counterrotating propeller. The principal objective of these studies was to develop an understanding of the sensitivity of the acoustic characteristics to certain key geometric and aerodynamic parameters of the tip vortex. The parametric studies described herein are:

- Influence of tip vortex strength and drag coefficient (C_t and C_d , respectively, sensitivity)
- Influence of tangential location of tip vortex (bt/s sensitivity)
- Influence of tip vortex trajectory (K_{vtx} sensitivity)
- Influence of decay rate of tip vortex (η sensitivity)
- Influence of progressive clipping of the aft rotor.

For the parametric studies, standard F-7/A-7 blade design parameters are used to calculate the gust harmonic spectra and unsteady loading noise through the present model; Figure 11 portrays a planform of these blades. The parametric studies are performed based on the aero-performance data of TP (test point) 3706 of a 90% rpm case with 9×8 F-7/A-7 blades at a take-off Mach number, obtained from GE Cell 41. For an unequal blade number configuration (such as, 9×8) but equal rpm, the steady loading and thickness noise and the noise due to wake/tip vortex interaction occur at distinctly different frequencies (Reference 11), as listed below:

- Steady loading and thickness noise of forward rotor

$$f_{s1q} = q * \frac{\text{rpm1}}{60} * B1 \quad q = 1, 2, 3, \dots \quad (23)$$

where f_{s1q} is the q^{th} harmonic of steady loading and thickness noise of the forward rotor, and $B1$ is the number of blades in the forward rotor, and $q = 1$ corresponds to BPF (blade passing frequency), $q = 2$ corresponds to $2 \times \text{BPF}$ of forward rotor, etc.

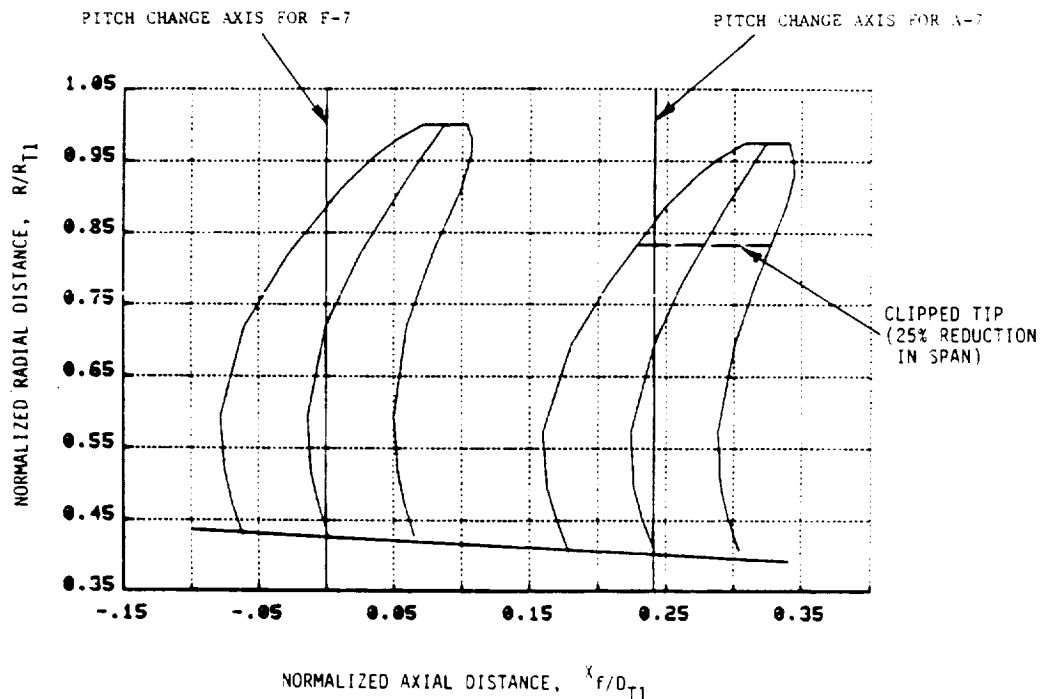


Figure 11. Planform of the F-7/A-7 Unducted Fan Blade Design, Showing the Extent of Clipping on the Aft Rotor.

- Steady loading and thickness noise of aft rotor

$$f_{s2r} = r * \frac{\text{rpm2}}{60} * B2 \quad r = 1, 2, 3, \dots \quad (24)$$

where f_{s2r} is the r^{th} harmonic of steady loading and thickness noise of the aft rotor; $B2$ is the number of blades in the aft rotor; and $r = 1$ corresponds to BPF; $r = 2$ corresponds to $2 \times \text{BPF}$ of the aft rotor, and so on.

- Noise due to wake/tip vortex interaction

$$f_{wqr} = f_{s1q} + f_{s2r}, \quad q = 1, 2, 3, \dots \quad (25)$$

For equal rpm's (say, $\text{rpm}_1 = \text{rpm}_2 = \text{rpm}$), normalized frequencies are defined as:

$$\bar{f}_{s1q} = \frac{f_{s1q}}{(\text{rpm}/60)} = qB1, \quad q = 1, 2, 3, \dots \quad (26)$$

$$\bar{f} = \frac{f_{s2r}}{(\text{rpm}/60)} = rB2, \quad r = 1, 2, 3, \dots \quad (27)$$

and

$$\bar{f}_{wqr} = \frac{f_{wqr}}{(\text{rpm}/60)} = qB1 + rB2, \quad q = 1, 2, 3, \dots \quad (28)$$

The spinning mode numbers associated with steady loading and thickness noise of forward and aft rotors are $qB1$ and $rB2$, respectively. The spinning mode number associated with the noise due to wake/tip vortex interaction is given by:

$$m_{wqr} = rB2 - qB1 \quad (29)$$

where m_{wqr} is the spinning mode number of the r^{th} harmonic or aft rotor unsteady noise, due to q^{th} gust harmonic of forward rotor.

Table 1 lists the tone designation, f_{wqr} , m_{wqr} , q , and r for increasing frequencies for a 9×8 blade configuration. Figure 12 is a schematic of the steady loading and unsteady loading noise spectra for the 9×8 blade number configuration.

In the following parametric studies, the sensitivity of each parameter was examined individually by varying the particular parameters from the basic stage of each. The value of each parameter at the basic stage is given as $C_i = 2.0$, $K_{vtx} = 2.0$, $bt/S = 0.5$, and $\eta = 1/4$.

3.1.1 Influence of Tip Vortex Strength and Drag Coefficient

Gust spectra and consequential interaction noise levels are affected by both rotor viscous wake and tip vortex flow field. In the present work effort, the viscous wake and the tip vortex flow fields are modeled independently and are then summed to obtain total unsteady gust loadings on the aft rotor. When the unsteady loading is dominated by the viscous rotor wakes, the tip vortex effect becomes small, and vice versa. The sensitivity of the strength of the viscous wake and the tip vortex on gust spectra and interaction noise levels is studied by parametrically

Table 1. Normalized Acoustic Frequencies and Spinning Modes Associated with Wake/Tip Vortex Interaction for a 9×8 Blade Number Configuration.

Tone Designation	\bar{f}_{wqr}	m_{wqr}	q	r
(A + F)	17	-1	1	1
(2A + F)	25	7	1	2
(A + 2F)	26	-10	2	1
(3A + F)	33	15	1	3
(2A + 2F)	34	-2	2	2
(A + 3F)	35	-19	3	1
(4A + F)	41	23	1	4
(3A + 2F)	42	6	2	3
(2A + 3F)	43	-11	3	2
(A + 4F)	44	-28	4	1
(5A + F)	49	31	1	5
(4A + 2F)	50	14	2	4
(3A + 3F)	51	-3	3	3
(2A + 4F)	52	-20	4	2
(A + 5F)	53	-37	5	1

\bar{f}_{wqr} - Normalized acoustic frequency

m_{wqr} - Spinning mode

q - Forward rotor gust harmonic

r - Aft rotor acoustic harmonic

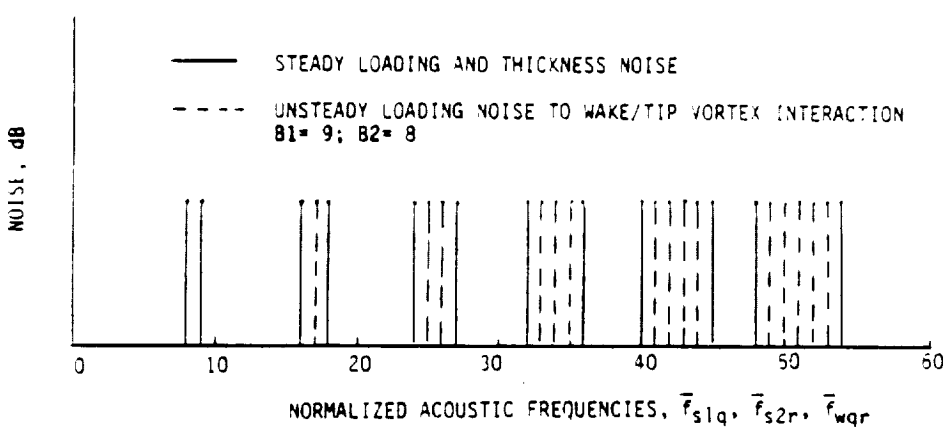


Figure 12. Schematic of a Narrowband Acoustic Spectrum of a 9×8 Blade Number Configuration.

**ORIGINAL PAGE IS
OF POOR QUALITY**

varying the circulation index of the tip vortex model and the drag coefficient (C_d) of the rotor viscous wake model.

The influence of the circulation of the tip vortex on gust spectra and its consequential sensitivity on the interaction noise is shown in Figure 13 where the parametrically varying C_i has a fixed value of $K_{vtx} = 2.0$ and $b/t_s = 0.5$. A "no tip" vortex is also included, for the sake of completeness. Figure 13 presents the predicted sensitivity of the circulation index on gust harmonic spectra at the tip streamline with three different values of C_d (0.03, 0.02, and 0.005); similarly, Figures 14 and 15 illustrate the C_i effect for these values of C_d at the streamlines of 70.7% and 45.4% span from the hub, respectively.

At the tip region (Figure 13), gust harmonic spectra for each C_i value have similar levels (regardless of C_d), even though the viscous wake gust spectra denoted by no tip are quite different from the nonzero C_i cases. The difference between no tip and nonzero C_i is the effect of the tip vortex. As demonstrated in Figure 15, the gust harmonics collapse into one line at the location far away from the tip vortex center where the tip vortex effect is minimal.

As shown in Figure 14, at the 70.7% span location from the hub, the spectra with $C_d = 0.03$ and 0.02 exhibit small spread, due to the different C_i values for the lower gust harmonics ($q = 1, 2, 3$, and 4); but the spectra with $C_d = 0.005$ shows a relatively large spread for three C_i values. This indicates that the sensitivity of tip vortex strength on the gust harmonics depends on the levels of drag

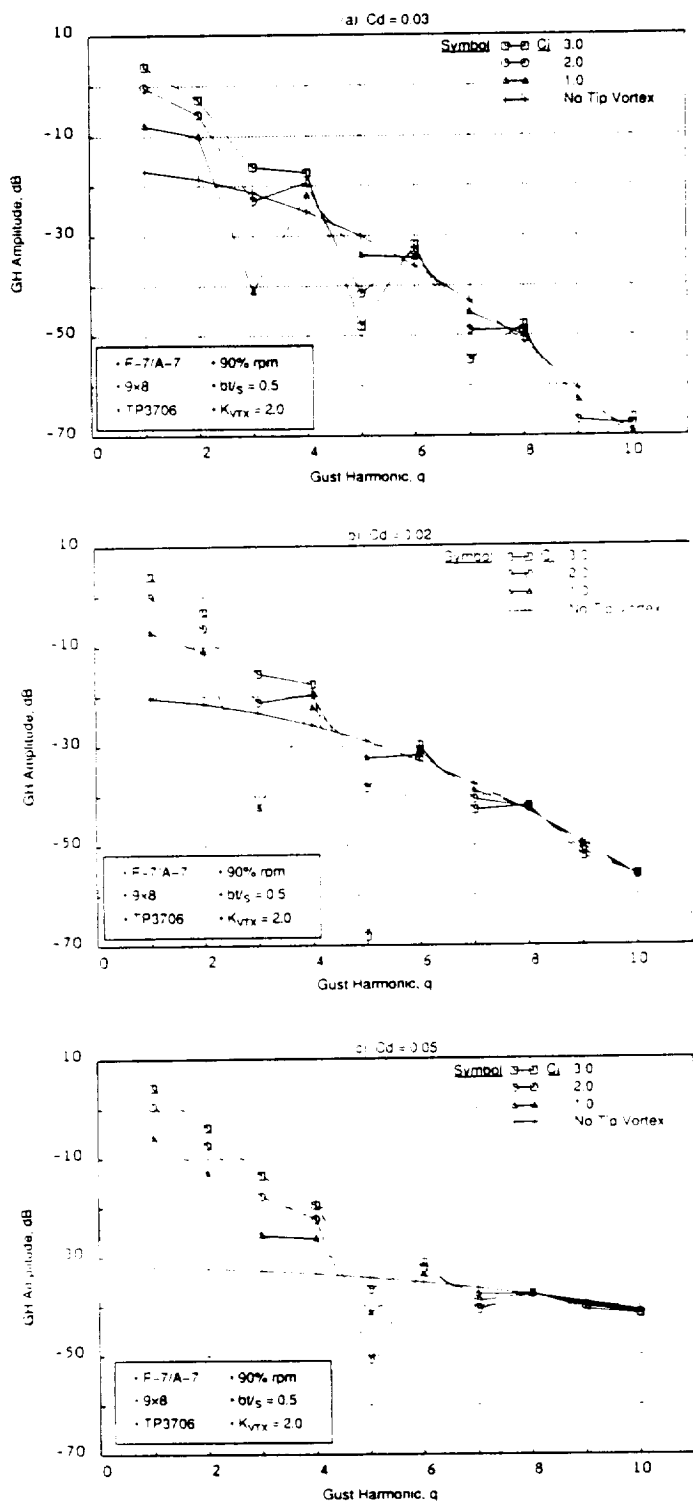


Figure 13. Predicted Effect of Tip Vortex Strength on Gust Harmonic Spectra with Three Different C_d Values at the Streamline of 100% Span from the Hub.

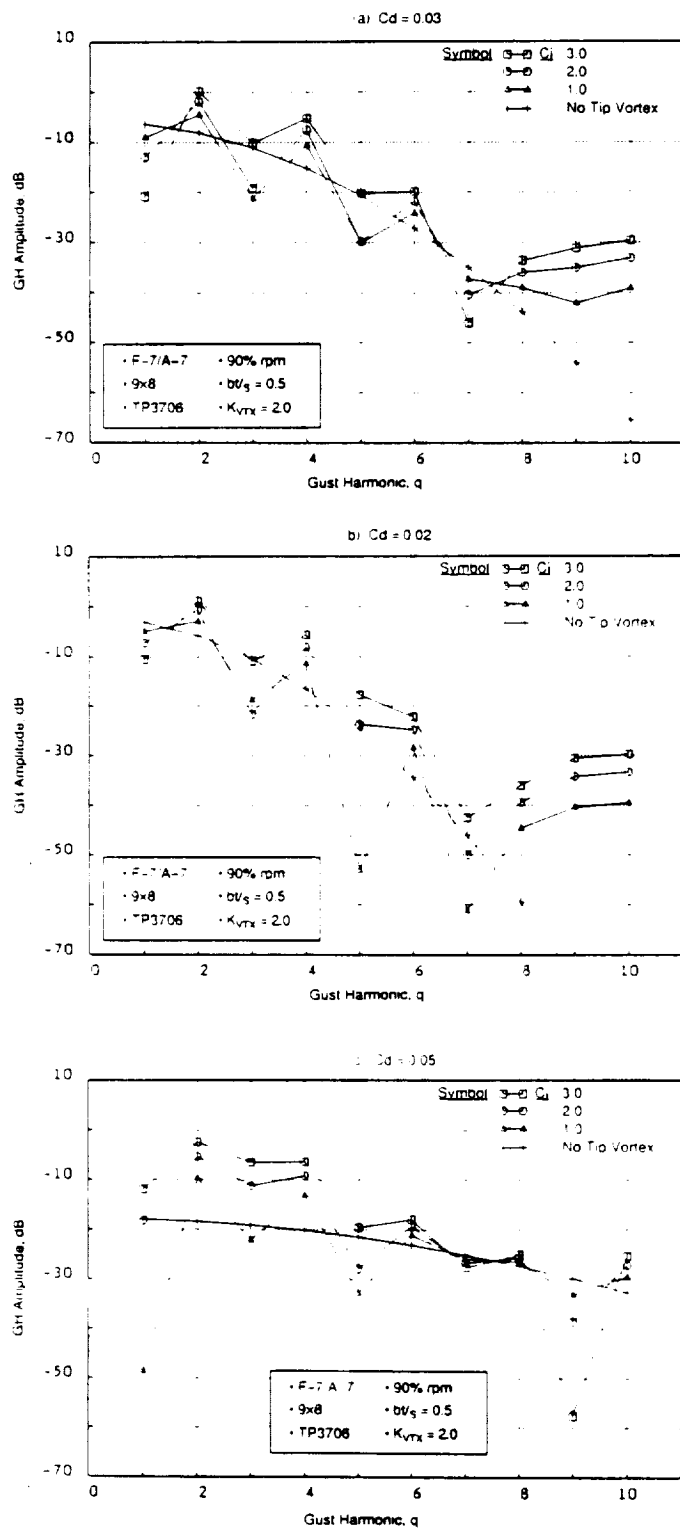


Figure 14. Predicted Effect of the Tip Vortex Strength on Gust Harmonic Spectra with Three Different C_d Values at the Streamline of 70.7% Span from the Hub.

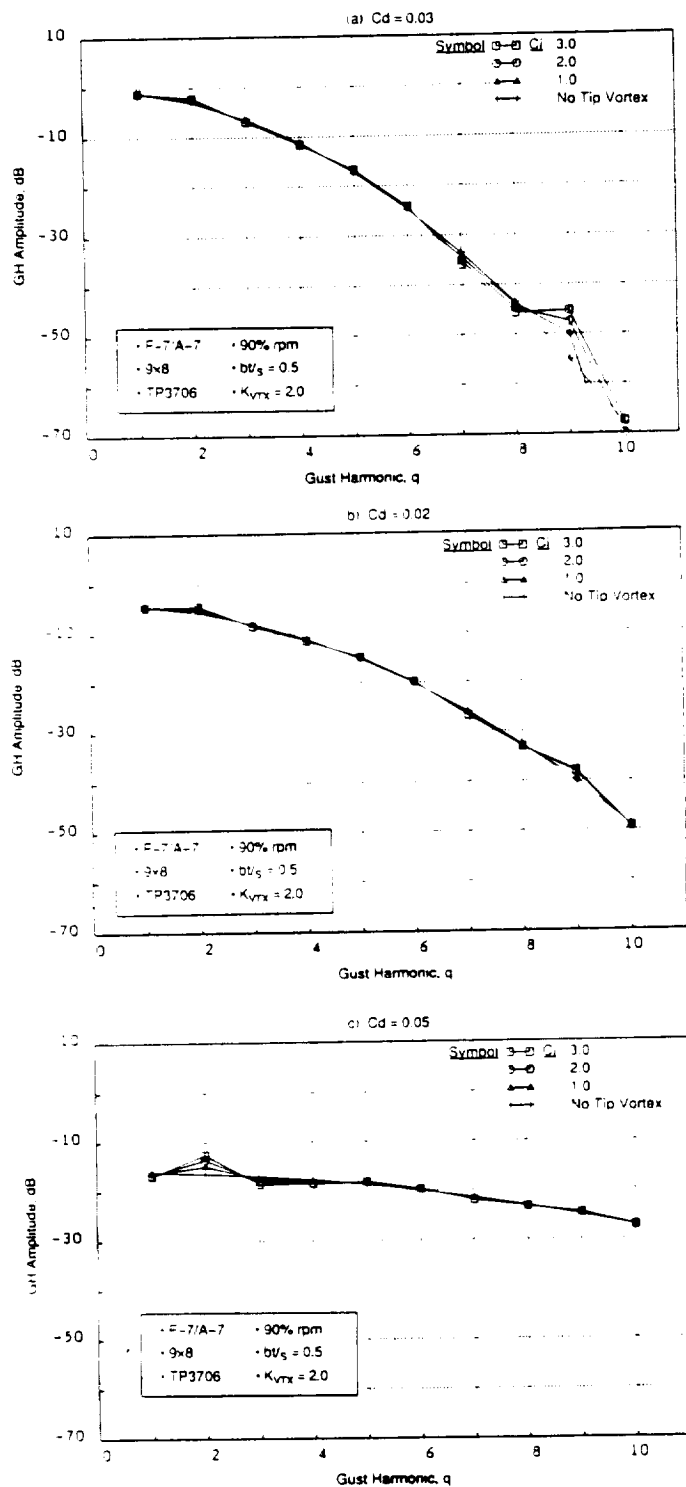


Figure 15. The Predicted Effect of Tip Vortex Strength on Gust Harmonic Spectra with Three Different C_d Values at the Streamline Location of 45.4% Span from the Hub.

coefficient. The effect of the tip vortex becomes minimal at the streamline of 45.4% span from the hub (Figure 15).

Figure 16 illustrates the predicted effect of the tip vortex strength (C_i) on the interaction tone SPL (sound pressure level) sum with $C_d = 0.005$. Since the value of C_d is small, the circulation index sensitivity is clearly shown as 4 to 6 dB; however, the directivity of SPL sum was preserved for the various C_i values. To examine the predicted effect of the drag coefficient on the interaction tone SPL sum with a fixed value of $C_i = 2.0$, Figure 17 is given for $C_d = 0.03, 0.02$, and 0.005 . Although the drag coefficient effect is seen at the forward arc of the emission angle, the C_d effect becomes negligible at the aft rotor. Thus, prediction of the averaged acoustic quantities of PNL, PNLT, or EPNL would be significantly influenced by the SPL sum directivity.

Figure 18 provides a summary of the predicted tip vortex effect for the C_d values of 0.03, 0.02, and 0.005 on the interaction tone sum directivity by comparing the SPL sum predictions, both with and without the tip vortex. The interaction tone sum directivity is computed both with and without the tip vortex model turned on. The differences between these two SPL directivities indicate the isolated tip vortex effect, since both cases contain the interaction tones induced by the rotor viscous wakes. As presented in Figures 13 through 15, the tip vortex effect becomes significant as the values of C_d are reduced. It should be emphasized that the accurate acoustic predictions, using the current model, depend upon

ORIGINAL PAGE IS
OF POOR QUALITY

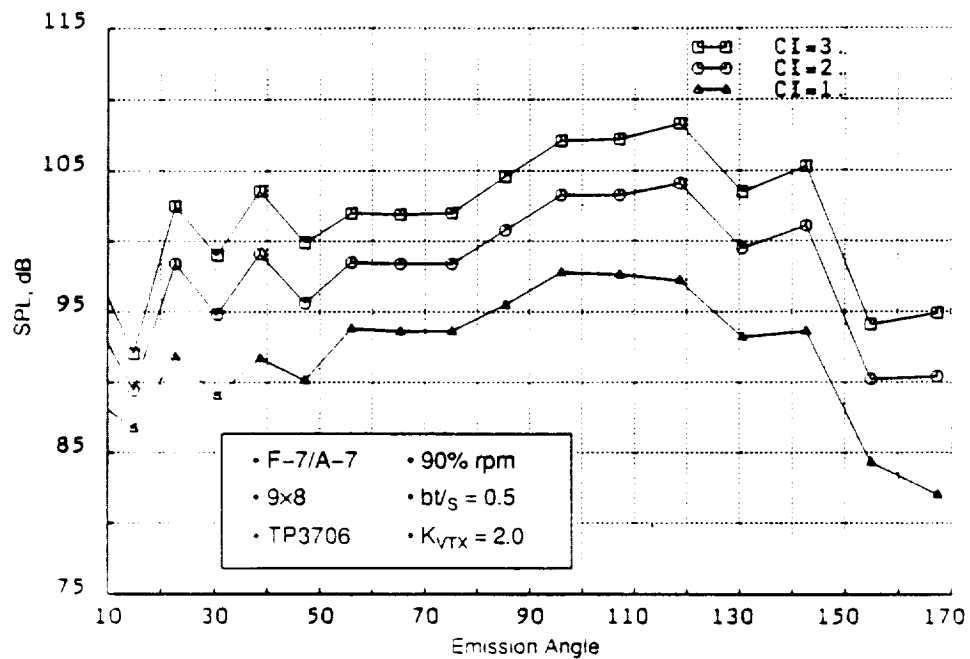


Figure 16. The Predicted Effect of the Tip Vortex Strength on Interaction Tone SPL Sum with $C_d = 0.005$.

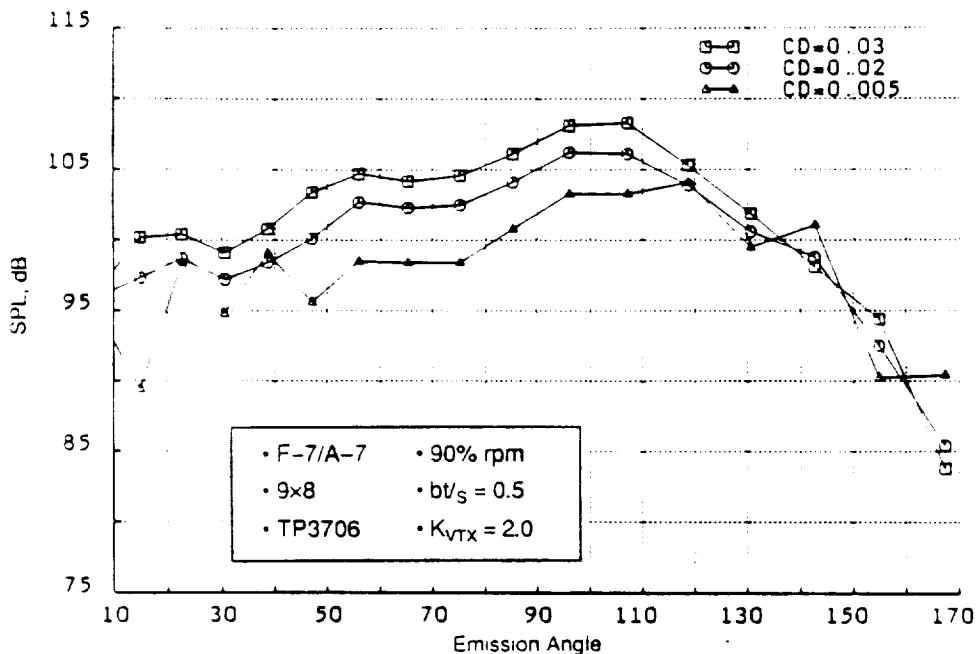


Figure 17. Predicted Effect of the Drag Coefficients on the Interaction Tone SPL Sum with $C_i = 2.0$.

ORIGINAL PAGE IS
OF POOR QUALITY

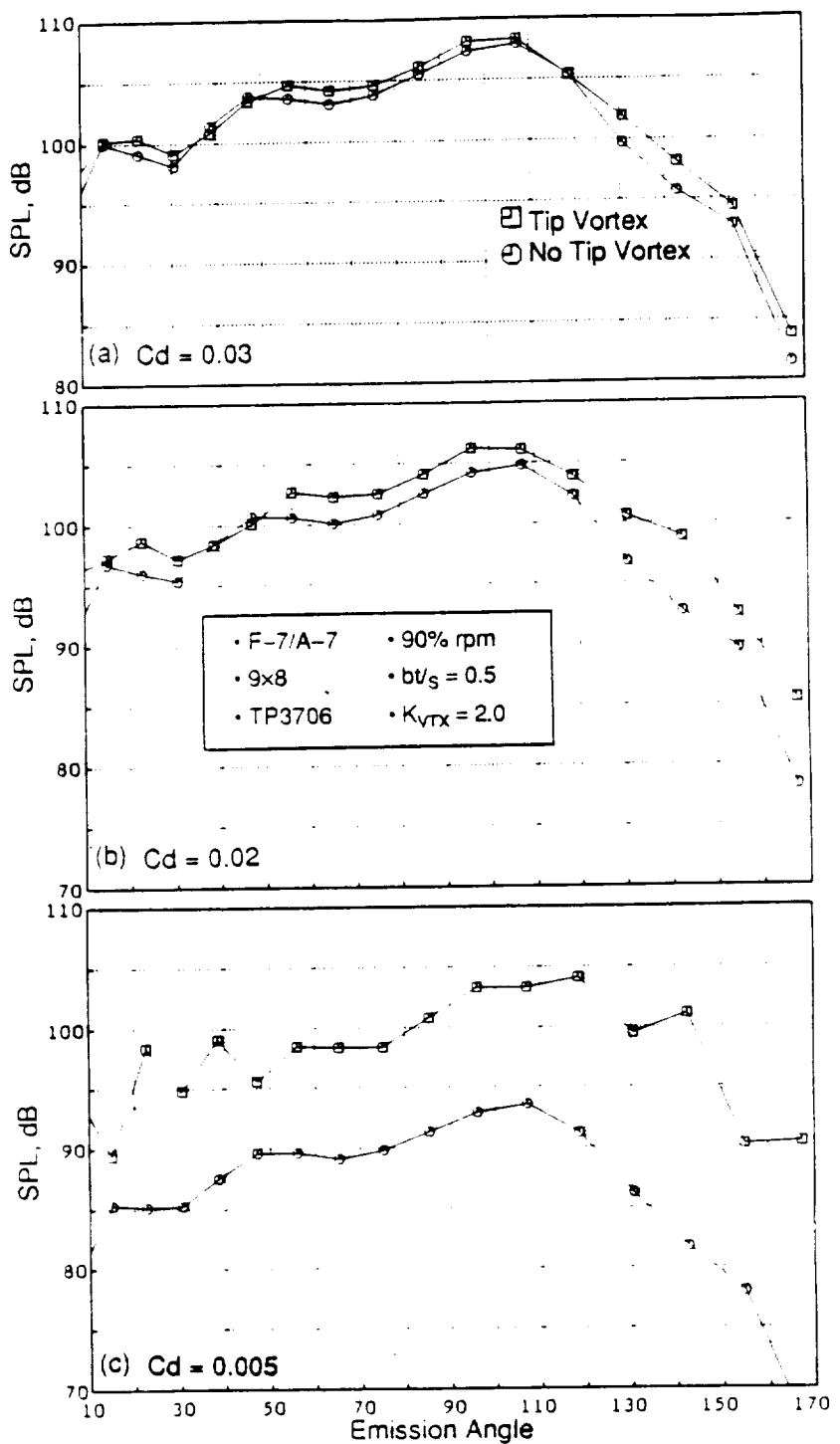


Figure 18. Predicted Tip Vortex Effect of the Drag Coefficients (0.03, 0.02, and 0.005) on Interaction Tone SPL Sum with $C_t = 2.0$.

the accuracy of the section local drag coefficients and the tip vortex strength (which are not available at the present time, due to the lack of experimental data).

3.1.2 Influence of Tangential Location of Tip Vortex

The tangential position of the tip vortex, relative to the wake centerline, is a critical parameter in determining the gust waveform shape and amplitude. Figure 19 compares the gust waveform shape for four values of tangential position of the tip vortex at three radial locations. The gust waveform shape for the case of wake alone (that is, no tip vortex) is included for the sake of completeness. The wake flow field is assumed to be symmetrical on either side of the blade (pressure or suction). Even though this assumption may not be valid, applicable data to model the asymmetry of the wake are lacking. Thus, the gust wave shape for $0.5 \leq x/S \leq 1.0$ is a mirror image of the gust waveform shape over $0.0 \leq x/S \leq 0.5$ without the tip vortex; however with tip vortex, a wavelength of the gust waveform shape becomes equal to blade-to-blade spacing and is not symmetrical between $0.0 \leq x/S \leq 0.5$ and $0.5 \leq x/S \leq 1.0$.

The gust velocity at the tip streamline and at 70.7% span from hub streamline are quite small for cases without the tip vortex effect, as compared to those cases with the tip vortex effect. At the hub streamline, this model predicts no tip vortex influence on the gust velocity. For $bt/S = 0.0$ (where tip vortex is located at the wake centerline), the upwash velocities at the tip and 70.7% streamlines shoot up at $x/S = 0.0$. For $bt/S = 0.25$, the presence of the tip vortex is indicated by the large increase at $x/S = 0.25$ at the tip and 70.7% streamlines; similarly for $bt/S = 0.33$, significant tip vortex influence is shown at $x/S = 0.33$. For $bt/S = 0.5$, the gust velocity shape is altered significantly (it is a downwash instead of an upwash, as was the case for other bt/S values).

Figure 20 shows the Fourier decomposition of the gust waveforms depicted in Figure 19 to yield the gust harmonic spectra. For $bt/S = 0.5$, the even-numbered gust harmonics are higher in amplitude (than the odd-numbered gust harmonics), due to two similar dips within one passage; one due to wake, and one due to the tip vortex. For $bt/S = 0.25$, the dips/hills due to tip vortex interact with the wake, and the resulting waveform is not symmetric (as was $bt/S = 0.5$) which causes higher gust spectral values for odd-numbered gust harmonics. Similar behavior can be seen from $bt/S = 0.33$. When $bt/S = 0.0$, the dips/hills due to wake and tip vortex yield a sharp gust profile at the wake centerline (similar to an impulse function). This results in high values for all gust harmonics. At the hub streamline, there is no tip vortex influence.

Next, the influence of the tangential location of tip vortex on interaction noise is considered, based on the case demonstrated in Figures 19 and 20. Figure 21 compares the predicted and measured interaction noise tones; that is, $1A + 1F$ through $2A + 3F$ tones at an observer angle of 131° for $bt/S = 0.5, 0.33, 0.25$, and 0.0 . The measured data were obtained from the GE Cell 41 data base. It is apparent that the tangential location of tip vortex strongly affects the $1A + 2F$ and $2A + 2F$ tones; for example, a 10-dB spread (depending on the values of bt/S). However, the sensitivity of the bt/S value on the other interaction tones is relatively small (less than 5 dB). However, Figure 19 reveals large underpredictions of the model on $1A + 2F$ and

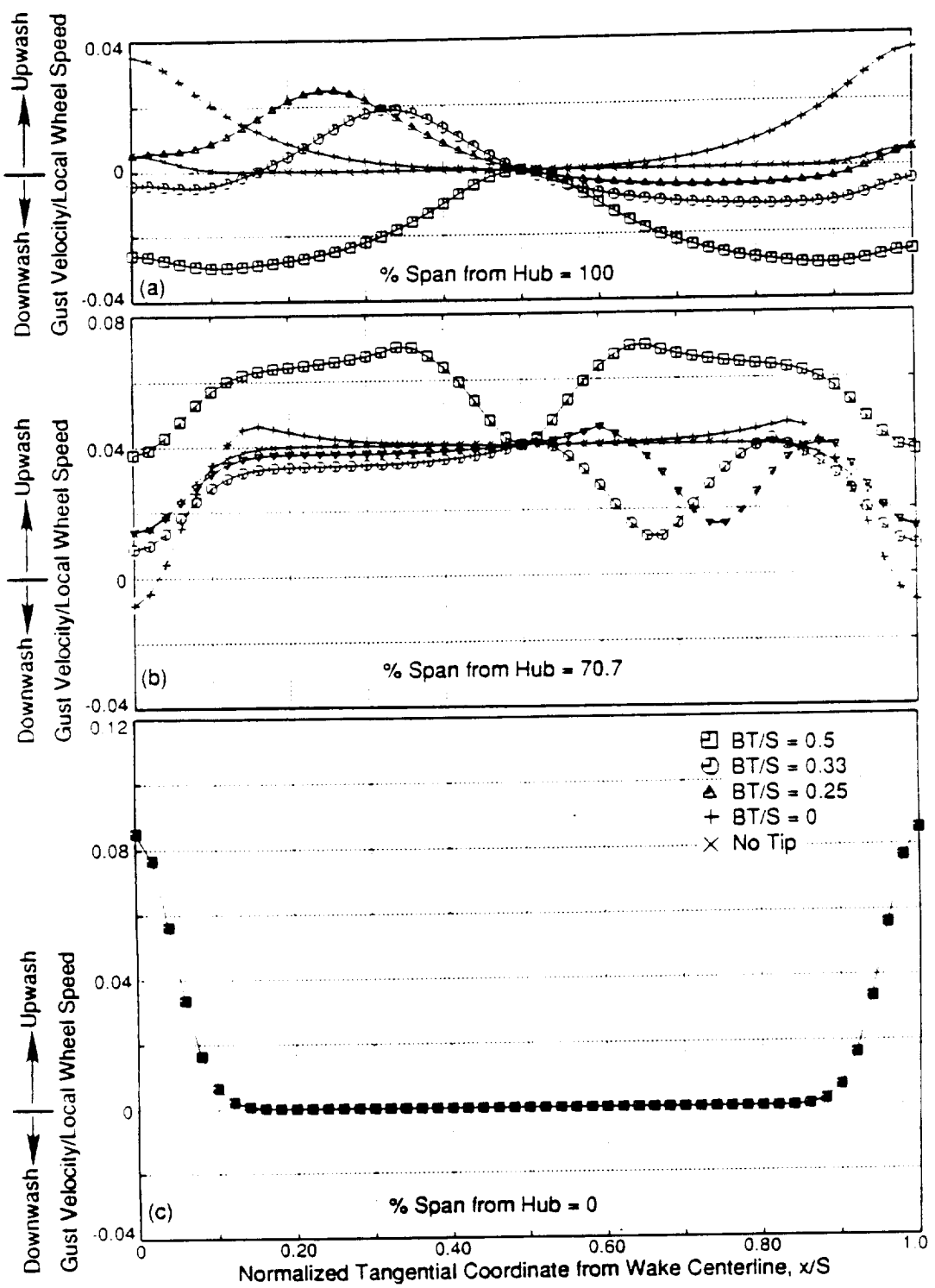


Figure 19. Predicted Tangential Distribution of Gust Velocity at Three Radial Locations for Various Tangential Locations of Tip Vortex, and for the Case of No Tip Vortex.

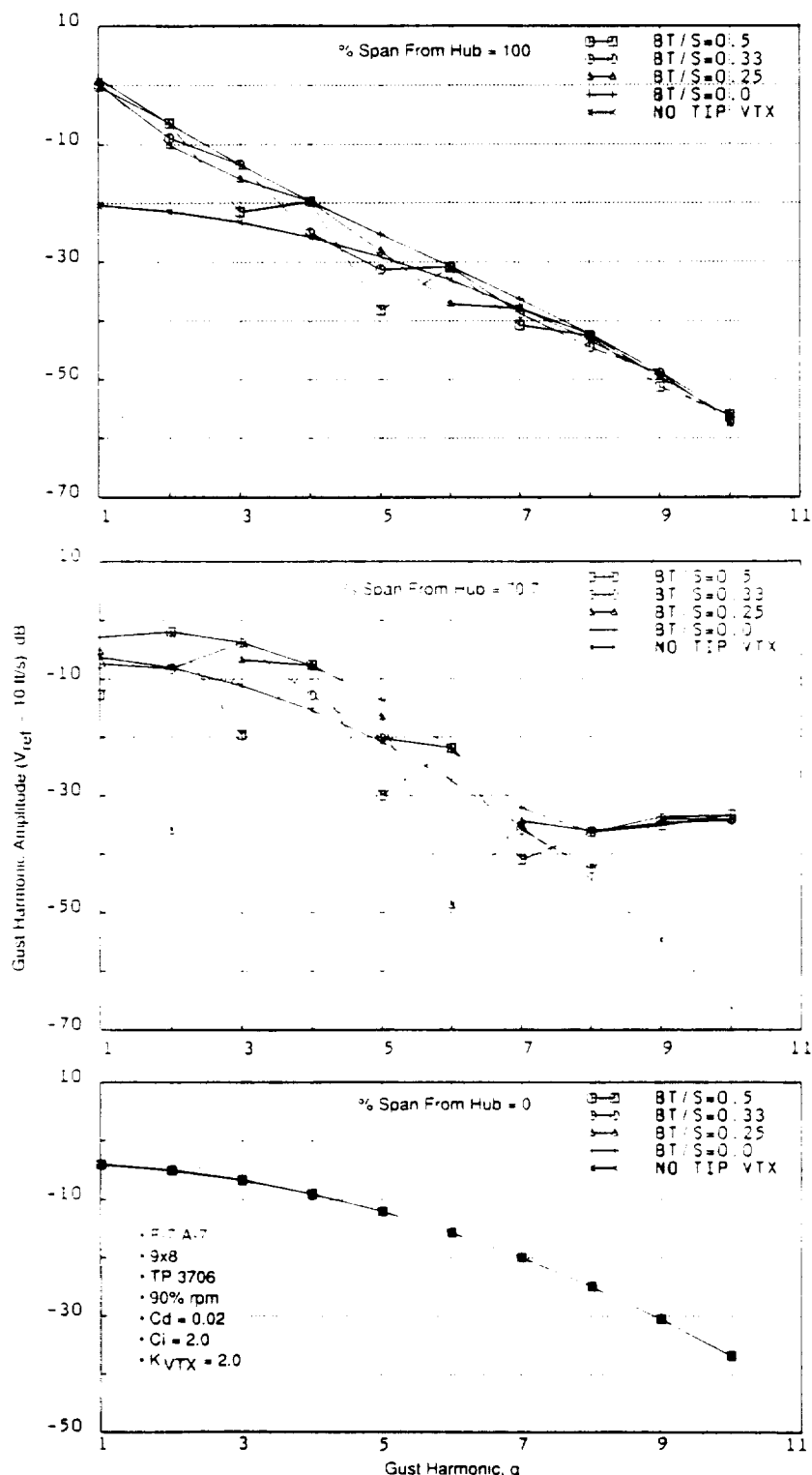


Figure 20. Predicted Effect of Tangential Location of Tip Vortex on Gust Harmonic Spectra at Three Radial Locations.

1A + 3F tones regardless of the value of bt/S . This indicates that further improvement and modification are needed on the model. Since values of bt/S depend on blade configurations and aeroperformance, it is difficult to determine the optimal value of bt/S without a detailed rotor aerodynamics data base at the present time.

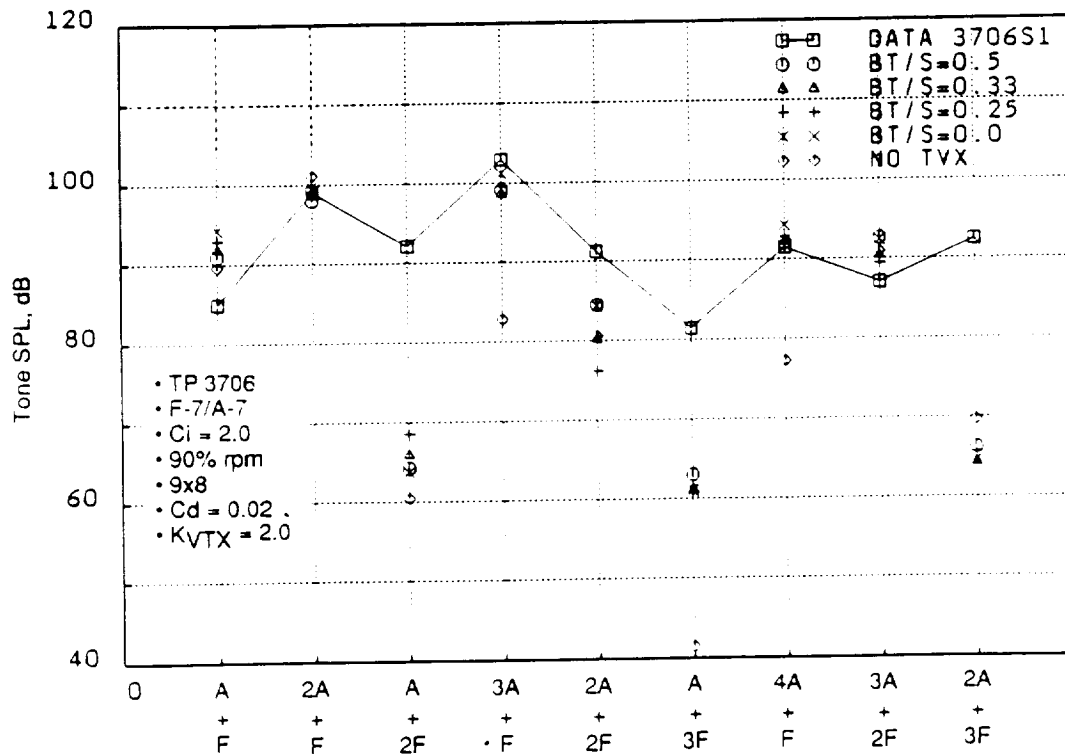


Figure 21. A Comparison of the Predicted and Measured Individual Interaction Tones.

Figure 22 depicts the sensitivity of tone SPL sum of interaction noise directivity to the tangential location of the tip vortex. The sum of interaction tones is not influenced by the different values of bt/S , up to the emission angle of 120° . The predictions of the SPL sum agree relatively well with the measured data (accurate within 2 to 5 dB), even though each individual tone prediction was not so good (Figure 21). Figure 22 indicates that the tangential location of the tip vortex has no significant impact on the interaction tone SPL sum. The value of $bt/S = 0.5$ has been used in this report.

3.1.3 Influence of Tip Vortex Trajectory

The influence of the tip vortex trajectory on gust spectra and its consequent influence on the interaction noise were studied by parametrically varying the K_{Vtx} (see Equation 22).

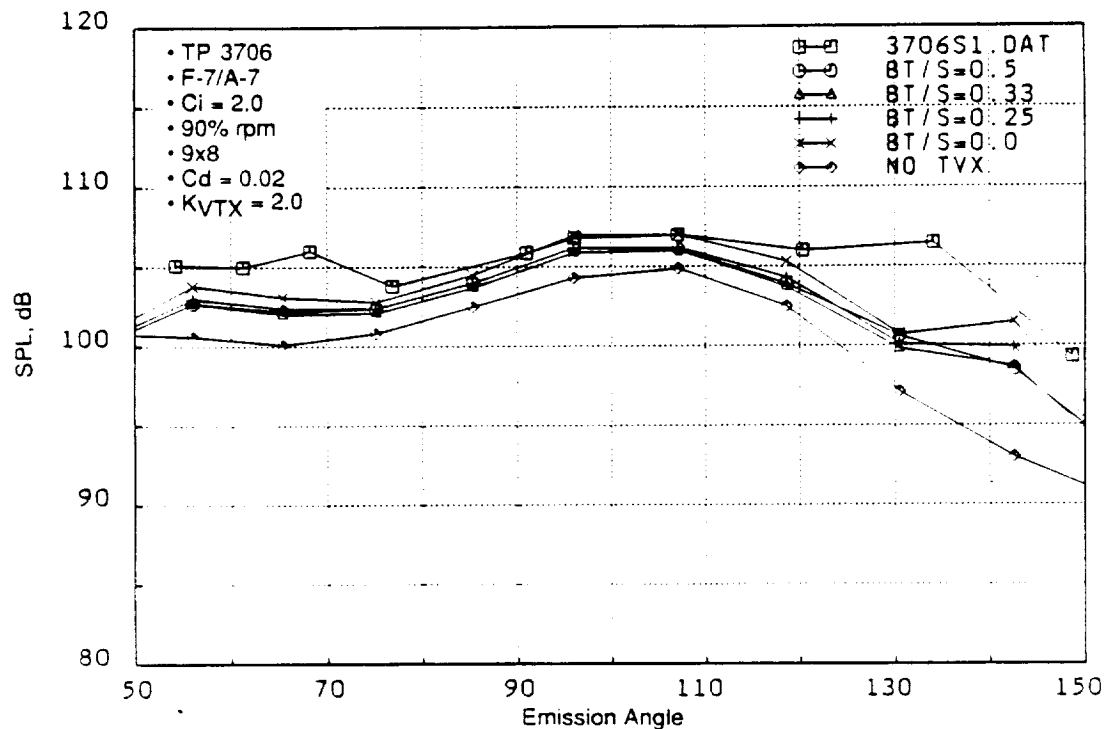


Figure 22. Sensitivity of the Tone SPL Sum of Interaction Noise to the Tangential Location of Tip Vortex.

Figure 23 indicates the predicted influence of the tip vortex trajectory on the gust harmonic spectra at three streamlines in the tip region. As K_{vtx} increases, the tip vortex moves radially inward. At the tip streamline, the gust harmonic spectrum for $K_{vtx} = 0.5$ has the highest levels (compared to $K_{vtx} = 1$ and 2), since the tip vortex for $K_{vtx} = 0.5$ is closest to the tip streamline. For the 89.1% streamline, the gust harmonic spectrum for $K_{vtx} = 1$ has the highest levels compared to $K_{vtx} = 0.5$ and 2, since the 89.1% streamline is closer to the tip vortex point of impact when $K_{vtx} = 1$. However, for the 70.1% streamline, gust spectrum levels for $K_{vtx} = 0.5$ and 1 are about same. This indicates the tip vortex effects induced by $K_{vtx} = 0.5$ and 1 are minor at this streamline location. The gust spectrum levels for $K_{vtx} = 2$ are quite different from others. The noted relative dominance of even-numbered gust harmonics over odd-numbered gust harmonics is due to the fact that the tangential location of the tip vortex is at the midpassage.

Figure 24 shows the influence of the tip vortex trajectory on each individual interaction tone at an observer angle of 91° along with the data. Apparently, the sensitivity of K_{vtx} on the acoustic predictions is insignificant. This probably happens because the gust spectra at different radial locations are enhanced for different values of K_{vtx} . The comparisons between data and predictions indicate that the K_{vtx} values do not improve the accuracy of the model. The differences between the predictions and data (up to 10 dB) are noted in Figure 24.

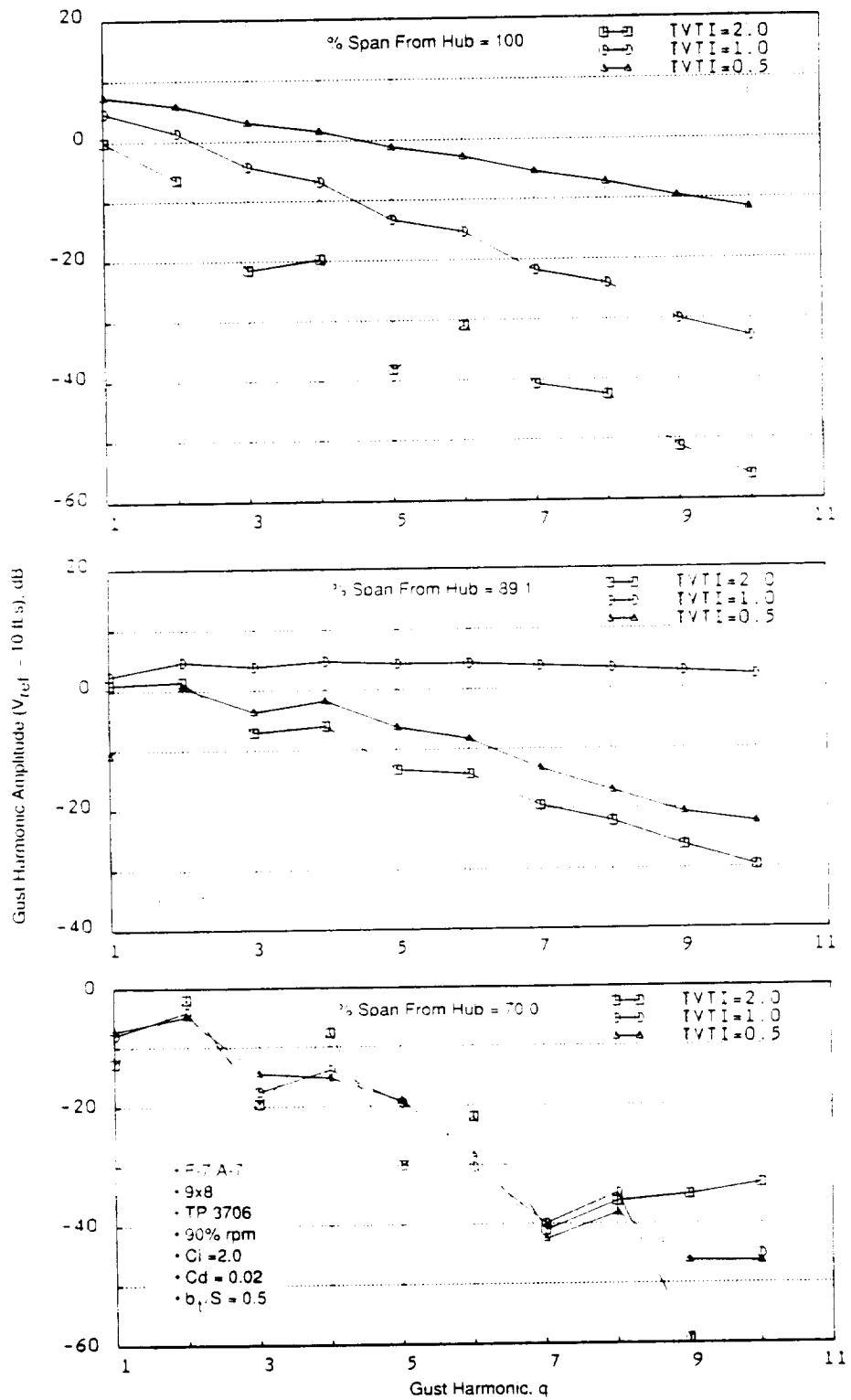


Figure 23. Predicted Influence of the Tip Vortex Trajectory on Gust Harmonic Spectra at Three Streamlines in the Tip Region.

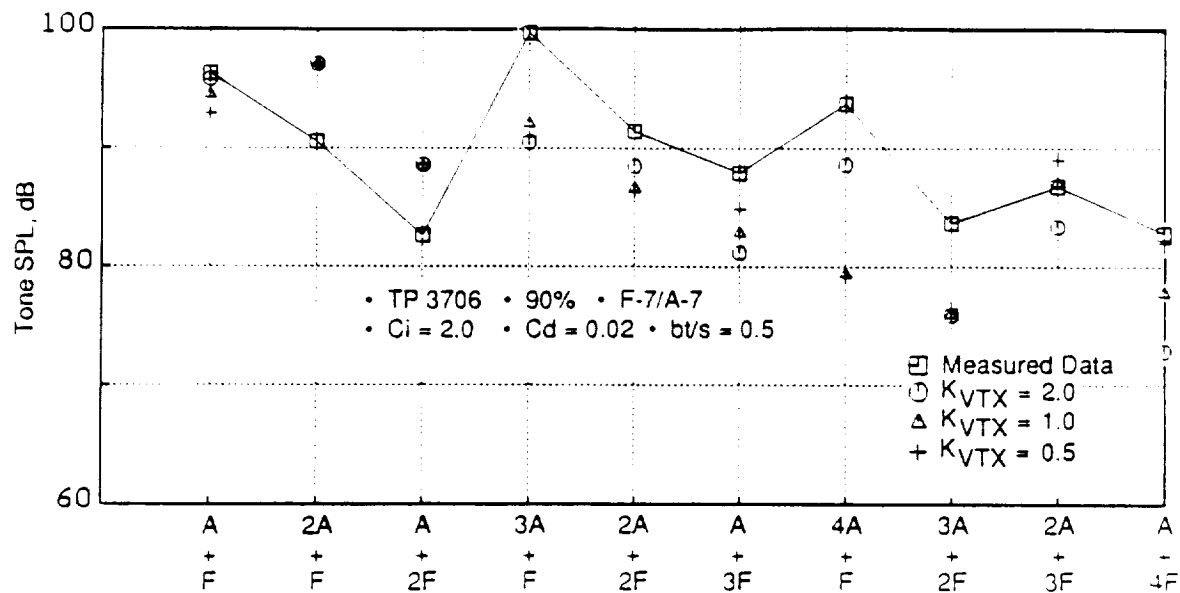


Figure 24. Predicted Influence of Tip Vortex Trajectory on Each Interaction Tone at Observer Angle of 91°.

Figure 25 shows the influence of tip vortex trajectory on the directivity of tone SPL sum of interaction noise. Variations in the tip vortex trajectory do not significantly alter the interaction tone SPL sum; however, the trajectory parameter does significantly affect the interaction noise prediction for the clipped aft rotor blades configuration, as shown in Subsection 3.1.5.

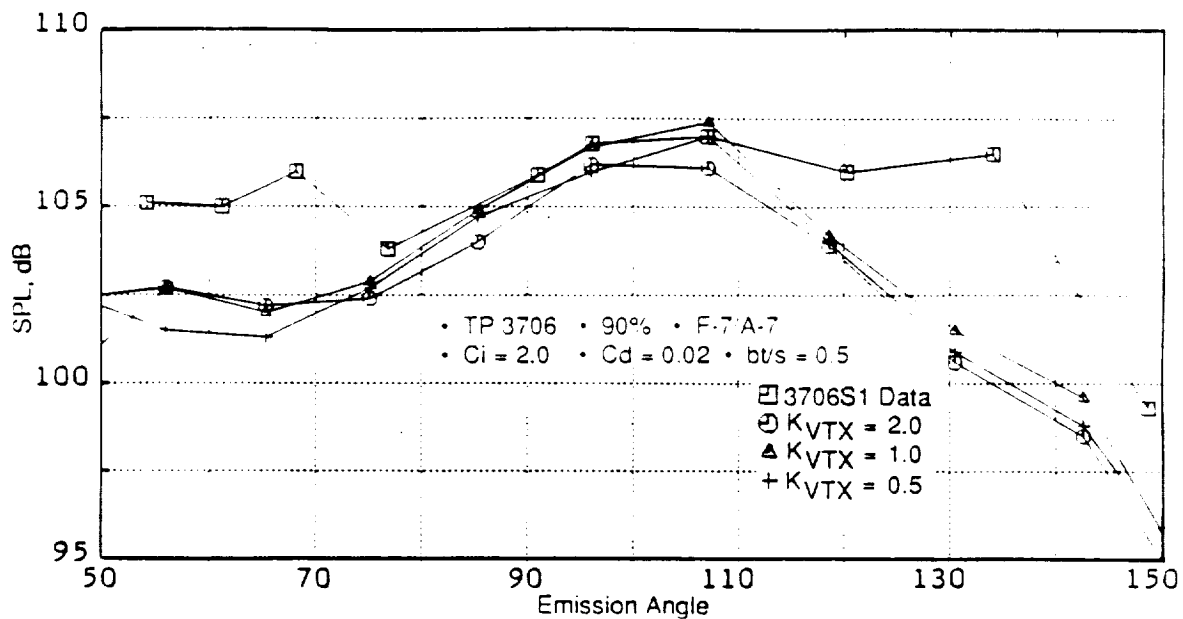


Figure 25. Predicted Influence of Tip Vortex Trajectory on Interaction Noise Tone SPL Sum.

3.1.4 Influence of Decay Rate of Tip Vortex

Also investigated was the influence of the decay rate of the tip vortex on gust harmonics and, thus, on the noise. As discussed in Section 2.2, a power law decay rate was proposed for the circulation of the tip vortex:

$$(\Gamma)_{vtx} \propto \frac{1}{(1 + s/c)^{\eta}} \quad (18)$$

The cycle corresponds to a typical cutback. Figure 26 demonstrates the predicted gust harmonic spectra for tip vortex decaying with different rates at the streamlines of the tip and 70.7% span from the hub. The case of no tip vortices also was included for the sake of comparison. For this study, $K_{vtx} = 2.0$ and $bt/S = 0.5$ are used.

The gust spectral levels for the nondecaying tip vortex are the highest. As the rate of decay increases from 0 to 1/4, to 1/2, the gust spectral levels decrease monotonically.

3.1.5 Influence of Progressive Clipping of Aft Rotor

As discussed in Subsection 3.1.1, the tip vortex is obviously a noise-generating mechanism. Thus, by clipping the aft rotor to minimize interactions between the tip vortex and the aft rotor blades, the interaction noise is reduced. This phenomenon has also been verified from the GE in-house UDF® acoustic data base. The thrust loss due to clipping and the associated required reduction in shp (shaft horsepower) can be made up either by increasing the rpm, or loading of the aft rotor; however in this parametric study, no attempt has been made to recover thrust loss resulting from clipping. This study was conducted with the objective of discovering the sensitivity (relating to the percent clipping of the aft rotor) on noise reductions. Consequently, this study considered four values of percent span clipping (5%, 10%, 15%, and 20%), in addition to 0% and 25% span clippings. Figure 11 presented the planforms of the standard F-7/A-7 and the F-7/A-7 with 25% clipping of span on the aft rotor.

Thrust and shp data are available only at 0% and 25% clippings for $M_\infty = 0.25$. Figure 27 shows the assumed interpolation of the thrust and shp of the aft rotor with the end points (0% and 25% clipping) coinciding with data for the 90% rpm case.

The steady loading and thickness noise and the wake/tip vortex interaction noise occur at distinctly different frequencies for unequal blade number configurations (Figure 12). As illustrated in Figure 12, tones associated with the steady loading and thickness noise were summed on a mean-squared pressure basis; this is also true for the tones associated with the wake/tip vortex interaction noise. Figure 28 demonstrates the predicted effect of progressive clipping of the aft rotor on the sum of steady loading and thickness noise. It is evident that the steady loading and thickness noise reduces uniformly as the percent clipping increases, a reflection of the assumed performance of clipped aft rotor (Figure 27). Predicted effect of the clipping

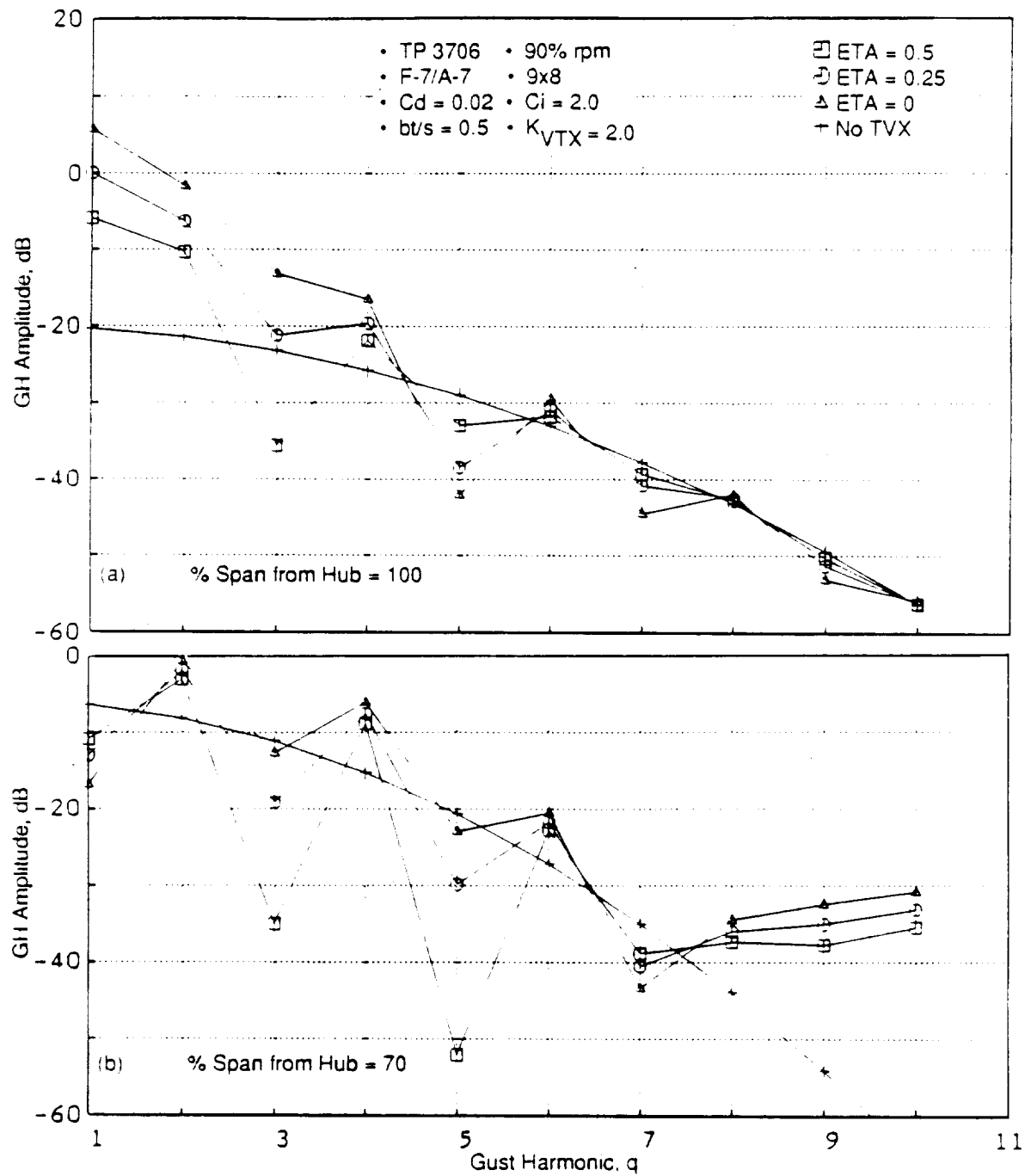


Figure 26. Predicted Gust Harmonic Spectra at Two Rotor-to-Rotor Spacings for the Tip Vortex at Different Decaying Rates and for the Case of No Tip Vortex at Two Streamline Locations.

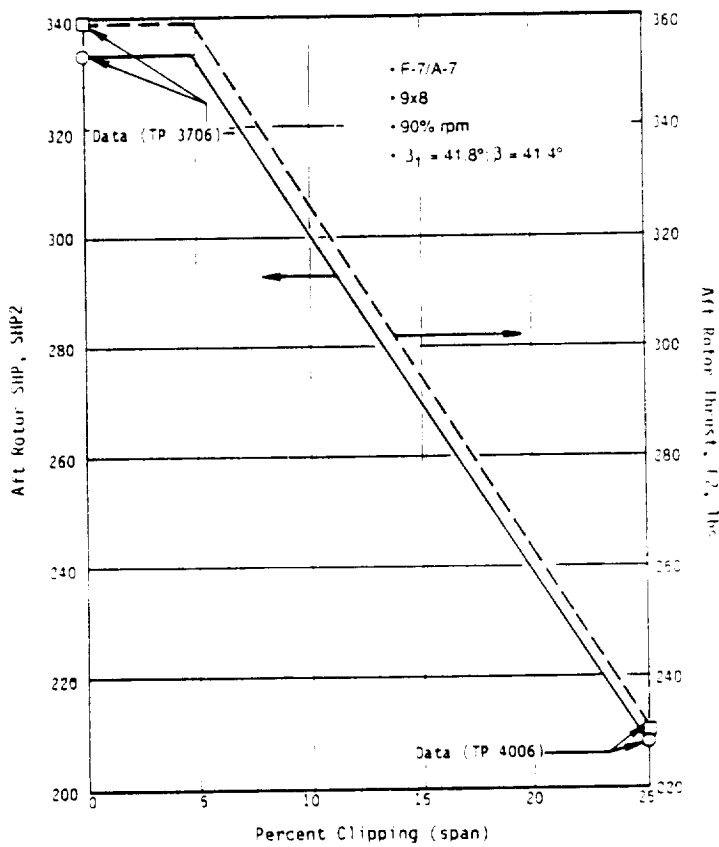


Figure 27. Assumed Performance of the Progressively Clipped Aft Rotor.

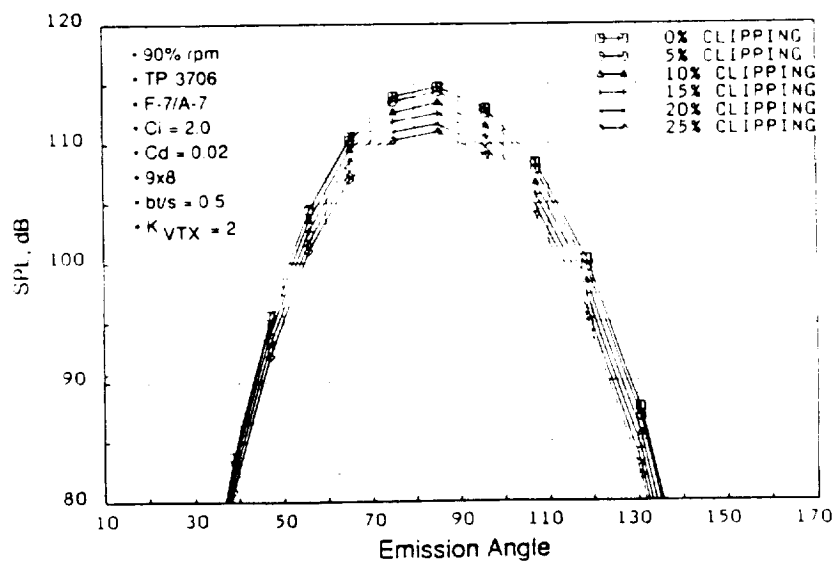


Figure 28. Predicted Effect of Progressive Clipping of the Aft Rotor on the Steady Loading and Thickness Noise.

sensitivity on the interaction tones is portrayed in Figure 29; whereas, the predicted effect on the OASPL (overall sound pressure level) is presented in Figure 30.

As discussed previously, unsteady loading interaction tone predictions depend on many empirical correction parameters. To predict the clipping effect on the interaction noise, the tip vortex strength (C_i) and the tip vortex tangential location (b_{tS}) were fixed at 2.0 and 0.5, respectively. Figure 29 (View A) shows the predicted effect of progressive clipping of the aft rotor on wake/tip vortex interaction noise by using $C_d = 0.02$ and $K_{VTX} = 2.0$. As previously stated (Subsection 3.1.1), the value of $C_d = 0.02$ induces the strong rotor viscous wakes which control the interaction noise generation and reduces the influence of the tip vortex. Since the tip vortex effect is small with a combination of these C_d and K_{VTX} , the clipping effect is also shown as small ($C_d = 0.02$).

On the other hand, View B of Figure 29 shows the significant clipping effect when the drag coefficient is reduced to 0.005 to amplify the effect of the tip vortex. With the value of $K_{VTX} = 2.0$, the tip vortex is located approximately at 17% span from the tip of the aft rotor; thus, a large reduction in interaction noise is obtained by going from 15% to 20% clipping, and there are no reductions for percent clippings less than 15% span, as evidenced in Figure 29, View B.

The predicted clipping effect with $C_d = 0.005$ and $K_{VTX} = 1.0$ is depicted

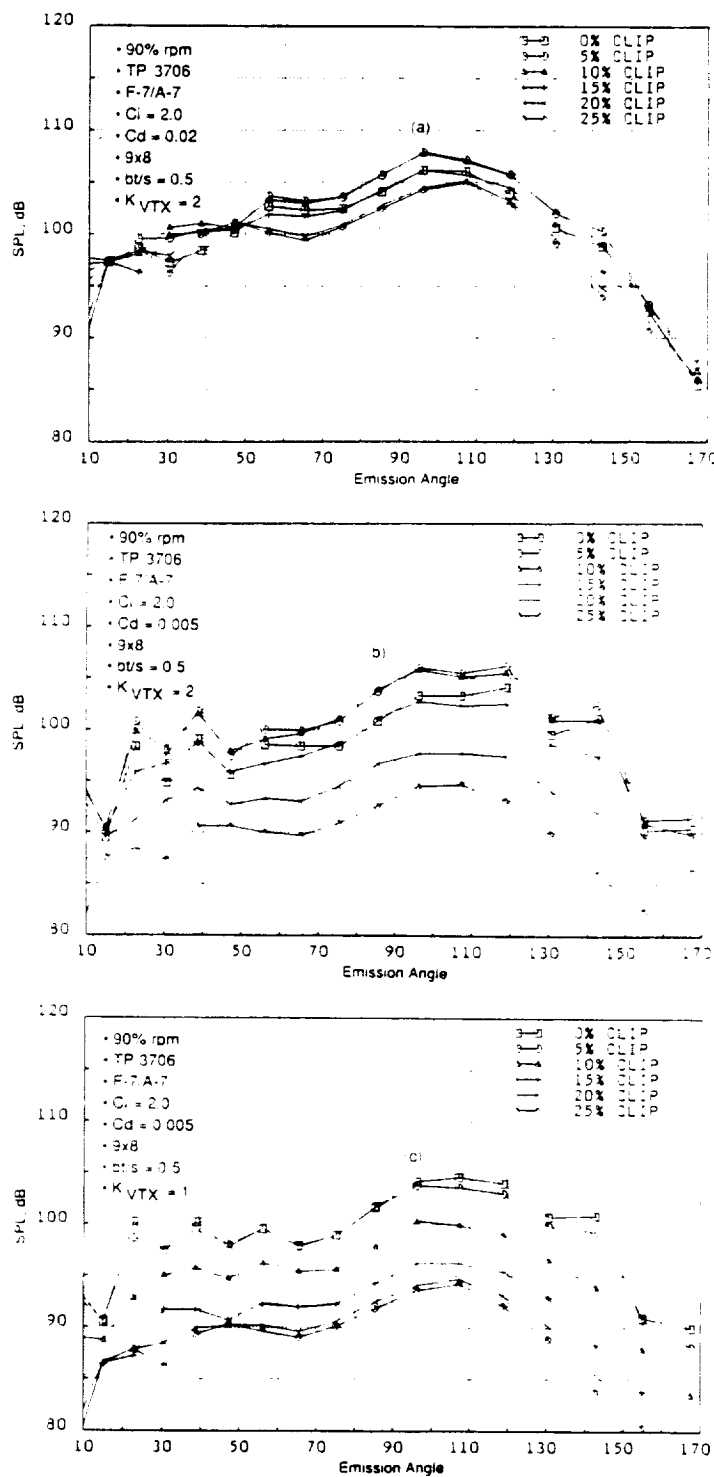


Figure 29. Predicted Effect of Progressive Clipping of the Aft Rotor on the Wake/Tip Vortex Interaction Noise.

ORIGINAL PAGE IS
OF POOR QUALITY

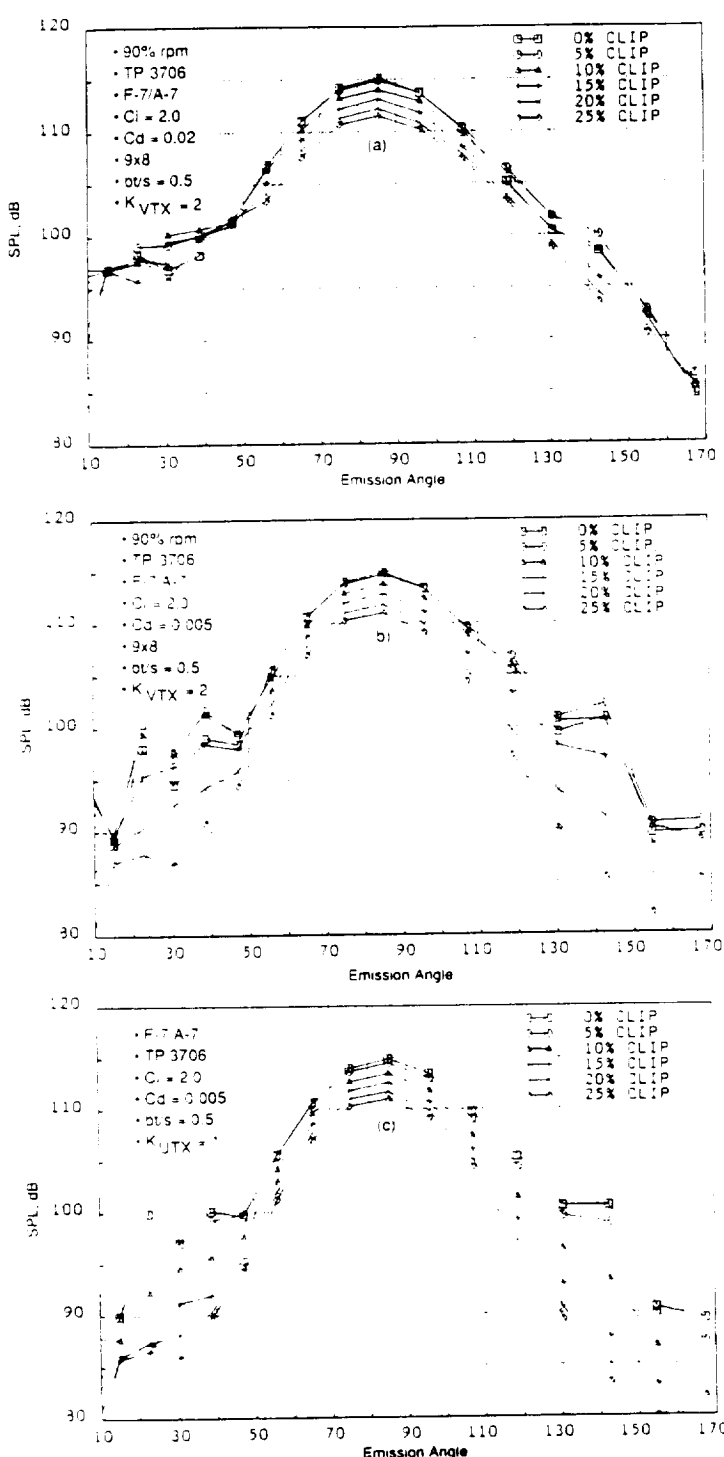


Figure 30. The Predicted Effect of Progressive Clipping of the Aft Rotor on the OASPL Directivity.

in Figure 29 (View C), where the only difference between Views B and C is the reduction of K_{Vtx} (from 2.0 to 1.0). With $K_{Vtx} = 1.0$, the tip vortex center is located at about 8% span; thus, a significant noise reduction is observed with the 10% and 15% clippings. Hardly any noise reduction is noted for clippings less than 5% or greater than 20%, since the influence of the tip vortex is concentrated at approximately 8% span.

Figure 30 (Views A through C) reveals predicted OASPL directivities for the various percent clippings with values of C_d and K_{Vtx} corresponding to those used in Figure 29 (Views A through C, respectively). The OASPL reduction due to the aft rotor clipping is clearly shown, but the magnitudes of reduction are not as significant as those of the interaction noise. This is primarily due to the relatively high levels of the aft rotor steady loading and thickness noise.

This study has demonstrated that the current tip vortex model can be used to predict the interaction noise reduction that can be attained by the clipping of the aft rotor. However, to determine the optimum value for percent clipping of the aft rotor, in terms of noise reductions at a nominal thrust loss, the empirical correction parameters of the current model need more refinements. This effort is currently in progress as part of a GE IR&D project.

3.2 Data - Predictions Evaluation

Systematic data/theory comparisons are performed to evaluate the applicability and limitations of the current tip vortex model. Figure 11 provided a planform of the standard F-7/A-7 blade design, along with the clipped aft rotor. Narrowband acoustic data, measured at Cell 41 for the F-7/A-7 (standard and clipped) blade geometries at a freejet Mach number of 0.25 and an axial distance of 0.2408 between pitch-change axes angle, were used to perform the following comparisons of data and theory. The acoustic data have been transformed from the freejet situation to an equivalent flight situation by accounting for the refraction effect of the freejet shear layer using ray theory, in order that a one-to-one comparison of data and theory can be performed. These comparisons, as discussed below, refer to a 90% rpm case (Test Points 3706 and 4110). Test Point 3706 is for the standard A-7 blade, and Test Point 4110 is for the clipped A-7 blade. For Test Point 4110, the aft pitch angle was opened to recover the thrust loss due to clipping, but the rpm was maintained to be the same for both standard and clipped configurations. Figure 31 identifies the shp and pitch angle data. The narrowband data employed has a bandwidth from 6 Hz to 5 kHz. Since the BPF is at about 1 kHz, the narrowband data contains tones up to about 5 harmonics of BPF.

Figure 31 compares measured and predicted directivities of the tone SPL sum of all of the steady loading and thickness noise for standard and clipped aft rotor blades. The tone SPL sum was obtained by adding only the tones associated with the steady loading and thickness noise of the forward and aft rotors on a mean-squared pressure basis. The measured reduction in steady loading noise due to the clipping of the aft rotor is well predicted; the directivities also are in relatively good agreement. Figure 32 compares the measured and predicted steady loading and thickness tones for standard and clipped aft rotor at an observer angle of 105°. The measured and predicted reductions in tone levels of the aft rotor BPF and its harmonics, indicated by 1A and 2A, due to clipping are in good agreement. The measured and predicted tone levels of the forward rotor BPF and its harmonics (denoted by 1F, 2F, and 3F) are also in good agreement. Actual tone data reveal a slower falloff with an increase in harmonics, as compared to the predictions; this may indicate the presence of some inflow distortion into the rotors.

Figures 33 through 36 compare the predicted and measured tone SPL sum for wake/tip vortex interaction noise for unclipped and clipped aft rotor cases. As previously discussed, the interaction tone predictions are sensitive to the empirical constants utilized in the tip vortex model. Therefore, several sets of the empirical constants are tested in the following data/theory comparisons and are specified in each figure. The term "no tip vortex" in the figures indicates that the tip vortex model was turned off for the specific predictions and that, these interaction tones are induced only by the forward rotor viscous wakes. The tone SPL sum was obtained (as in the case of steady loading and thickness noise) by adding all of the interaction noise tones on a mean-squared pressure basis.

The predictions presented in Figure 33 were performed using the empirical constants of $C_d = 0.02$, $C_i = 2$, $K_{vtx} = 2.0$, and $bt/S = 0.5$ for the tip vortex model. As discussed, the value of $C_d = 0.02$ produces such strong viscous wakes that the tip vortex effect is masked. However,

ORIGINAL PAGE
OF POOR QUALITY

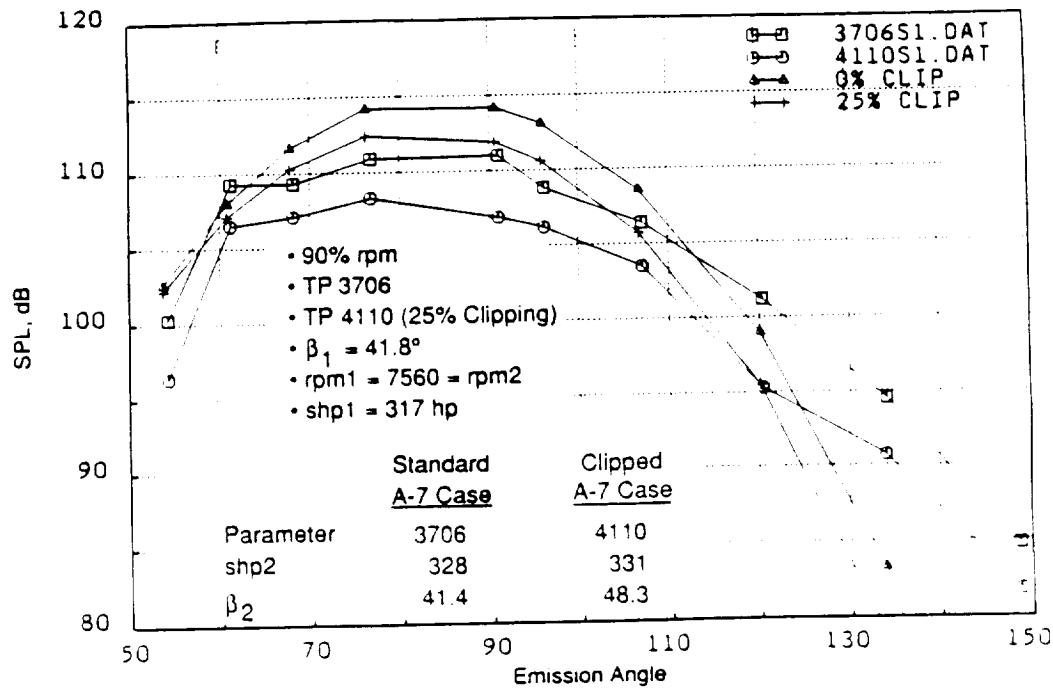


Figure 31. Comparison of the Measured and Predicted Effect of Clipping of the Aft Rotor on Steady Loading and Thickness Noise.

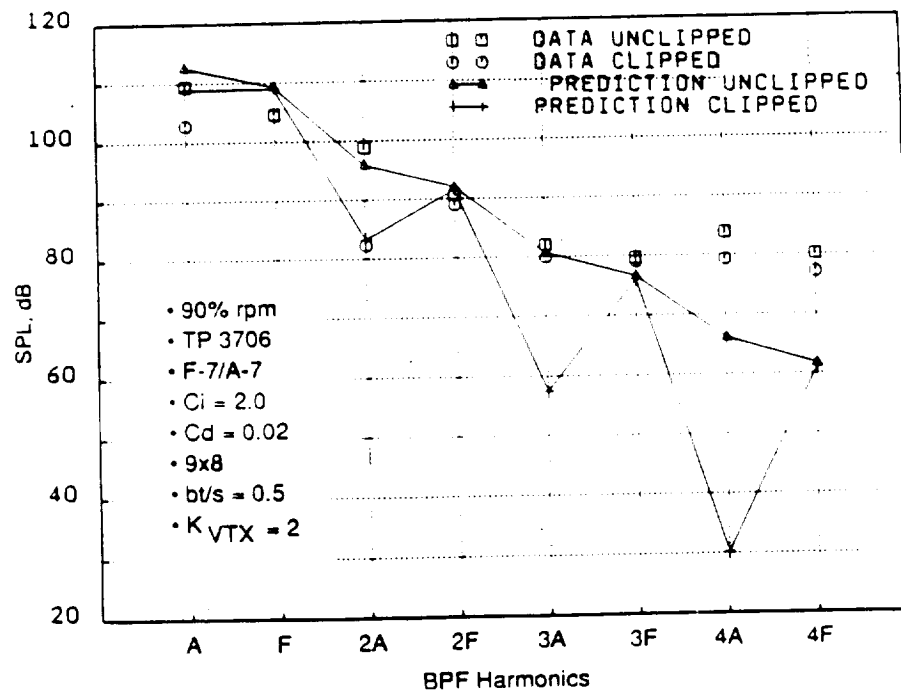
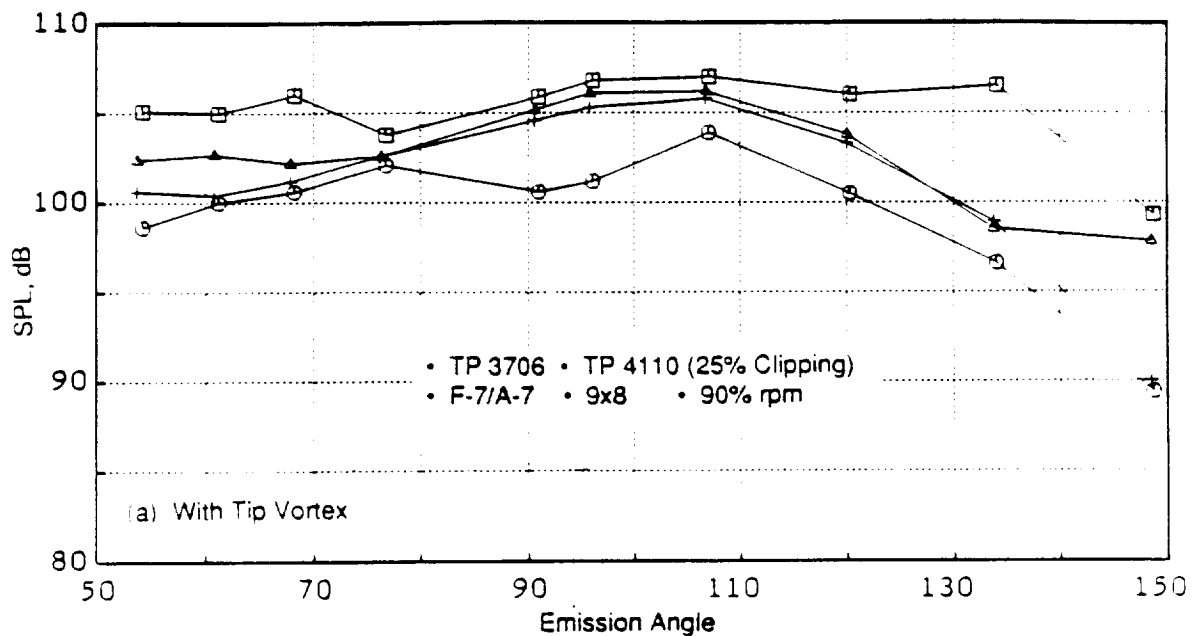


Figure 32. Comparison of the Measured and Predicted Steady Loading and Thickness Tones for Standard and Clipped Aft Rotor at 105° Observer Angle.



(a) With Tip Vortex

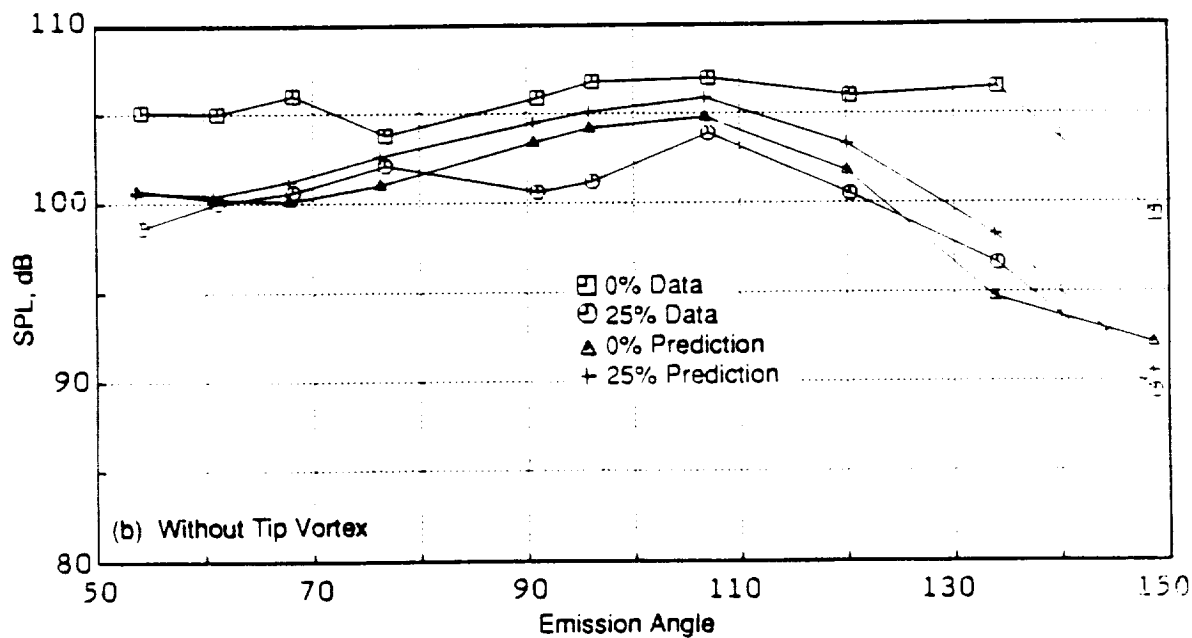


Figure 33. Comparison of the Measured and Predicted Effect of Clipping of the Aft Rotor on Interaction Tone SPL Sum With and Without the Tip Vortex Model ($C_d = 0.02$, $C_1 = 2$, $K_{VIX} = 2.0$, $bt/S = 0.5$).

ORIGINAL PREDICTION
OF POOR QUALITY

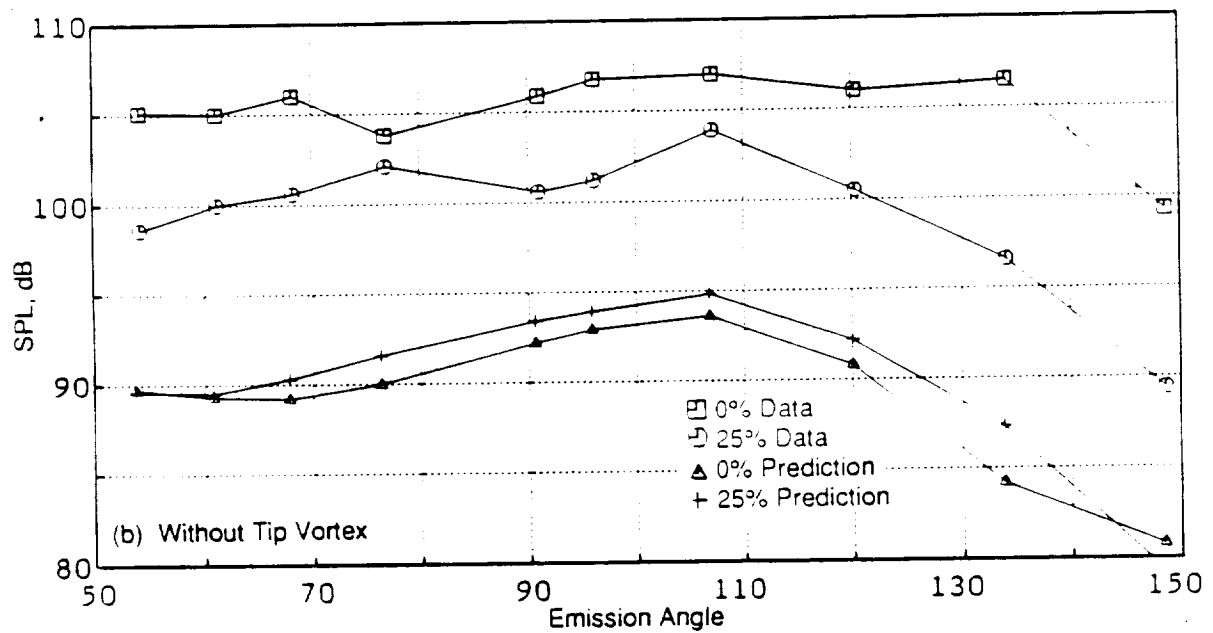
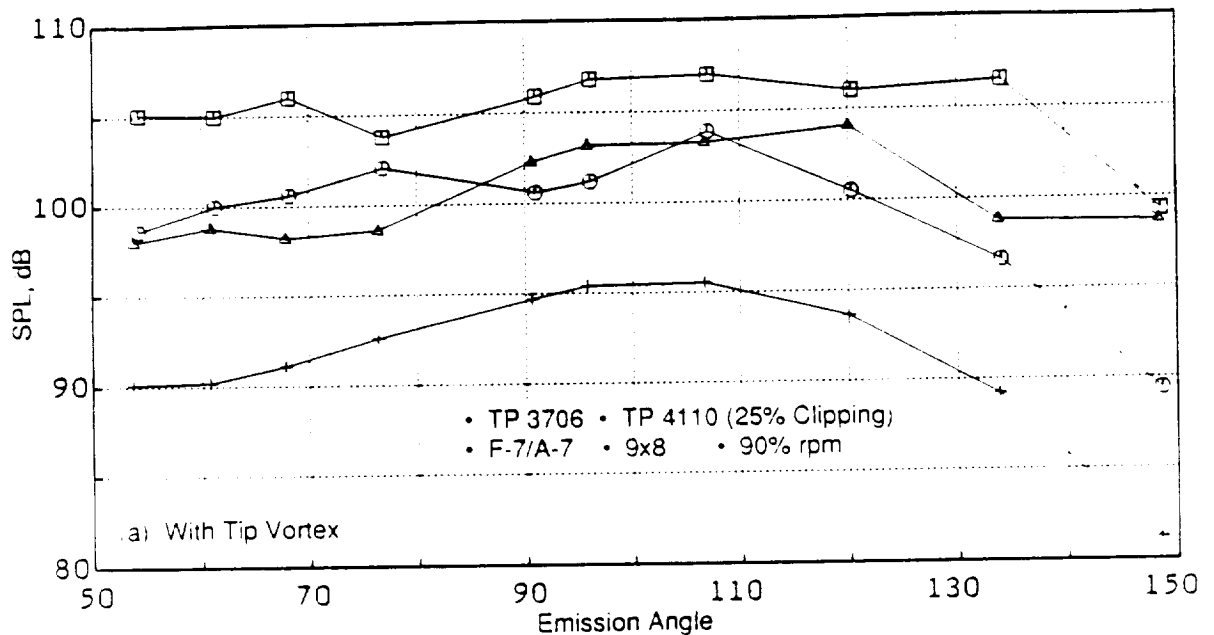
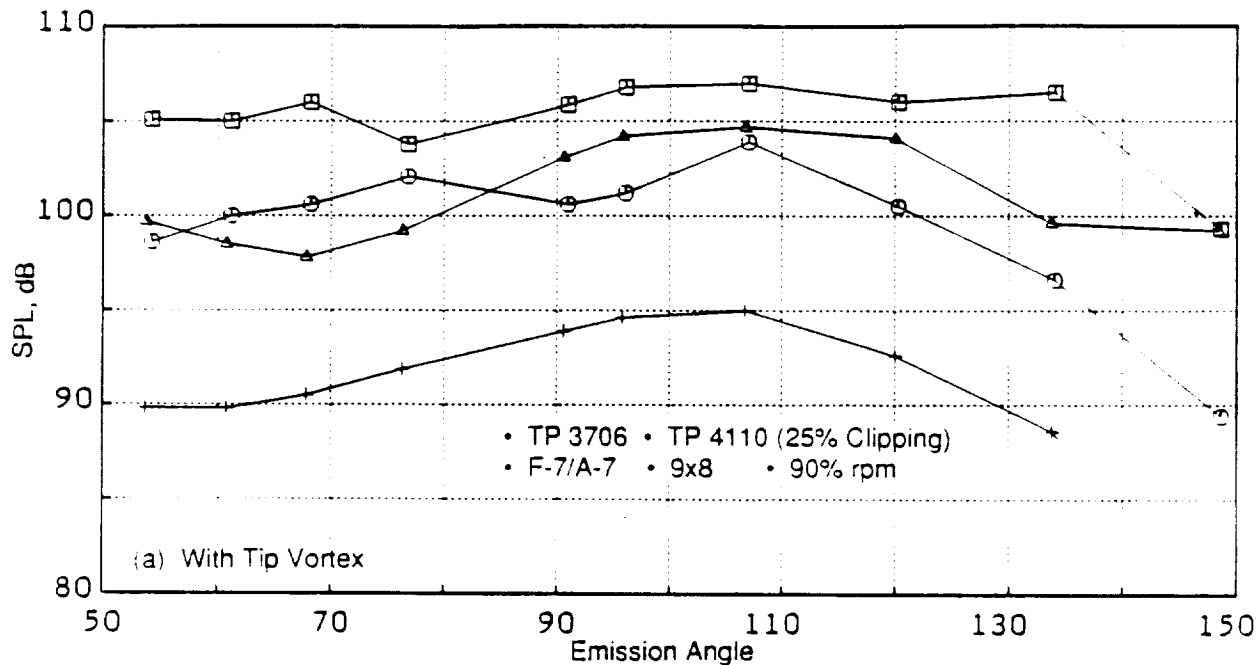
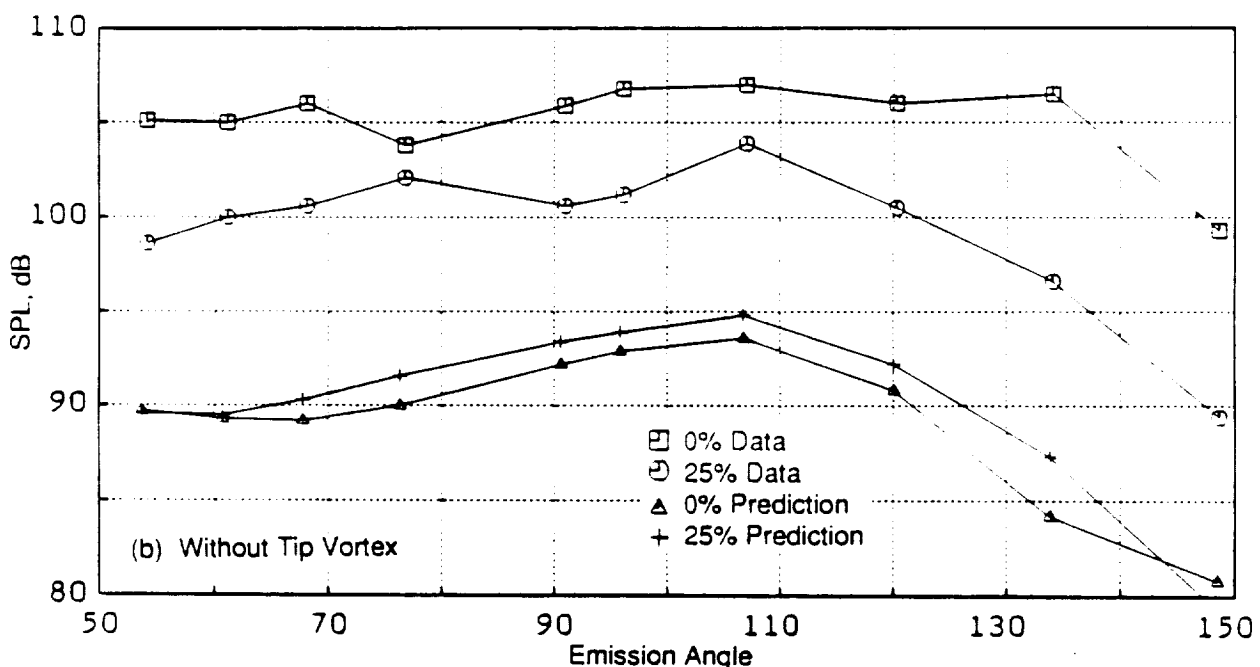


Figure 34. Comparison of the Effect (Measured and Predicted) of Clipping of the Aft Rotor on Interaction Tone SPL Sum With and Without the Tip Vortex Model ($C_d = 0.005$, $C_t = 2$, $K_{Vtx} = 2.0$, $bt/S = 0.5$).



(a) With Tip Vortex



(b) Without Tip Vortex

Figure 35. A Comparison of the Measured and Predicted Effect of the Clipping of the Aft Rotor on Interaction Tone Sum With and Without the Tip Vortex Model ($C_d = 0.005$, $C_r = 1$, $K_{VX} = 2.0$, $\text{bt/S} = 0.5$).

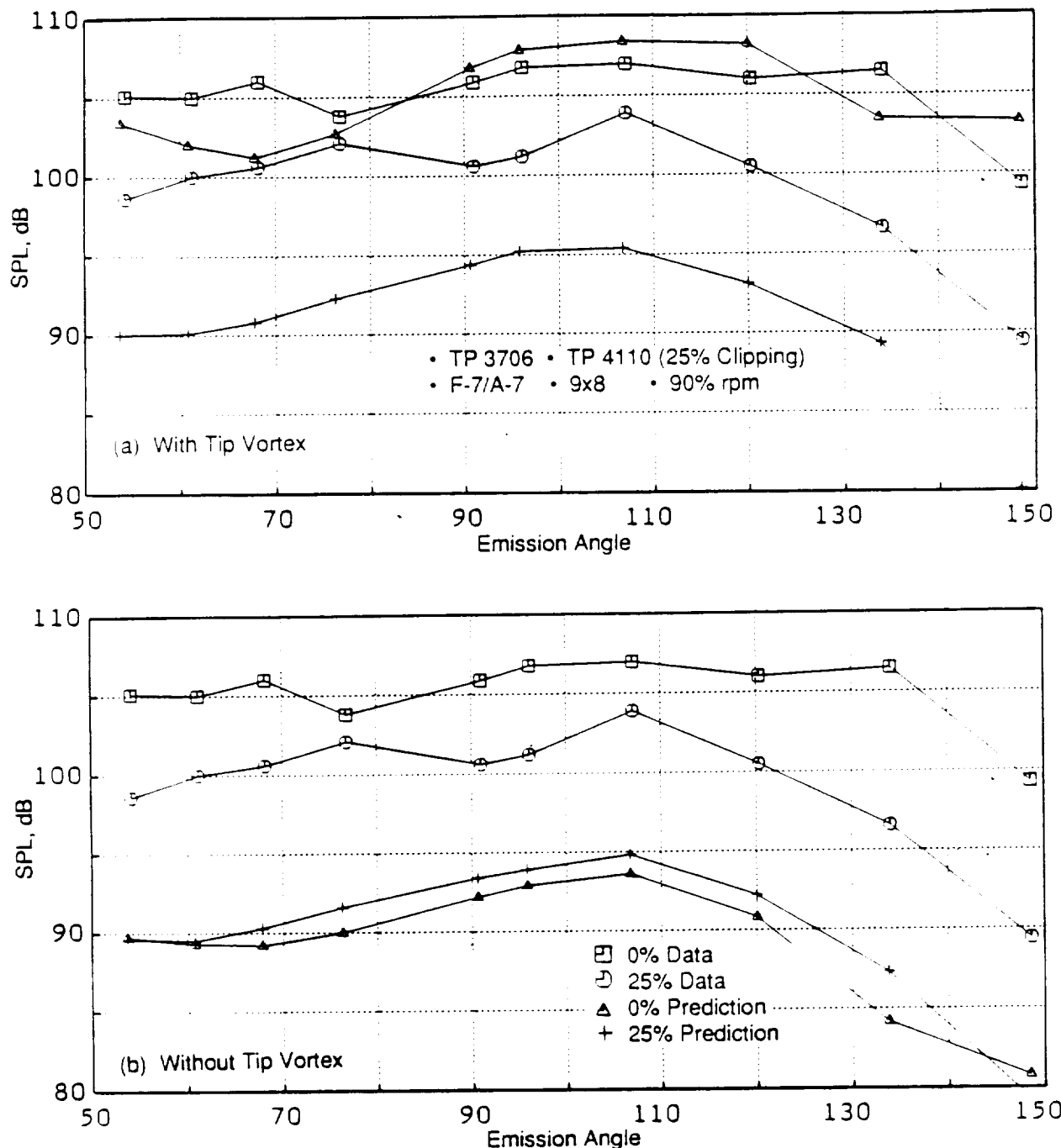


Figure 36. A Measured and Predicted Effect Comparison of Clipping of the Aft Rotor on Interaction Tone Sum With and Without the Tip Vortex Model ($C_d = 0.005$, $C_1 = 3$, $K_{VIT} = 2.0$, $bt/S = 0.5$).

the predictions with no tip vortex indicate that the clipping blade increases the interaction tone sum, which contradicts the data. The predictions in Figure 34 are performed with a C_d of 0.005; results indicate the accurate predictions of the clipping effect, but with the underpredictions of the SPL. Without the tip vortex model, Figure 34 shows that predictions for both the standard and clipped blades are underpredicted and that, the interaction tone noise is still higher for the clipped case than for the standard case. The Figure 35 predictions are performed with the same empirical parameters as in Figure 34, except that the tip vortex value is reduced from 2.0 to 1.0, in order to locate the tip vortex center closer to the tip of the standard blade. As a result, the prediction for the standard blade agrees relatively well with the data, but the clipped blade is still underpredicted. Finally, Figure 36 presents the predictions made with the same empirical constants used in Figure 35, except C_i is increased to 3.0. With this set of parameters, the data/theory comparisons show good predictions for the standard aft blade configuration; however, the inaccurate prediction of the clipped blades was still present. Since predictions with no tip vortex are not affected by the K_{vtx} and C_i values, the no tip vortex comparisons in Figures 34 through 36 are identical to each other.

Next, data and theory comparisons of the individual interaction tone directivity contained within the interaction tone sum of Figure 36 are examined utilizing the empirical constants of $C_d = 0.005$, $C_i = 3$, $K_{vtx} = 1$ and $bt/S = 0.5$. Figure 37 compares predicted and actual data for 1A + 1F, 2A + 1F, 1A + 3F, 2A + 2F and 3A + 1F interaction tones (Table 1 identifies these interaction tones), both with and without the tip vortex model. For each interaction tone, the predicted ΔdB between standard and clipped aft rotors is in better agreement with the data for cases with tip vortex influence, as compared to those without tip vortex. Note that predictions for the clipped aft rotor (with or without the tip vortex model) have altered only slightly. However for most individual interaction tones, the predictions for the standard aft rotor with the tip vortex model have increased, relative to those without the tip vortex model. In general, it is obvious that the current acoustic prediction model including viscous wake/tip vortex model can not predict accurate individual interaction tones, even though (as demonstrated in Figures 33 through 36) the interaction tone sum can be well-predicted.

To examine the effect of the rotor viscous wake alone, Figure 38 demonstrates the predicted spanwise variation of the streamwise distance per chord, normalized wake centerline defect, and the semiwake width for Test Point 3706, with the C_d values of 0.02 and 0.005. This figure does not contain the tip vortex effect. It is seen that due to relatively large s/c values in the tip region, the wake has decayed much more (compared to the hub region). The semiwake width determines the shape of the gust harmonic spectra, and the wake centerline defect determines the amplitude of the gust spectra (Reference 3). The harmonic falloff rate increases as the semiwake width increases. The amplitude of the gust spectra increases with a corresponding increase in the wake centerline defect. Due to the deeper (larger values of the wake centerline defect) and the narrower (smaller values of semiwake width) wakes in the hub region, compared to the tip region, the gust harmonic levels that are due to wake alone are much higher in the hub region than in the tip region. Therefore, the contribution of the wakes from the outer 25% span in the tip region probably is not a significant contribution to the total interaction noise. Accordingly, the outer 25% span of the aft rotor was clipped; the total interaction

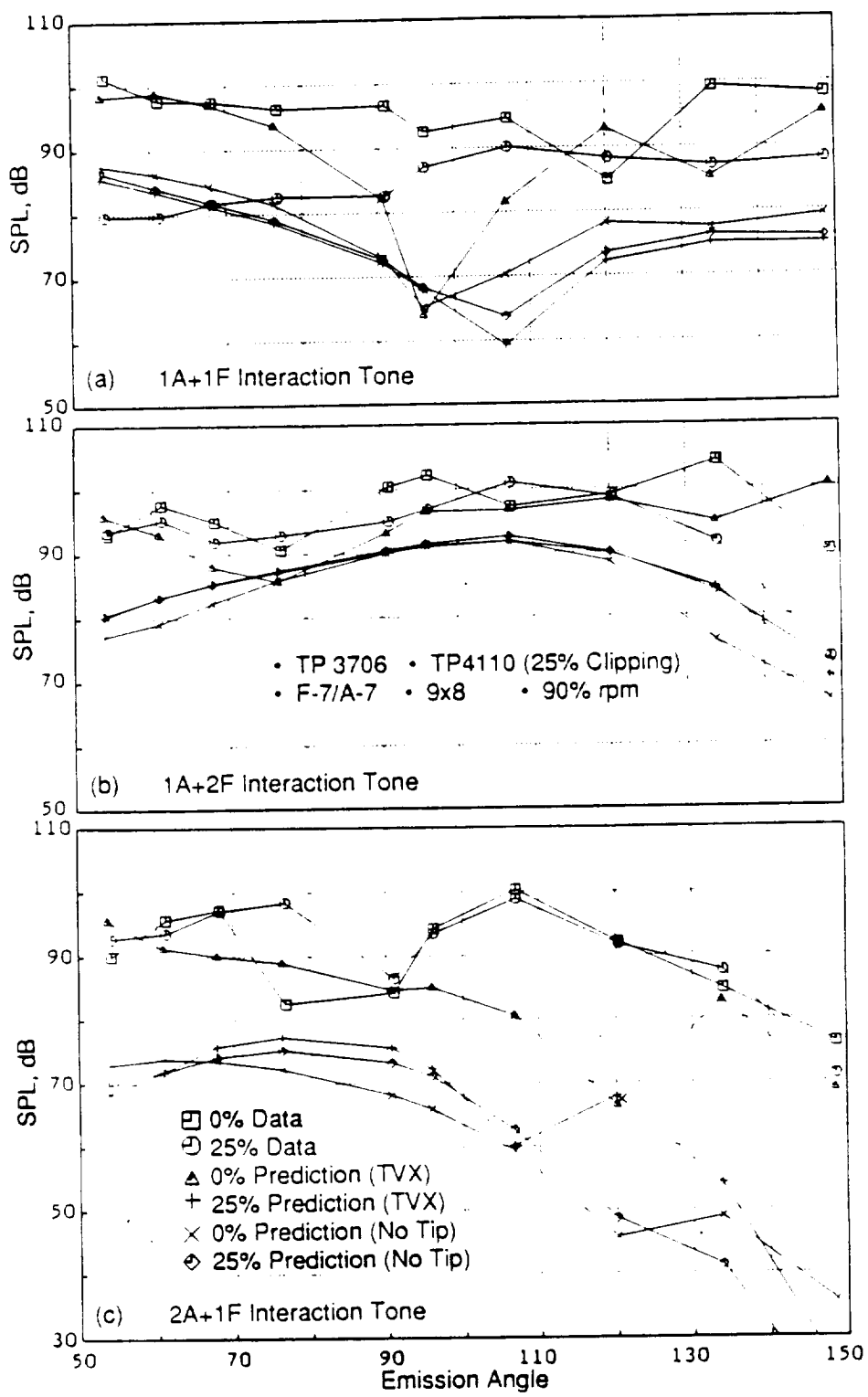


Figure 37. Comparison of the Measured and Predicted Effect of Clipping of the Aft Rotor on Individual Interaction Tones, With and Without the Tip Vortex Model ($C_d = 0.005$, $C_t = 3$, $K_{TVX} = 1.0$, $bt/S = 0.5$).

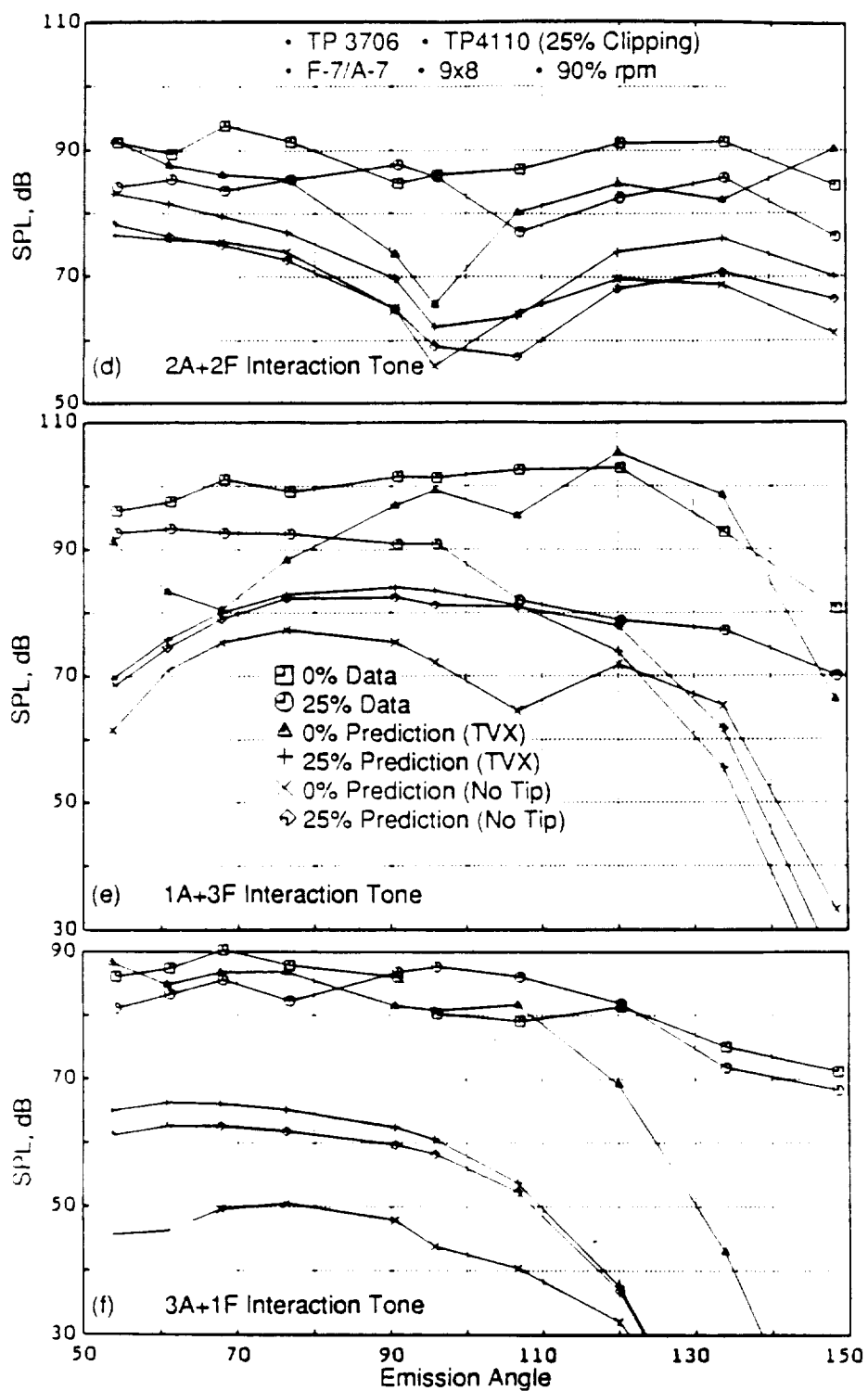


Figure 37. Comparison of the Measured and Predicted Effect of Clipping of the Alt Rotor on Individual Interaction Tones, With and Without the Tip Vortex Model ($C_d = 0.005$, $C_t = 3$, $K_{TV} = 1.0$, $bt/S = 0.5$), Concluded.

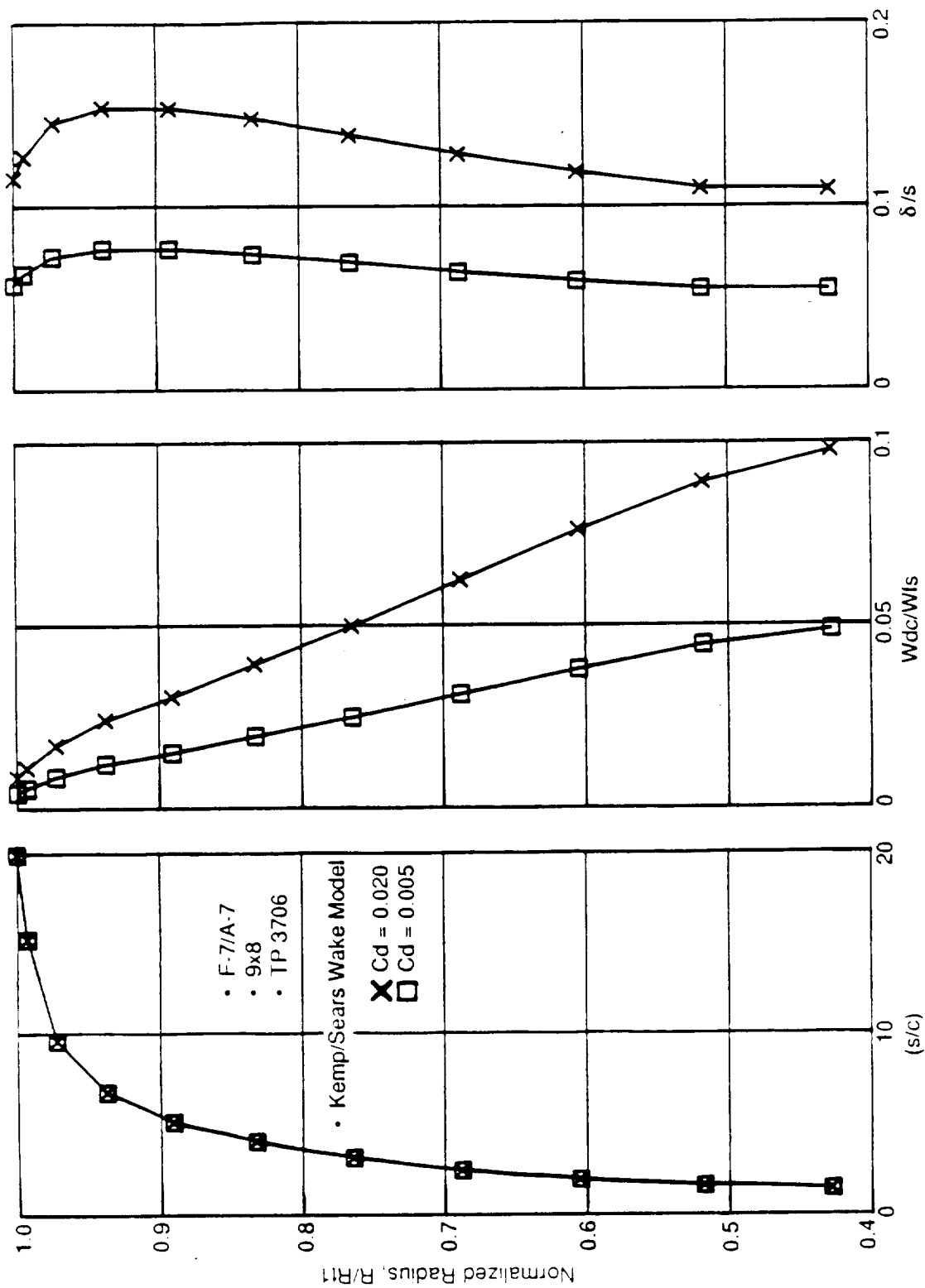


Figure 38. The Predicted Spanwise Variation of Normalized Streamwise Distance, Wake Centerline Defect, and Semiwake Width.

noise is not predicted to be much different from the standard blade case (for the wake alone model).

A set of data and theory comparisons also were generated for 80% rpm for standard (Test Point 3704) and clipped (Test Point 4104) aft rotor blades. Aeroperformance data for these two test points are contained in Figure 39, where the pitch angle of the clipped aft rotor is opened more (than that of the standard aft rotor) to recover performance loss caused by the clipping. Figure 39 compares the measured and predicted directivities of the tone SPL sum of steady loading and thickness noise for standard and clipped aft rotor configurations. As in the case of 90% rpm (Figure 31), the predicted reduction in steady loading and thickness noise due to clipping of the aft rotor is in relatively good agreement with the data.

Figure 40 compares measured and predicted effects of clipping of the aft rotor on interaction tone SPL sum, with and without tip vortex model. The predictions are performed with the empirical constants of $C_d = 0.005$, $C_i = 3$, $K_{vtx} = 1$, $bt/S = 0.5$, as in Figure 36 of the 90% rpm case. As in the case of 90% rpm (Figures 33 through 36), when the tip vortex model is included in the predictions, the predicted ΔdB between standard and clipped aft rotor is in better agreement with the data, as compared to those where the tip vortex model is not included. The predicted ΔdB with the tip vortex model between standard and clipped aft rotor, however, is greater than the measured ΔdB . Since the C_i (or strength) of the tip vortex is computed based on the average lift coefficient over the outboard 30% of the span in the current model (Section 2.2), the strength of the tip vortex is reduced at lower rpm; hence, the prediction at 80% rpm (due to clipping) is seen as lower than that predicted at 90% rpm. The measured ΔdB due to clipping at 80% rpm is seen as greater than that at 90% rpm (Figures 36 and 40). Hence, the predicted change (with the tip vortex model) of the effect of clipping with rpm contradicts other data with this particular set of empirical constants.

Figure 41 summarizes the comparisons for the measured and predicted effect of clipping of the aft rotor on 1A + 1F, 2A + 1F, 1A + 2F, 3A + 1F, 2A + 2F, and 1A + 3F interaction tones at 80% rpm, with and without tip vortex. Figure 41 indicates that predictions for the standard aft blade are in relatively good agreement with the data using the tip vortex model, although data/theory comparisons for the clipped blade need improvement. In general, the predicted ΔdB (due to clipping of the aft rotor) when the tip vortex model is included is still in better agreement with the data, as compared to those predictions not including the tip vortex model.

These comparisons of data and theory show that the current model can be utilized to investigate the noise characteristics of the UDF® blade configuration and can, eventually, become a useful design tool when the empirical constants used in the present model will be determined accurately from well-controlled experimental studies.

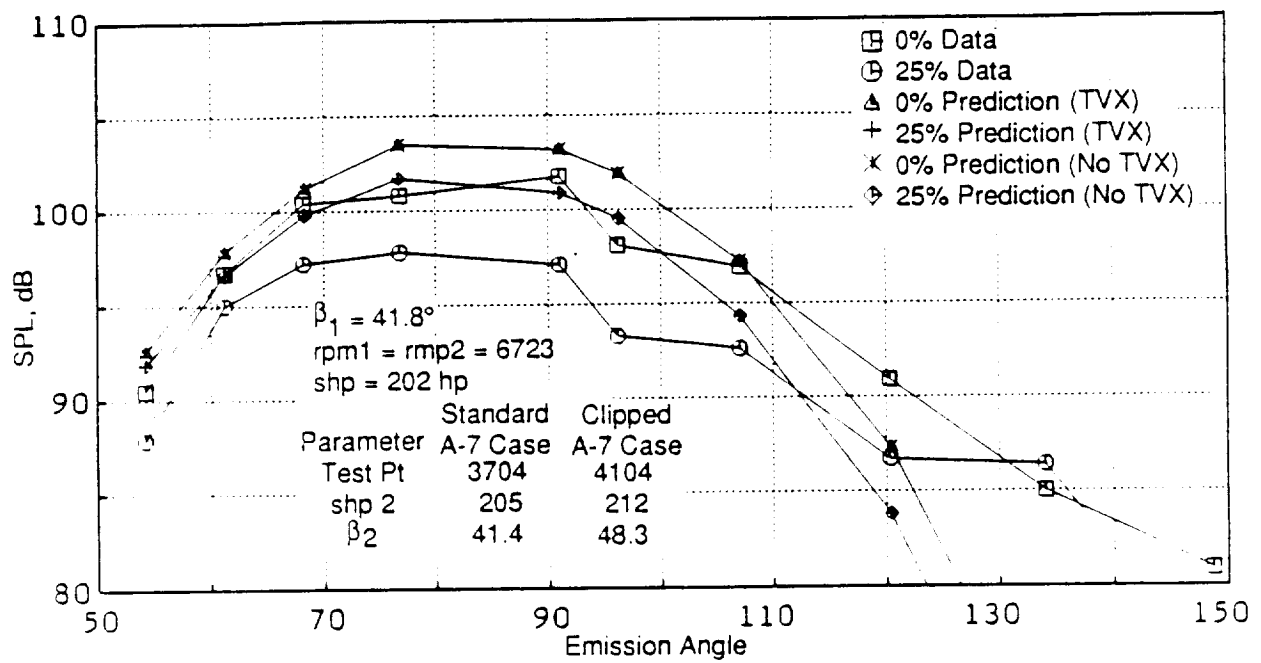


Figure 39. Comparison of the Measured and Predicted Effect of Clipping of the Aft Rotor on Steady Loading and Thickness Noise for 80% rpm.

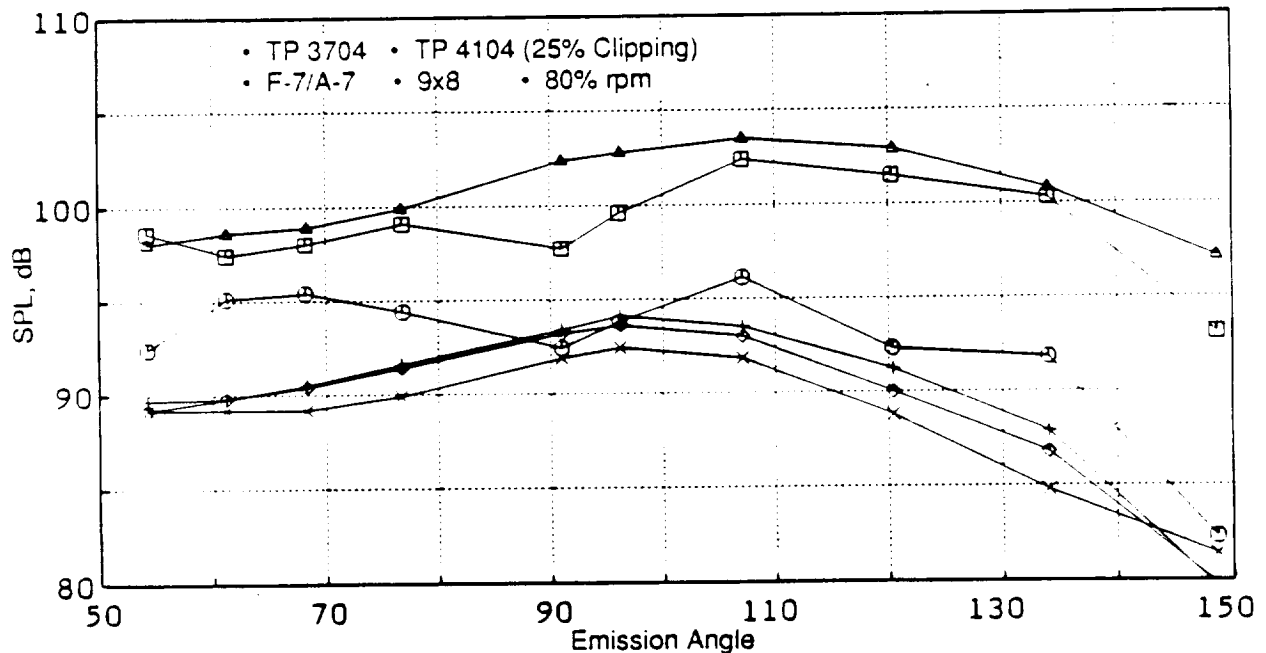


Figure 40. Measured and Predicted Effect of Clipping of the Aft Rotor on Interaction Tone SPL Sum With and Without the Tip Vortex Model ($C_D = 0.005$, $C_L = 3$, $K_{TVX} = 1.0$, $bT/S = 0.5$).

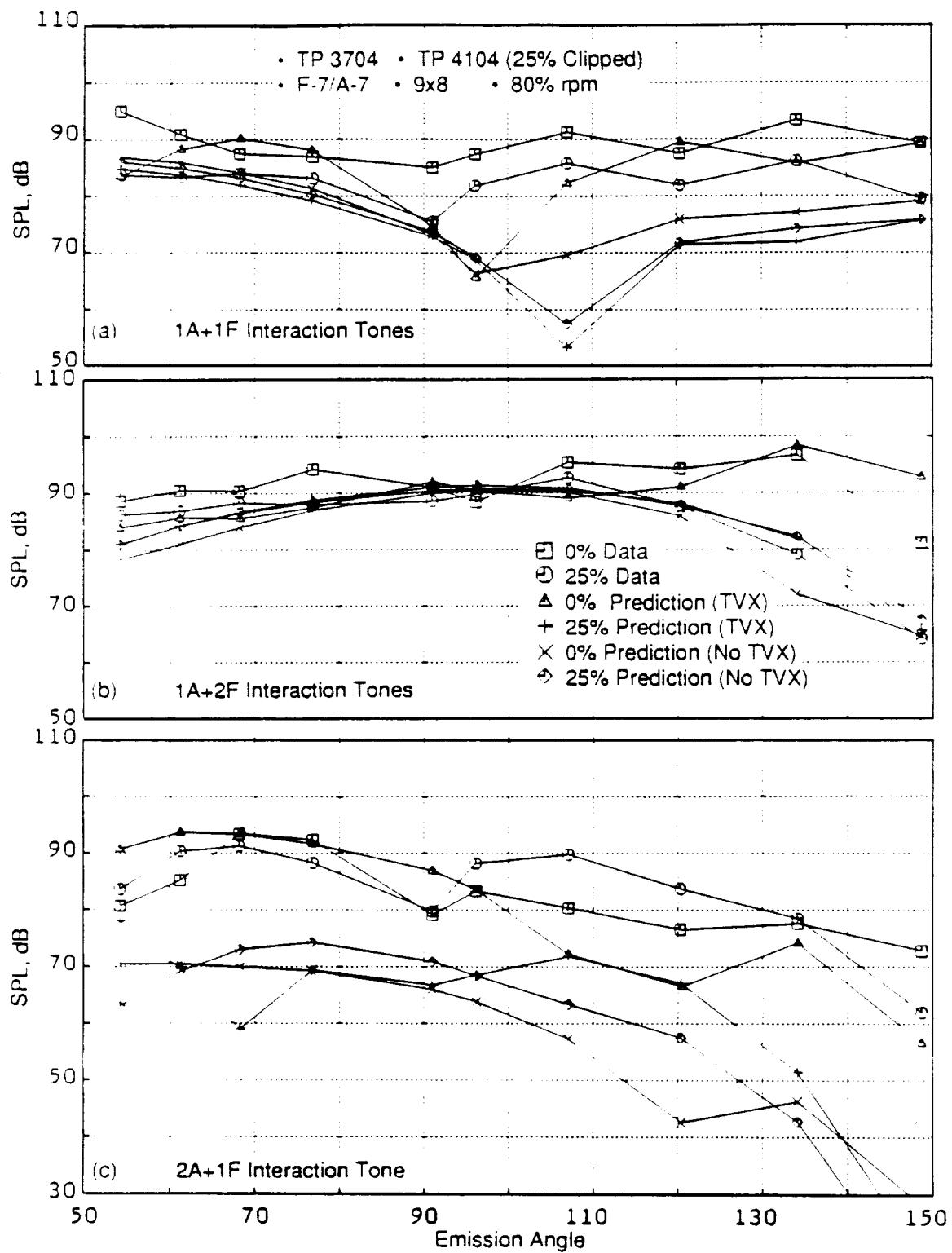


Figure 41. Comparison of the Measured and Predicted Effect of Clipping of the Aft Rotor on Individual Interaction Tones, With and Without the Tip Vortex Model ($C_d = 0.005$, $C_i = 3$, $K_{vtx} = 1$, $\text{bt/S} = 0.5$).

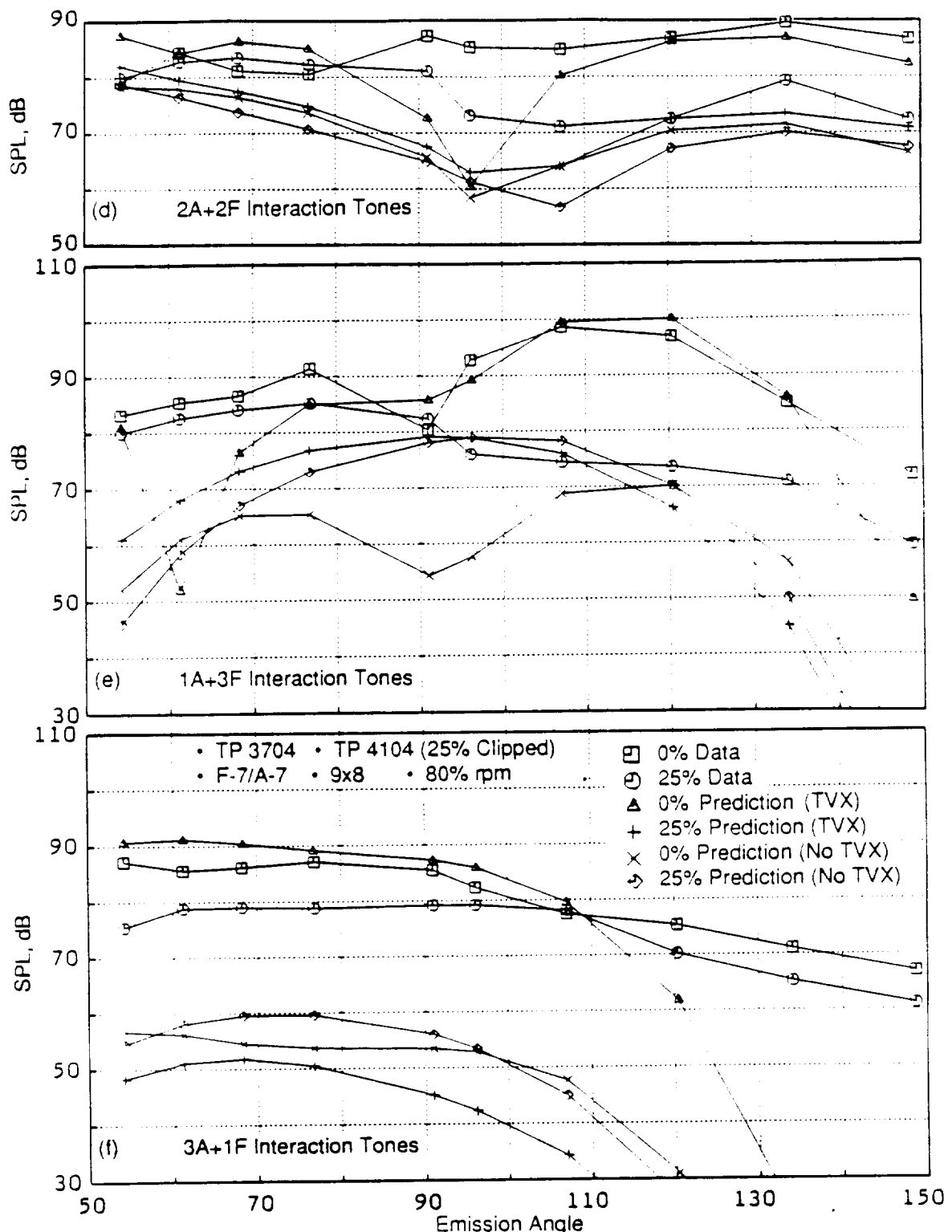


Figure 41. Comparison of the Measured and Predicted Effect of Clipping of the Alt Rotor on Individual Interaction Tones, With and Without the Tip Vortex Model ($C_d = 0.005$, $C_t = 3$, $K_{vtx} = 1$, $bt/S = 0.5$), Concluded.

4.0 Conclusions and Recommendations

This report has documented the analytical modeling, limited data and model prediction comparisons, and certain key parametric studies pertaining to the tip vortex as a part of the noise-source mechanism for unsteady loading noise of counterrotating propellers. The viscous rotor wake effect is also modeled in order to compute the unsteady loading noise. The upwash field created by the combined tip vortex and the viscous rotor wake was analytically modeled employing an approach previously taken for fan tone noise. The strength, size, and streamwise development of the tip vortex are empirically modeled, based on fixed wing and helicopter rotor data. The present work should be considered as a basic frame model containing a number of empirical constants. These constants cannot be defined accurately at the present time, due to insufficient aerodynamics data for the UDF® blades configurations. However, the model has been structured in such a manner that it can be improved and refined with minor modifications when detailed UDF® aerodynamics data become available. Some of the significant conclusions and recommendations for future work are presented in the following sections.

4.1 Conclusions

The following significant conclusions are a product of the above-described analyses:

- The measured reduction in interaction noise due to clipping of the aft rotor is very well predicted by the tip vortex model; however, the wake-alone model (that is, without the tip vortex) could not predict the measured reduction in interaction noise due to clipping.
- The tangential location of tip vortex affects the gust harmonic spectra which, in turn, has a relatively small bearing on the interaction noise (an average of 5 dB). The influence of the bt/S value on the interaction tones sum predictions is minor.
- Tip vortex trajectory does not have a noticeable impact on the interaction noise for the standard aft blade configuration; however, it controls the effectiveness of the clipping on interaction noise levels for the clipped aft blade configuration.
- The decay rate of the tip vortex has a very significant effect on the noise reduction achievable due to an increase in rotor-to-rotor spacing.
- The section local drag coefficient and the tip vortex strength interact with each other and have a strong influence on the interaction tones.

4.2 Recommendations

Various physical parameters of the tip vortex, such as the tangential location and strength of the tip vortex, had to be extracted from the measured acoustic data. An improved aerodynamic model of the tip vortex would reduce the amount of empiricism in the model. These improvements can be attained either through experimental measurements of flow fields or through flow-field computations.

An axisymmetric model is recommended for the tip vortex (rather than an unwrapped annulus model), due to the significant geometric and aerodynamic radial variations of the blades. Such an approach may require a numerical solution rather than the analytical (closed form) solution that has been possible with the unwrapped annulus or rectilinear array of vortices adopted in the existing model.

In the current tip vortex model, an axial velocity component of the tip vortex has not been considered, which may affect the upwash perturbation velocity as much as the tangential component of the tip vortex.

5.0 References

1. Arndt, W.E., "Propfans Go Full-Scale," *Aerospace America*, pp. 100-103, January 1984.
2. Rauscher, M., "Introduction to Aeronautical Dynamics," John Wiley and Sons, Inc., p. 373, 1953.
3. Majjigi, R.K., and Gliebe, P.R., "Development of a Rotor Wake/Vortex Model," Final Report, Volume I, NASA CR-174849, June 1984.
4. Majjigi, R.K., and Gliebe, P.R., "Development of a Rotor Wake/Vortex Model," User's Manual for Computer Program, Volume II, NASA CR-174850, June 1984.
5. Tangler, J.L., Wohlfeld, R.M., and Miley, S.J., "An Experimental Investigation of Vortex Stability, Tip Shapes, Compressibility, and Noise for Hovering Model Rotors," NASA CR-2305, September 1973.
6. Rorke, J.B., and Wells, C.D., "A Hover Performance Analysis Combining the Strip-Momentum and Prescribed Wake Theories." Proceedings - Third CAL/AVLabs Symposium Aerodynamics of Rotary Wing and V/STOL (vertical/short takeoff and landing) Aircraft, Volume I, Rotor/Propeller Aerodynamics, Rotor Noise, held at Buffalo, New York, June 18 through 20, 1969.
7. Grow, T.L., "Effect of a Wing on its Tip Vortex," *J. Aircraft*, Volume 6, Number 1, pp. 37-41, January/February 1969.
8. Mason, W.H., and Marchman, J.F., III, "The Far-Field Structure of Aircraft Wake Turbulence," *AIAA Paper Number 72-40*, 1972.
9. Sears, W.R., "Some Aspects of Nonstationary Aerofoil Theory," *Journal of Aeronautical Sciences*, Volume 8, pp. 104-118, 1941.
10. Amiet, R.K., "Effects of Compressibility in Unsteady Lift Theories," *Unsteady Aerodynamics* (R.B. Kinney, ed.), Proceedings of a Symposium on Unsteady Aerodynamics, University of Arizona, pp. 631-653, March 18 through 20, 1975.
11. Goldstein, M.E., "Aeroacoustics," McGraw-Hill, New York City, New York, 1976.
12. Johnsen, I.A., et al., editors, "Aerodynamic Design of Axial Flow Compressors," NASA SP-36, 1965.
13. Lakshminarayana, B., "Methods of Predicting the Tip Clearance Effects in Axial Flow Turbomachinery," *ASME Journal of Basic Engineering*, Volume 92, Series D, pp. 467-482, September 1970.

14. Lamb, H., "Hydrodynamics," 6th Edition, Dover Publications, p. 224, New York, 1945.
15. McCormick, B.W., Tangler, J.L., and Sherrieb, H.E., "Structure of Trailing Vortices," J. Aircraft, Volume 5, Number 3, pp. 260-267, May/June, 1968.
16. Donaldson, C., Snedeker, R.S., and Sullivan, R.D., "Calculation of Aircraft Wake Velocity Profiles and Comparison with Experimental Measurements," J. Aircraft, Volume 11, pp. 547-555, September 1974.
17. Kemp, N.H., and Sears, W.R., "The Unsteady Forces due to Viscous Wakes in Turbomachines," Journal of Aeronautic Sciences, Volume 22, Number 7, pp. 478-483, July 1955.

6.0 Nomenclature

a	Radius of the core of the tip vortex
AR	Aspect ratio (span/chord)
b _r	Radial distance of the center of the tip vortex from rotor tip
b _t	Tangential location of the center of the tip vortex in the interblade passage relative to wake centerline
B ₁	Number of blades in the forward rotor
B ₂	Number of blades in the aft rotor
c	Chord
c _a	Axial Chord
C _D	Local section drag coefficient
C _i	Circulation index (Equation 13.1)
C _L	Local section lift coefficient
dBA	A-weighted dB level
D _{tip}	Tip diameter
D _{T1}	Tip diameter of forward rotor
D _{T2}	Tip diameter of aft rotor
f _{s1q}	q^{th} harmonic of steady loading and thickness noise of forward rotor (see Equation 20)
f _{s2r}	r^{th} harmonic of steady loading and thickness noise of aft rotor (see Equation 21)
f _{wqr}	r^{th} harmonic of aft rotor unsteady noise due to q^{th} gust harmonic
HTR	Hub/tip-ratio
K _{vtx}	Empirical constant for tip vortex trajectory (see Equation 19)
M _∞	Aircraft Mach Number

M,N,p	Parameters associated with the tip vortex (see Equations 3-5)
m_{wqr}	Spinning mode number of r^{th} harmonic of aft rotor unsteady noise due to q^{th} gust harmonic of forward rotor
η	Exponent for decay of circulation of tip vortex (see Equation 16)
OASPL	Overall sound pressure level
PNL	Perceived noise level
q	Gust harmonic
R	Radius
r	Radial distance from center of vortex core
R_{hub}	Hub radius
R_{tip}	Tip radius
R_{vtx}	Radial location of tip vortex
R_{T1}	Tip radius of forward rotor
RPM1	RPM of forward rotor
RPM2	RPM of aft rotor
S	Blade-to-blade tangential spacing
s	Streamwise distance
SPL	Sound pressure level
S_{tip}	Blade-to-blade tangential spacing at the tip
UDF	Unducted fan
$V_{a/c}$	Aircraft flight velocity
V_{tip}	Tip speed
V_θ	Tangential velocity created by tip vortex
$(V_\theta)_{\max}$	Maximum value of tangential velocity created by tip vortex
V_∞	Freestream velocity

W_{dc}	Wake centerline defect (relative to forward rotor)
W_{FS}	Freestream velocity (relative to forward rotor)
x, y	Coordinates of the unwrapped annulus (see Figure 2)
X_f	Axial distance from pitch change axis of forward rotor
X_{PCA}	Axial distance between pitch change axes
Z_{vtx}	Axial location of tip vortex

Greek Symbols

Γ	Circulation
$(\Gamma)_{vtx}$	Circulation of the tip vortex
δ	Semiwake width
τ	Tip clearance
ω	Angular velocity of the tip vortex

Appendix A

User's Manual for Blade Tip Vortex Model Computer Program

The tip vortex model computer program developed for counterrotating propulsors is described in this appendix. This computer program is based on a similar program for evaluating turbofan/compressor rotor/stator interaction and also has an option to include a hub vortex (References 3 and 4). This study concentrated on developing the tip vortex model only. This appendix is divided into the following sections:

- A. Description and Flow Chart of the Computer Program
- B. Listing of the Computer Program
- C. Definition of Input/Output Parameters
- D. A Sample Input/Output Case.

A. Description and Flow Chart of the Computer Program

The computer program predicts the wake/tip vortex flow distributions of the forward rotor and the resultant upwash gust velocity field at the aft rotor. Based on a meridional-plane stream surface subdivision of the rotor-to-rotor flowpath annulus, the program is designed to use the following as input:

- Forward rotor inlet and exit aerodynamic vector diagram parameters
- Blade section properties such as solidity, chord, and sweep
- Aerodynamic properties (such as section drag and lift coefficients), as a function of immersion.

The viscous wake and tip vortex model is programmed to predict blade-to-blade circumferential distributions of the flow field at the one-fourth-chord point of the aft rotor in a reference frame fixed to the aft rotor. The computer program has all of the logic built into it to predict the flow field due to a hub vortex, but the empirical relationships for the hub vortex characteristics have not yet been developed. The computer program is designed to transform the forward rotor-fixed wake and tip vortex combined flow velocity profiles into a reference frame fixed to the aft rotor to evaluate the gust velocity profiles. Fourier analysis of the gust velocity profiles yields the gust harmonic spectrum. An analysis for evaluating the spanwise distortion and clocking of the wake/tip vortex sheet is incorporated into the program to predict the spanwise aerodynamic phase lag of the wake/tip vortex velocity field; thereby obtaining the spanwise distribution of the amplitude and relative phase of the gust upwash harmonic content. A flow chart of this computer program is presented in Figure A-1. The computer program output (specifically, gust harmonic spectrum and aerodynamic phase lag) forms input to the computation of the unsteady lift force computation and, subsequently, noise due to wake/tip vortex interaction.

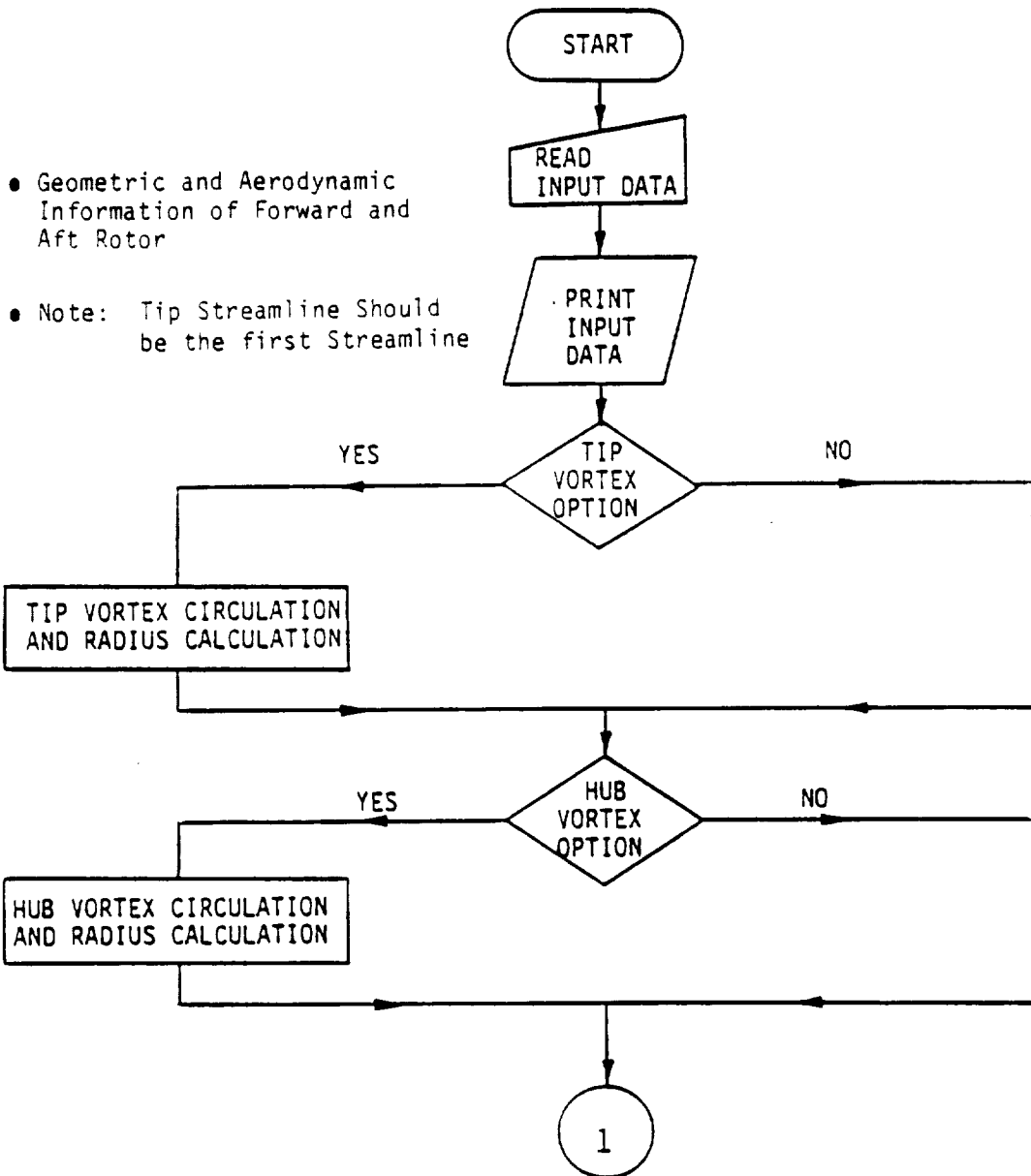


Figure A-1. Program Flow Chart for the Rotor Wake/Tip Vortex Model.

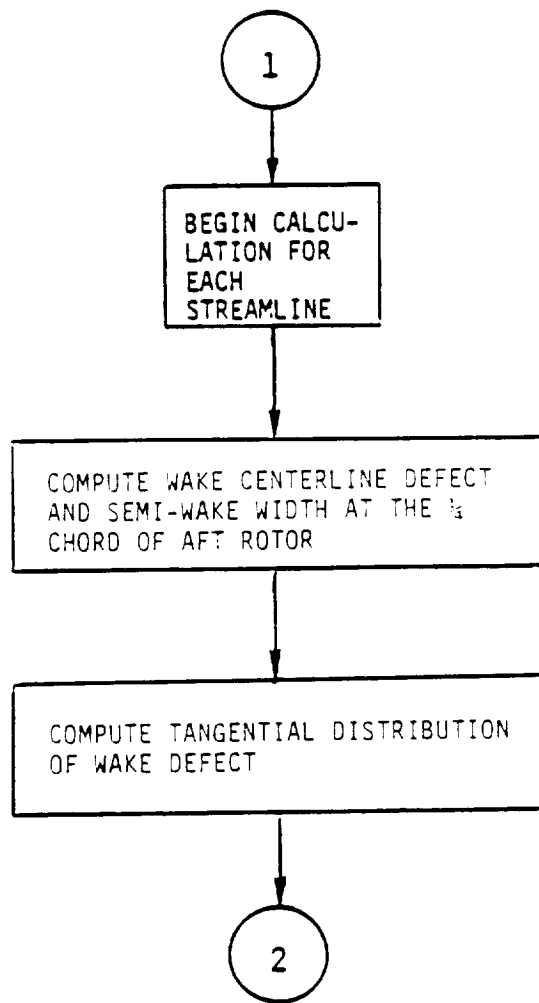


Figure A-1. Program Flow Chart for the Rotor
Wake/Tip Vortex Model (Continued).

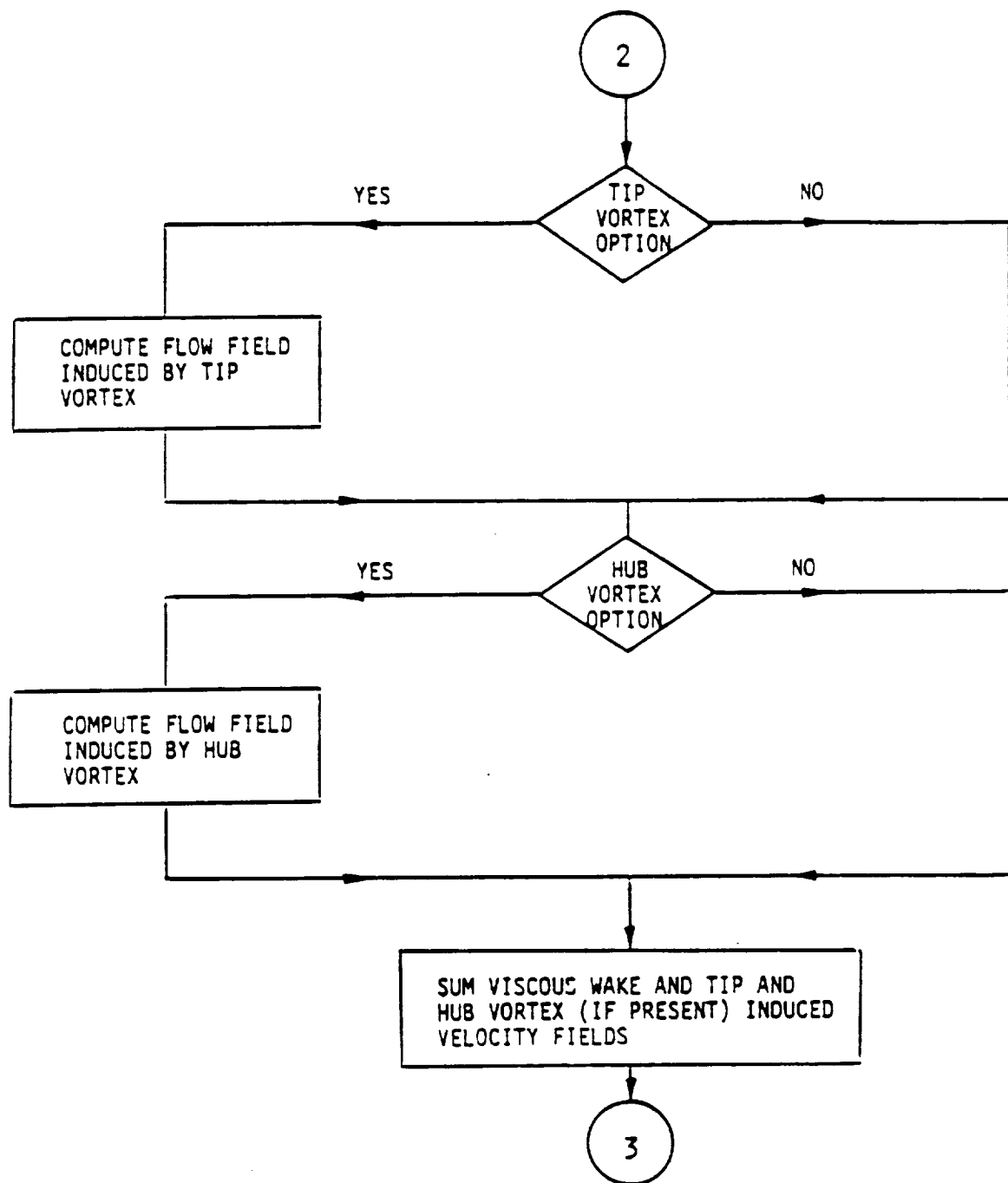


Figure A-1. Program Flow Chart for the Rotor Wake/Tip Vortex Model (Continued).

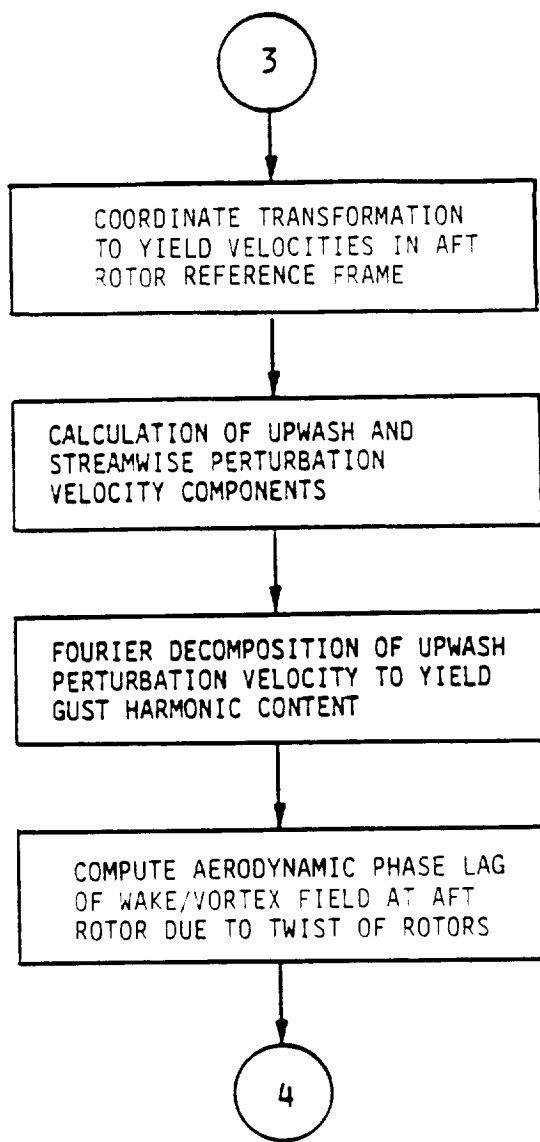


Figure A-1. Program Flow Chart for the Rotor Wake/Tip Vortex Model (Continued).

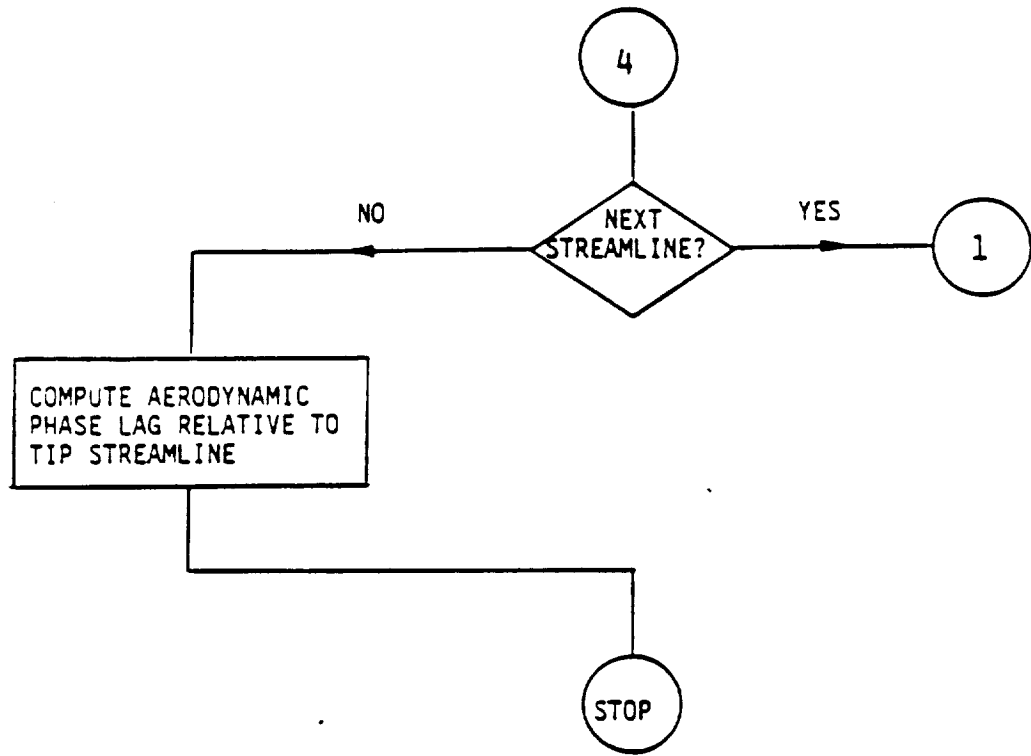


Figure A-1. Program Flow Chart for the Rotor Wake/Tip Vortex Model (Concluded).

The following specific features are incorporated into the computer program.

- Three models of predicting the centerline defect and semiwake width:
 - Linear-rational-function model (see Reference 3)
 - Kemp and Sears model
 - Mugridge and Morfey model.
- Two wake shape functions; namely:
 - Gaussian profile ($e^{-\ln 2 \eta^2}$)
 - Hyperbolic secant profile [$\operatorname{sech}(a\eta)$, $a = \cosh^{-1} 2$].
- Tip and hub vortices are incorporated in the program with options to include both, neither, or either one of them. Certain existing empirical relationships have been used in estimating the strength and radius of the tip vortex; however at this time, no such information is available for the hub vortex model. When such correlations for estimating the strength and radius of hub vortex become available, they can be incorporated into the computer program. The computer code also gives the trajectories of the centers of hub and tip vortices.

The computer program source code contains approximately 1000 lines. It consists of:

- Main program, which manipulates input, output, and all of the subroutines. It also computes the tip-to-hub aerodynamic phase lag, once all of the streamline computations have been performed.
- Subroutine RWTVM, which combines the flow fields due to wake and tip vortex and performs the coordinate transformation from the one fixed to the forward rotor, to the one fixed to the aft rotor.
- Subroutine WAKE1, which computes the wake centerline defect and semiwake width.
- Subroutine WAKE2, which computes the tangential wake profiles.
- Subroutine VORTX1, which computes the vortex strength and radius of tip and hub vortices.
- Subroutine VORTX2, which computes the velocity field induced by tip and hub vortices.
- Subroutine HRMONIC, which computes the harmonic content of rotor wake/vortex gust.
- Subroutine GAMCAL, which computes the ratio of specific heats for air as a function of ambient temperature.

- Subroutines PITCH1 and PITCH2, which compute the blade coordinate changes (and, thus, spacing) due to changes in pitch angle, relative to design setting for forward and aft rotors, respectively.
- Subroutine LSPFIT, which is an interpolation/integration subroutine.

B. Listing of the Computer Program

A listing of the computer program in the DEC/FORTRAN-77 language is included in this section.

C WAKE/TIP VORTEX GUST HARMONIC COMPUTATION MODEL
 C R.K.MAJJIGI NOV 11, 1985
 COMMON/COM12/ NZ,DTR,RTD,VO,CO,SXOCH(51)
 C COMMON/RWAKE1/ ISHAP, BETAW, NWHM, VREF, IWAKE
 C COMMON/HMONIC/ST(300), VPN(300), FCA(21), FCB(21), FCDB(21)
 COMMON/PRINTD/IPTT, IPR
 C COMMON/BLADE1/ THETA1(51), SIGR1(51) , DPINT1(51) ,
 1 CHORD1(51), TMOC1(51) , ALPHA1(51) ,
 1 Z1(51), ZMC1(51) , YMCL(51) ,
 1 BETAP1(51), MCA1(51) , FA1(51) ,
 1 BETPP1(51), DELBP1 , SCD1(51) ,
 1 EM1 , NB1
 C COMMON/BLADE2/ THETA2(51), SIGR2(51) , DPINT2(51) ,
 1 CHORD2(51), TMOC2(51) , ALPHA2(51) ,
 1 Z2(51), ZMC2(51) , YMCL(51) ,
 1 BETAP2(51), MCA2(51) , FA2(51) ,
 1 BETPP2(51), DELBP2 , SCD2(51) ,
 1 EM2 , NB2
 C COMMON /VTEX1/ IPTVTX, IHVTX, TAU, ALPHR, DUMMY, WT00, BL
 COMMON /VTEX2/ SAODS(2), SCIRCO(2), SOO(2), SVSDV0(2), SCL(2) ,
 1 SFRL(2)
 COMMON /VTEX3/ SBN(2) , SBR(2) , SDIST, RAWDS, R, VINRVT(300,2) ,
 1 VISRVT(300,2), HTR, VINRVT(300) , VISRV(300)
 COMMON /VTEX4/ CLAV, CRV, WT00T, ABR(51) , CI, TVTI
 C CHARACTER*40 CRUDF1, CRUDF2, PRINTF, L0TF
 CHARACTER DAT*9,TIM*8
 C DIMENSION Z(10), ZMC(10), YMCL(10)
 DIMENSION TMOC(10), BETAP(10), THETA(10) , ALPHA(10) , CHORD(10)
 DIMENSION CLL(51), EMRL(51)
 DIMENSION CL2(51), EMR2(51)
 DIMENSION XC1(51), YC1(51), XI(51), YI(51), AAA(51) , XC2(51) , YC2(51)
 DIMENSION EMR(51), SPARE(51)
 DIMENSION SCD(10)
 DIMENSION AEROPH(51)
 C REAL MCA, MCA1, MCA2
 C DATA RG/1716.26/
 DATA IWAKE, IRW, IQMAXR/2, 1, 10/
 IWAKE=1 LINEAR RATIONAL FUNCTION MODEL FOR ROTOR WAKE
 IWAKE=2 SILVERSTEIN/KEMP & SEARS MODEL FOR ROTOR WAKE (DEFAULT)
 IWAKE=3 MUGRIDGE & MORFEEY MODEL FOR ROTOR WAKE
 DATA WTIV_PCTCL,BETAW,IPRNTW,ISHAPE/0.,0.,0.,2/
 DATA VREF, IHVTX, TAU/10.0,0,10.0/
 C DATA PCTVTX/30./
 C C CI=CIRCULATION INDEX FOR TIP VORTEX CALCULATIONS
 C CI=1.0 (DEFAULT)
 C

```

      DATA CI / 1.0 /
C
C   TVTI=TRIP VORTEX TRAJECTORY INDEX ,TVTI=2.0 (DEFAULT)
C
C   DATA TVTI/2.0/
C
C   NAMELIST/INPUT/NCASE,VO,TAMB,PAMB,NP,
C   1 2,NZ,
C   1 ISHAPE,BETAW,NWHM,VREF,NSTEP,IPRNTW,
C   1 XPCA,WTIV,PCTCL,
C
C   1 DT,NB,SHP,RPM,CHORD,TMOC,ALPHA,THETA,
C   1 BETAP,DELBP,BETA34,HTR,ZMC,YMC,
C   1 SCD,IRW,IWAKE,
C   1 ITVTX,IBVTX,SBN,PCTVTX,
C   1 TAU,CI,TVTI
C
C   C
C   C
C   C
C   C   INITIALIZE CONSTANTS
C
C   PI=3.1415926
C   TPI=2.0*PI
C   DTR=PI/180.0
C   RTD=1.0/DTR
C   KASE=0
C
C   OPEN(15,STATUS='OLD')
C   READ(15,9000) CRUDF1
C   I1=1
C   IF(CRUDF1(1:1).EQ.'1') THEN
C   DO I=1,40
C   IF(CRUDF1(I:I).EQ.'1') I1=I+1
C   END DO
C   END IF
C   DO I=I1,40
C   IF(CRUDF1(I:I).EQ.'1'.OR.CRUDF1(I:I).EQ.' ') THEN
C   NC=I-1
C   CRUDF1=CRUDF1(1:NC)//'.'DAT'
C   GO TO 8001
C   END IF
C   END DO
C   OPEN(UNIT=10,FILE=CRUDF1,STATUS='OLD',SHARED)
C   READ(15,9000) CRUDF2
C   I1=1
C   IF(CRUDF2(1:1).EQ.'1') THEN
C   DO I=1,40
C   IF(CRUDF2(I:I).EQ.'1') I1=I+1
C   END DO
C   END IF
C   DO I=I1,40
C   IF(CRUDF2(I:I).EQ.'1'.OR.CRUDF2(I:I).EQ.' ') THEN
C   NC=I-1
C   CRUDF2=CRUDF2(1:NC)//'.'DAT'
C   GO TO 8002
C   END IF

```

```

END DO
OPEN(UNIT=11,FILE=CRUDF2,STATUS='OLD',SHARED)
READ(15,9000) PRINTF
I1=1
IF(PRINTF(1:I1).EQ.'(') THEN
DO I=1,40
IF(PRINTF(I:I1).EQ.'()') I1=I+1
END DO
END IF
DO I=I1,40
IF(PRINTF(I:I1).EQ.'.' OR PRINTF(I:I1).EQ.' ') THEN
NC=I-1
LOTF=PRINTF(1:NC)//'.LCT'
PRINTF=PRINTF(1:NC)//' PRN'
CALL SFATT(26,LOTF,1,ISTAT)
READ(15,9002) ILOTT
GO TO 9001
END IF
END DO
FORMAT(A)
FORMAT(I1)
CALL SFATT(16,PRINTF,1,ISTAT)
READ INPUT DATA FILE
C
C
CONTINUE
C
READ(10,INPUT,ERR=800,END=999)
NRSEC=0
BETA34=0.
ISECT=0
CALL READNL(10,0,INPUT,'INPUT',1,' ',1,IBW,IEW)
CLOSE(10)
C SET PROGRAM VARIABLES/CONSTANTS - ROTOR 1
DT1=DT
NBL=NB
NHM1=NHM
SHB1=SHP
RPM1=FRPM
DELBP=DELBP
IF(BETA34.NE.0.) THEN
CALL LSPPIT(Z,BETAP,NZ,.75,BET34,1,0,AAA)
DELBP1=BETA34-BET34
END IF
HTR1=HTR
ITDO1=ITDO
ILDO1=ILDO
ALE1=ALE
BTE1=BTE
KTM1=KTM
DXTM1=DXTM
YOD1=DIST/DT1
XLM1=XLM
DO 90 ISL=1,NZ
Z1(ISL)=Z(ISL)
ZMC1(ISL)=ZMC(ISL)
YMC1(ISL)=YMC(ISL)
CHORD1(ISL)=CHORD1ISL
TMOC1(ISL)=TMOC(ISL)
BETAP1(ISL)=BETAP(ISL)
69

```

```

THETA1 (ISL)=THETA (ISL)
ALPHA1 (ISL)=ALPHA (ISL)
SCD1 (ISL)=SCD (ISL)
CONTINUE
C-----
C
C OPEN(11,STATUS='OLD')
C READ INPUT DATA FILE
C
C READ(11,INPUT,ERR=900,END=999)
NRSEC=0
C
C BETA34=0.
CALL READNL(11,0,INPUT,'INPUT',1,' ','INPUT',1,IBW,IEW)
C SET PROGRAM VARIABLES/CONSTANTS - ROTOR 2
DT2=DT
NB2=NB
NBM2=NBM
SHP2=SHP
RPM2=RPM
DELB2=DELB
DELB2=DELB2
IF(BETA34.NE.0.) THEN
CALL LSPFFIT(Z,BETAP,NZ,.75,BET34,1,0,AAA)
DELB2=BETA34-BET34
END IF
HTR2=HTR
ITDO2=ITDO
ILD02=ILD0
ALE2=ALE
BTE2=BTE
XTM2=XTM
DXTM2=DXTM
YOD2=DIST/DR2
XLM2=XLM
DO 91 ISL=1,NZ
Z2 (ISL)=Z (ISL)
ZMC2 (ISL)=ZMC (ISL)
YMC2 (ISL)=YMC (ISL)
CHORD2 (ISL)=CHORD (ISL)
TMOC2 (ISL)=TMOC (ISL)
BETAP2 (ISL)=BETAP (ISL)
THETA2 (ISL)=THETA (ISL)
ALPHA2 (ISL)=ALPHA (ISL)
SCD2 (ISL)=SCD (ISL)
CONTINUE
C-----
C
C OPEN(26,STATUS='NEW')
C OPEN(16,STATUS='NEW')
WRITE(16,500)
500  WRITE(16,505)
FORMAT(//,1HO,16X,15H*** RWTVM ***//,
1 4X,33HUDF ROTOR GUST PREDICTION PROGRAM//)
FORMAT(4X,'BETAP SURFACE APPROXIMATION MODEL'//
1 4X,'WAKE/VORTEX MODEL INCLUDED'///)
C
WRITE(26,9500)
9500 FORMAT(//,16X,17H*** RWTVM ***//,
1 4X,35H"UDF ROTOR GUST PREDICTION PROGRAM"//)

```

ORIGINAL PAGE IS
OF POOR QUALITY

```

C CALL DATE(DAT)
CALL TIME(TIM)
WRITE(16,517) CRUDF1,CRUDF2,DAT,TIM
FORMAT(16,'FORWARD CRUDFILE IS ',A40//2X,'AFT CRUDFILE IS ',A40//)
1 2X,'DATE; ',A9,' TIME; ',A8//)

C WRITE(26,9517) CRUDF1,CRUDF2,DAT,TIM
FORMAT(2X,' FORWARD CRUDFILE IS ',",",A40,'',/"/
1 2X,' AFT CRUDFILE IS ',",",A40,'',/"/
1 2X,'DATE; ',",",A9,' TIME; ',",",A8,'',/"/)

C KASE=KASE+1
WRITE(16,510)KASE
FORMAT(7X,'*** ROTOR 1 INPUT PARAMETERS - CASE NO.',I3,4H '***//')
WRITE(16,515)DT1,NB1,SHPL,RPM1,VO,TAMB,PAMB,NP
WRITE(16,511)KASE
FORMAT(7X,'*** ROTOR 2 INPUT PARAMETERS - CASE NO.',I3,4H '***//')
WRITE(16,515)DT2,NB2,SHP2,RPM2,VO,TAMB,PAMB,NP
WRITE(16,515)DT10X,28PROPELLER TIP DIAMETER DT = F8.4,5H FT.//'
1 10X,28NUMBER OF BLADES NB = I5//'
1 10X,28SHAFT HORSEPOWER SHP = F10.2//'
1 10X,28ROTATIVE SPEED (RPM) = F10.1//'
1 10X,28FLIGHT VELOCITY VO (FPS) = F8.2//'
1 10X,28HAMBIENT TEMPERATURE TAMB = F8.2,8H DEG. F//'
1 10X,28HAMBIENT PRESSURE PAMB = F8.3,5H PSIA//'
1 10X,28NUMBER OF PROPELLERS NP = I3//')

C WRITE(16,516)XPCA,IRW,IWAKE
FORMAT(10X,'XPCA = ',F7.4/10X,' IRW = ',I2/
1 10X,'IWAKE= ',I2)

C ***** PRELIMINARY AERODYNAMIC PARAMETER CALCULATIONS *****
C
C RPS1=RPM1/60.0
B1=NB1
UT1=PI*DT1*RPS1
TO=TAMB+459.7
PO=144.0*NAMB
RHO=PO/(RG*TO)
CALL GAMCAL(TAMB,GAMMA)
CO=SQRT(GAMMA*RG*TO)
EMT1=UT1/CO
EMO=VO/CO
EMH1=SORT(EMT1**2+EMO**2)
WCON1=0.25*GAMMA*PO*CO*EMO*EMT1*B1*DT1*DT1
PCON1=GAMMA*PO*B1/(4.0*PI*SQRT(2.0))
ADVRI=VO/(RPS1*DT1)
WRITE(16,520) EMT1,EMO,EMH1
FORMAT(15X,20HTIP SPEED MACH NO. =F8.4/
1 15X,20HFLIGHT MACH NO. =F8.4/
1 15X,20HELICAL MACH NO. =F8.4//)

C RPS2=RPM2/60.0
B2=NB2
UT2=PI*DT2*RPS2

```

ORIGINAL PAGE IS
OF POOR QUALITY

```

EMT2=UT2/CO
EMH2=SQRT(EMT2**2+EMO**2)
WCON2=0.25*GAMMA*PO*CO*EMO*EMT2*B2*DT2*DT2
PCON2=GAMMA*PO*B2/(4.0*PI*SQRT(2.0))
ADVR2=VO/(RPS2*DT2)
WRITE(16,520) EMT2,EMO,EMH2
C
C *** BLADE SECTION PROPERTIES CALCULATION - ROTOR 1 ***
C
C CALL PITCH1
C
THMODI=1.0
CONTINUE
DO 10 IZ=1,NZ
SIGRI(IZ)=BI*CHORD1(IZ)/(PI*Z1(IZ))
EMRI(IZ)=SQRT(EMO**2+EMT1**2*(IZ)**2)
CLCON=2.0/(GAMMA*EMRI(IZ)*EMRI(IZ))
DPINT1(IZ)=GAMMA*EMT1*Z1(IZ)*EMRI(IZ)*THETA1(IZ)/SIGRI(IZ)
DPINT1(IZ)=THMODI*DPINT1(IZ)
CLI(IZ)=CLCON*DPINT1(IZ)
YC1(IZ)=EMRI(IZ)*CLI(IZ)*CHORD1(IZ)*Z1(IZ)
CONTINUE
10
C
C
IZVTX=1
ZVTX=Z1(1)-(PCTVVTX*(Z1(1)-HTR1))/100.
DO 12 IZ=1,NZ
IF (Z1(IZ).LE.ZVTX) THEN
IZVTX=IZ
GO TO 721
END IF
END DO
CONTINUE
SCLAV=0.0
SCAV=0.0
DO IZ=1,IZVTX
SCLAV=SCLAV+CL1(IZ)
SCAV=SCAV+CHORD1(IZ)
END DO
FIZVTX=FLOAT(IZVTX)
CLAV=SCLAV/FIZVTX
CAV=SCAV/FIZVTX
C
C *** ROTOR EFFECTIVE AERODYNAMIC HORSEPOWER AND DISK LOADING ***
C
XI(1)=HTR1
XI(2)=1.0
YI(1)=0.0
IF(Z1(1).LT.Z1(NZ)) GO TO 21
XI(1)=1.0
XI(2)=HTR1
YI(1)=0.0
CONTINUE
CALL LSPFIT(Z1,YC1,NZ,XI,YI,2,-1,AAA)
IF(Z1(1).GT.Z1(NZ)) YI(2)=-YI(2)
21

```

```

      SHPE1=WCON1*YI(2)/550.0
      IF (ABS(SHP1-SHPE1).LE..0.01) GO TO 710
      THMOD1=SHP1/SHPE1
      GO TO 700

C *** PRINT-OUT BLADE SECTION PROPERTIES - ROTOR 1 ***
C
 710  CONTINUE
      WRITE(16,570)
      FORMAT(1X,'TABLE OF BLADE SECTION PROPERTIES - ROTOR 1'//
      1 2X,7HSECTION,2X,4HR/RT,4X,5HCHORD,3X,4HTM/C,4X,SHALPHA,
      1 3X,5HBETAP,3X,3HMCA,5X,2HCL,6X,'CD',//)
      IPRT=1
      IF (NZ.GT.15) IPRT=NZ/10
      DO 25 IZ=1,NZ,IPRT
      WRITE(16,575) IZ,Z1(IZ),CHORD1(IZ),TMOC1(IZ),ALPHAI(IZ),
      1 BETPP1(IZ),MCAL(IZ),FAI(IZ),CLI(IZ),SCDI(IZ)
 25  CONTINUE
      FORMAT(16,2X,3F8.4,2F8.2,4F8.4)

C *** BLADE SECTION PROPERTIES CALCULATION - ROTOR 2 ***
C
C     CALL PITCH2
C
 73   THMOD2=1.0
      IZCL=1
      IF (PCTCL.EQ.0.) GO TO 701
      ZCL=2*(1)-PCTCL*(Z2(1)-HTR2)/100.
      DO IZ=1,NZ
      IF (Z2(IZ).LE.ZCL) THEN
      IZCL=IZ
      GO TO 701
      END IF
      END DO
      CONTINUE
      DO 11 IZ=1,NZ
      SIGR2(IZ)=B2*CHORD2(IZ)/(PI*22(IZ))
      EMRR(IZ)=SQR(EMO**2+(Z2(IZ)*EMT2+THETA1(IZ))*THMOD1
      1 *Z1(IZ)*EMT1)**2
      EMR2(IZ)=EMRR(IZ)
      CLCON=2.0/(GAMMA*EMR2(IZ)*EMR2(IZ))
      DPINT2(IZ)=THMOD2*DPINT2(IZ)
      DPINT2(IZ)=CLCON*DPINT2(IZ)
      CL2(IZ)=CLCON*DPINT2(IZ)
      YC2(IZ)=EMRR(IZ)*CL2(IZ)*CHORD2(IZ)*Z2(IZ)
      CONTINUE
 11  CONTINUE
C
C *** ROTOR EFFECTIVE AERODYNAMIC HORSEPOWER AND DISK LOADING ***
C
      XI(1)=HTR2
      XI(2)=Z2(IZCL)
      YI(1)=0.0
      NZCL=NZ-IZCL+1
      IF (Z2(1).LT.Z2(NZ)) GO TO 22

```

```

X1(1)=Z2(IZCL)
X1(2)=HTR2
Y1(1)=0.0
C
CONTINUE
CALL LSPEFIT(Z2(IZCL),YC2(IZCL),NZCL,X1,Y1,2,-1,AAA)
IF(Z2(1).GT.Z2(NZ)) Y1(2)=-Y1(2)
SHPE2=WCON2*Y1(2)/550.0
IF(LABS(SHP2-SHPE2).LE.0.01) GO TO 711
THMOD2=SHP2/SHPE2
GO TO 701

C ** PRINT-OUT BLADE SECTION PROPERTIES - ROTOR 2 ***
C
711
CONTINUE
WRITE(16,571)
FORMAT(//18X,'TABLE OF BLADE SECTION PROPERTIES - ROTOR 2'//)
1 2X,7HECTION,2X,4HR/RT,4X,5HCHORD,3X,4HTM/C,4X,5HALPHA,
1 3X,5HBETAP,3X,3HMC,A,5X,2HFA,6X,2HCL,//
DO 26 IZ=IZCL,NZ,IPRT
WRITE(16,575)IZ,Z2(IZ),CHORD2(IZ),THOC2(IZ),ALPHA2(IZ),
1 BETEP2(IZ),MCA2(IZ),FA2(IZ),CL2(IZ)
CONTINUE

C ** ROTOR 1 ***
AA1 =0.25*PI*DT1*DT1*(1.0-HTR1+HTR1)
DL11=SHP1/(DT1*DT1)
DL21=SHP1/A1
CPQ1=550.0*SHP1/(RHO*(RPS1**3)*(DT1**5))
WRITE(16,578)
FORMAT(//15X,'ROTOR 1')
WRITE(16,580) SHPE1,A1,DL11,DL21,CPQ1
FORMAT(//15X,21HEFFECTIVE AERO SHP = F8.2/
1 15X,21HROTOR ANNULUS AREA = F8.3,6H SQ FT/
1 15X,21HDISK LOADING SHP/D2 = F8.2/
1 15X,21HDISK LOADING SHP/AA = F8.2/
1 15X,21HPOWER COEFFICIENT CP= F8.3//)
C
C ** ROTOR 2 ***
AA2 =0.25*PI*DT2*DT2*(1.0-HTR2+HTR2)
DL12=SHP2/(DT2*DT2)
DL22=SHP2/A2
CPQ2=550.0*SHP2/(RHO*(RPS2**3)*(DT2**5))
WRITE(16,579)
FORMAT(//15X,'ROTOR 2')
WRITE(16,580) SHPE2,A2,DL12,DL22,CPQ2
C
C *** CALCULATE ROTOR - ROTOR GUST LOADING HARMONICS ***
C
IF IRW.LE.0) GO TO 660
DO 650 IZ=1,NZ
IZR=IZ
RMC1=SQRT(YMC1(IZ)*YMC1(IZ)+ZMC1(IZ)*ZMC1(IZ))
IF(RMC1.GT..00001) THEN
PSII=ATAN2(ZMC1(IZ),YMC1(IZ))
YMC1P=RMC1*COS(PSII+DELBP1*GTR)
ZMC1P=RMC1*SIN(PSII+DELBP1*GTR)
ELSE

```



```

END IF
YMC2P=RMC2*COS(PSI2+DELBP2*DTR)
ZMC2P=RMC2*SIN(PSI2+DELBP2*DTR)
THMC2=2.0*YMC2P/Z2(IZ)
THLE2=THMC2-CHORD2(IZ)*COSBP2/Z2(IZ)
THQC2=THMC2-.5*CHORD2(IZ)*COSBP2/Z2(IZ)
THMC2=-THMC2
THLE2=-THLE2
THQC2=-THQC2
CH1AX=CHORD1(IZ)*SINBP1
XQCHQC=(ABS(XPCA)-2MCP-CHORD1(IZ)*SINBP1/2.)+
1 DT2/DT1*(ZMC2P-CHORD2(IZ)*SINBP2/4.)/CH1AX
DTHW1=2.*XQCHQC*TBL1*CH1AX/Z1(IZ)
THW1=THTE1+DTHW1
DELPHW=THW1-THQC2
IF(IZ.EQ.1) DPHTIP=DELPHW
DELPHW=DELPHW-DPHTIP
AEROPH(IIZZ)=DELPHW*RTD
C
3000 CONTINUE
C
WRITE(16,670)
FORMAT(//15X,'HUB-TO-TIP AERODYNAMIC PHASE LAG')
WRITE(16,680)
FORMAT(8X,'STREAMLINE NO.',5X,'AERO PHASE LAG, DEG.')
680 DO 3010 IZ=1,NZ
WRITE(16,690) IZ,AEROPH(IZ)
CONTINUE
FORMAT(10X,I3,F19.6)
STOP
3010 FORMAT(10X,I3,F19.6)
690 END
C -----
C
SUBROUTINE RWVM(IZR,N,IPRNTW,WTIV,THMOD1)
COMMON/RWAKE1/ ISHAPE,BETAW,NWHM,VREF,IWAKE
DIMENSION THETAW(300),BETA(300),WT(300),WS(300),WN(300),VT(300),
1 VN(300),VS(300),ALPHA(300),VTP(300),VPS(300),
1 WTO(300),WTIF(300),WSC(300),
1 WNC(300),PHI(10),WTOT(300)
C
COMMON/PRINTD/ IPRV,IPR
COMMON/COM12/ NZ,DT,RTD,VO,CO,SXOCH(51)
COMMON/HMONIC/ ST(300),VPN(300),FCA(21),FCB(21),FCDB(21)
COMMON/FANVTX/ NSTR,SSIGR(51),SSMNA(51),SSTHET(51),SSEMT(51)
COMMON/BLADE1/ THETAI(51),SIGRI(51),DPINT1(51),
1 CHORD1(51),TMOC1(51),ALPHAI(51),
1 Z1(51),ZMC1(51),YMC1(51),
1 BETAP1(51),MCA1(51),FA1(51),
1 BETPP1(51),DELBP1 ,SCDI(51),
1 EMT1 ,NB1
C
COMMON/BLADE2/ THETA2(51),SIGR2(51),DPINT2(51),
1 CHORD2(51),TMOC2(51),ALPHA2(51),
1 Z2(51),ZMC2(51),YMC2(51),
1 BETAP2(51),MCA2(51),FA2(51),
1 BETPP2(51),DELBP2 ,SCD2(51),
1 EMT2 ,NB2
C

```

```

COMMON /VTEX1/ IPUTX, IHBUTX, TAU, ALPHR, CHORD, WT00, B1
COMMON /VTEX2/ SAODS(2), SCIRCO(2), SOO(2), SVSDVO(2), SCL(2),
  1  SFRL(2)
COMMON /VTEX3/ SBN(2), SBR(2), SDIST, RAWDS, R, VINRVT(300,2),
  1  VISRVT(300,2), HTR, VINRV(300), VISRV(300)
COMMON /VTEX4/ CLAV, CAV, WT00T, ABR(51), CI, TVTI
C      CI=CIRCULATION INDEX FOR TIP VORTEX
C      TVTI=TOP VORTEX TRAJECTORY INDEX
C
C      REAL MCA1, MCA2
C      PI=4.*ATAN(1.)
C      B1=NB1
C      B2=NB2
C      IPR=0
C      DO IP=0,11
C        IF (IZR.EQ.1+IP*IPRT) THEN
C          IPR=1
C          WRITE(16,1100)
C          WRITE(16,1110)
C
C      C INDEX OVER STREAMLINE NUMBER - IZR
C      WRITE(16,1200) IZR
C      GO TO 10
C      END IF
C      END DO
C
C      VVTR=EMT2/EMT1
C      FOPT=1.0
C      SADIN=90.0-BETPP1(IZR)
C      SADIN=90.0-BETPP2(IZR)
C      SEMA=VO/CO
C      SIGS1=SIGR2(IZR)
C      SEMT=EMT1*Z1(IZR)
C      VWHEEL=SEMT*CO
C      R=Z1(IZR)
C      SIG1=SIGR1(IZR)
C      SXOCH1=SXOCH(IZR)
C      STHETA=STHETAI(IZR)*THMOD1
C      ISTR=IZR
C      CD=SCDI(IZR)
C      IF (IPR.EQ.1) WRITE(16,1210)CD
C
C      =====
C      C SIMILARITY AND CORRELATION CALCULATIONS
C      C
C      C WAKE PARAMETERS
C      C
C      BETA0=ATAN2((1.-STHETA)*SEMT,SEMA)
C      ALPHR=BETA0
C      ALPHS=ATAN2(STHETA*SEMT,SEMA)
C      IF (IPUTX.EQ.0.AND.IHBUTX.EQ.0) GO TO 300
C      IF (IZR.NE.1) GO TO 310
C      SIG1=SIG1

```

```

SEMAT-SEMA
STHETAT-STHETA
SEMTT-SEMT
CALL VORTX1 SIGIT,SEMAT,STHETAT,SEMTT)
GO TO 310
300  IF(IZR.EQ.1) WRITE(06,1120)
C   W(N) EVALUATED AT STATOR 1/4 CHORD POINT
C
      SXOCH1=SXOCH1+0.25*B1*B2*SIG1/SIG1
WT00=SEMA/(SEMT*COS(BETA0))
BNB=NBL
C
      SDIST=SXOCH1/COS(BETA0)
      CALL WAKE1 (IWAKE,CD,SDIST,WT00,ALPHR,BETA0,SIG1,WTDC,DLO)
      IF(IPR.EQ.1) THEN
        WRITE (16,1130) WT00
        WRITE (16,1140) WTDC
        WRITE (16,1145) SXOCH1(IZR)
        WRITE (16,1150) SDIST
        WRITE (16,1160) DLO
      END IF
C=====
C   DETERMINE RELATIVE, ABSOLUTE, AND PERTURBATION VELOCITIES
C=====
C   SPECIFY ANALYSIS TRAVERSE DISTANCE STEP SIZE
C
      RN=FLOAT(N)
      NPS=(N-1)/2
      S=2.*PI/BNB
      NI=N-1
      RNI=FLOAT(NI)
      SI=S/RNI
      RNPS=FLOAT(NPS)
      THETAW(1)=-RNPS*SI
      ST(1)=THETAW(1)/(2.*ABS(THETAW(1)))
C
      DO 510 I=2,N
      THETAW(I)=THETAW(I-1)+SI
      ST(I)=THETAW(I)/(2.*ABS(THETAW(1)))
      CONTINUE
C   DETERMINE INVISCID DISTRIBUTION OF WT
C
      BETAO=BETA0*OTR
      WTINC=WTIV/RNI
      WT0(I)=WT00
      WTIF(I)=1.0
      ND2=(N+1)/2
      N22=ND2+1
      DO 520 I=2,ND2
      WTIF(I)=WTIF(I)-WTINC
      CONTINUE
      DO 530 I=N22,N

```

```

DUB0 : (CHARLOTTE) RWTVM FOR;6
      WTIF(1)=WTIF(1)+WTIV/2.+ (N22-I)*WTINC
      CONTINUE
C   DETERMINE TANGENTIAL ANGLE DISTRIBUTION
C
      BETAW=BETAW*DTR
      BETA(1)=BETA0
      DO 540 I=2,N
      BETA(I)=BETA(1)
      CONTINUE
C
      IMIDDL=(N+1)/2
      DO 550 I=1,IMIDDL
C   SPECIFY EXIT-FLOW TOTAL RELATIVE VELOCITY PROFILE
C
      DLSPPP=DL0*S
      DLSTOP=DLSPPP/2.
      DL=DLSTOP
      DT=THETAW(I)/DL
      DT1=(THETAW(I)+S)/DL
C
      CALL WAKE2 (IWAKE,ISHAPE,DT,PP)
      WT(I)=WTDC*(1.-PP)
      WT(I)=WT(I)*WTIF(I)+WT0(I)-WTDC
      II=I
      BETA(I)=BETA(I)+BETAW*EXP(PP)
      CALL WAKE2 (IWAKE,ISHAPE,DT1,PP1)
      PPT=PP+PP1
      WTOT(I)=WTDC*(1.-PPT)
      WTOT(I)=WTOT(I)*WTIF(I)+WT0(I)-WTDC
      CONTINUE
C
      IMIDDL=IMIDDL+1
      DEL=WTOT(IMIDDL)-WT(IMIDDL)
      DO 560 I=IMIDDL,N
      DT=THETAW(I)/DL
      DT1=(THETAW(I)-S)/DL
      CALL WAKE2 (IWAKE,ISHAPE,DT,PP)
      WT(I)=WTDC*(1.-PP)
      WT(I)=WT(I)*WTIF(I)+WT0(I)-WTDC
      BETA(I)=BETA(I)+BETAW*EXP(PP)
      CALL WAKE2 (IWAKE,ISHAPE,DT1,PP1)
      PPT=PP+PP1
      WTOT(I)=WTDC*(1.-PPT)
      WTOT(I)=WTOT(I)*WTIF(I)+WT0(I)-WTDC
      II=I
      CONTINUE
C
      DO 570 I=1,N
      WTOT(I)=WTOT(I)-DEL
      BETDEL=BETA(I)-BETA(1)
      WS(I)=WTOT(I)*COS(BETDEL)

```

```

WN(I)=WTOT(I)*SIN(BETDEL)
I=I
CONTINUE

570
C      IF (ITPVTX.EQ.0.AND.IHBVTX.EQ.0) GO TO 600
C      CALCULATE VORTEX INDUCED VELOCITY FIELD
C
NST=N
RADUS=B1/(2.*PI)
CALL VORTX(ISTR,NST,SIGIT,SEMAT,STHETAT,SEMTT,SEMT,SIG1)
C      INTEGRATE WAKE AND VORTEX GUST DESCRIPTIONS
C
N0=(N-1)/2
N1=(N+1)/2
DO 610 I=1,N1
IF (ITPVTX.EQ.0.AND.IHBVTX.EQ.0) VISRV(I)=0.
IF (ITPVTX.EQ.0.AND.IHBVTX.EQ.0) VINRV(I)=0.
WSC(I)=VISRV(I)+WS(N0+1)
WNC(I)=VINRV(I)+WN(N0+1)
CONTINUE

C      N2=2*NO
DO 620 I=N1,N
IF (ITPVTX.EQ.0.AND.IHBVTX.EQ.0) VISRV(I)=0.
IF (ITPVTX.EQ.0.AND.IHBVTX.EQ.0) VINRV(I)=0.
WSC(I)=VISRV(I)+WS(I-NO)
WNC(I)=VINRV(I)+WN(I-NO)
CONTINUE

80 620
C      N3=2*N-1
DO 630 I=N,N3
WSC(I)=WSC(I-N2)
WNC(I)=WNC(I-N2)
CONTINUE

630
C      DO 640 I=1,N3
WS(I)=WSC(I)
WN(I)=WNC(I)
WT(I)=(WSC(I)**2+WNC(I)**2)**0.5
AAA=WS(I)/WT(I)
IF (AAA.GE.-1.0) AAA=-1.0
BETA(I)=ACOS(AAA)+BETA0
RLI=FLOAT(I)
RLN3=FLOAT(N3)
ST(I)=(RLI-1.)/(RLN3-1.)
ST(I)=ST(I)*2.
CONTINUE

640
C      DO 650 I=N,N3
THETAW(I)=THETAW(I-N2)
CONTINUE

650
C      WTHN1=WT(N1)*SIN(BETA(N1))
WXN1=WT(N1)*COS(BETA(N1))
VXN1=WXN1
VTN1=1.+VVTR-WTHN1
VTN1=(VXN1**2+VTN1**2)**0.5

```

```

DUB0: | CHARLOTTE | RWTVM.FOR;6
      ALPHA(N1)=ACOS(VXN1/VTN1)
      ALPDN1=ALPHA(N1)-ALPHA(N1)
      VS(N1)=VTN1*COS(ALPDN1)

C      DO 660 I=1,N3
C
C DETERMINE ABSOLUTE VELOCITY PROFILE
C
      WTH=WT(I)*SIN(BETA(I))
      VX=WX
      VT=VX
      VTH=1.0+VVTR-WTH
      VT(I)=(VX**2+VTH**2)**0.5
      ALPHA(I)=ACOS(VX/VT(I))

C
C DETERMINE ABSOLUTE VELOCITY COMPONENTS
C
      ALPDEL=ALPHA(I)-ALPHA(N1)
      VS(I)=VT(I)*COS(ALPDEL)
      VN(I)=VT(I)*SIN(ALPDEL)

C
C DETERMINE TOTAL PERTURBATION VELOCITY
C
      VPN(I)=VN(I)
      VPS(I)=VS(I)-VS(N1)
      VTP(I)=(VPS(I)**2+VPN(I)**2)**0.5

C      CONTINUE
C=====
C
C PRINT NUMERICAL VELOCITY PROFILES
C
      DO 700 I=1,N3
      THETAW(I)=THETAW(I)*RTD
      BETA(I)=BETA(I)*RTD
      ALPHA(I)=ALPHA(I)*RTD
      CONTINUE
C
      IF (IPRNTW.LE.0) GO TO 800
C
      IF (IPR.EQ.1) THEN
      WRITE (16,1410)
      WRITE (16,1420)
      DO 710 I=1,N3,10
      WRITE (16,1430) I,THETAW(I),ST(I),WT(I),WS(I),VN(I),BETA(I)
      CONTINUE
C
      WRITE (16,1500)
      WRITE (16,1510)
      DO 720 I=1,N3,10
      WRITE (16,1520) I,THETAW(I),ST(I),WT(I),VS(I),VN(I),ALPHA(I)
      CONTINUE
C
      WRITE (16,1600)
      WRITE (16,1610)
      DO 730 I=1,N3,10

```

WRITE (16,1620) I, THETAW(I), ST(I), VTP(I), VPS(I), VPN(I)

CONTINUE

END IF

C
C
C

C CALCULATE HARMONIC CONTENT OF ROTOR EXIT FLOW

C=====

C=====

C IF (FOPT.NE.1.0) GO TO 810

CALL HRMNIC (ISTR,N,NWHM,VREF,VMWHEEL)

CONTINUE

C FORMAT STATEMENTS

C=====

1100 FORMAT (//,10X,'ROTOR WAKE/VORTEX FLOW PROGRAM')

1110 FORMAT (//2X,'CASE NUMBER',I4)

1120 FORMAT (//2X,'TIP VORTEX NOT INCLUDED')

1200 FORMAT (//,2X,'---- STREAMLINE NUMBER',I3,' ----')

1210 FORMAT (//5X,'CD',=,F8.4)

1300 FORMAT (//2X,'LINEAR RATIONAL FUNCTION ROTOR WAKE PROFILE')

1330 FORMAT (5X,'WFS/UT',5X,'=',F8.4)

1340 FORMAT (5X,'WD/UT',6X,'=',F8.4)

1345 FORMAT (5X,'X/C',8X,'=',F8.4)

1350 FORMAT (5X,'SDIST',6X,'=',F8.4)

1360 FORMAT (5X,'WAKE WIDTH',IX,'=',F8.4)

81400 FORMAT (//,2X,'ROTOR WAKE GUST DESCRIPTION FOR CASE',I4)

1410 FORMAT (//5X,'VELOCITY PROFILE RELATIVE TO FORWARD ROTOR')

1420 FORMAT (9X,'I',5X,'THETAW',5X,'S',8X,'WT',7X,'WS',7X,

1 'WN',7X,'BETA')

1430 FORMAT (7X,I4,F9.2,4F9.5,F11.5)

1500 FORMAT (//5X,'VELOCITY PROFILE RELATIVE TO AFT ROTOR')

1510 FORMAT (9X,'I',5X,'THETAW',5X,'S',8X,'VT',7X,'VS',7X,'VN',

1 'BX','ALPHA')

1600 FORMAT (//5X,'PERTURBATION VELOCITY PROFILE RELATIVE TO AFT ROTOR')

1610 FORMAT (9X,'I',5X,'THETAW',5X,'S',7X,'VPT',6X,'VPS',6X,

1 'VPN')

1620 FORMAT (7X,I4,F9.2,4F9.5)

1720 FORMAT (7X,I4,F9.2,3F9.5)

2000 FORMAT (//,1X,'HARMONIC CONTENT OF ROTOR WAKE/VORTEX FLOW')

2010 FORMAT (//5X,'STREAMLINE NUMBER',I3)

2020 FORMAT (//8X,'NH',3X,'MODULUS',4X,'PHASE',4X,

1 '20*LOG(MODULUS), DB')

2030 FORMAT (7X,I3,F10.6,F11.6,F14.2)

2100 FORMAT (//,2X,'TIP-TO-HUB AERODYNAMIC PHASE LAG')

2110 FORMAT (//5X,'STREAMLINE NO.',2X,'AERO PHASE LAG')

2120 FORMAT (10X,I3,F19.6)

2240 FORMAT (8X,I4,F12.2,F9.2)

C
C
C

990 RETURN

END

C----- WAKE -----

C SUBROUTINE TO CALCULATE WAKE CENTERLINE DEFECT AND SEMI-WAKE WIDTH

C SUBROUTINE WAKE1 (IWAKE,CD,SDIST,WT00,ALPHR,BETA0,SIG1,WTDC,DLO)

```

C PI=4.0*ATAN(1.)
C GO TO (100,200,300), IWAKE
C LINEAR RATIONAL FUNCTION FOR ROTOR WAKE PROFILE
C
100  CONTINUE
    CDEXP1=CD**(0.125)
    CDEXP2=CD**(.025)
    IF(SIG1.GE.1.0) GO TO 101
    DL0C=(10.2375*SDIST*CDEXP1+0.034125)/
    1(0.357*SDIST*CDEXP1+1.0)
    DL0=DL0C*SIG1
    GO TO 102
CONTINUE
    DL0=(10.31875*SDIST*CDEXP1+0.048)/
    1(0.268125*SDIST*CDEXP1+1.0)
102  CONTINUE
    WTDC=CDEXP2*((0.3675*SDIST+1.95)/(7.65*SDIST+1.0))
    GO TO 400
C SILVERSTEIN/ KEMP & SEARS MODEL FOR ROTOR WAKE
C
200  CONTINUE
    WTDC=SQRT(CD)*(1.21*(SDIST+.3)**(-1.))
    DL0=SQRT(CD)*SIG1*(0.68*(SDIST+.15)**.5)
    GO TO 400
C MUGRIDGE & MORFEY MODEL FOR ROTOR WAKE
C
300  CONTINUE
    A1A=2.0
    WTDC=SQRT(CD)*A1A/SQRT(2.)*( (SDIST+2.*CD)**(-.5) )
    DL0=CD*SIG1*(.5+EXP(-.16/CD*SDIST))*(WTDC)**(-1.0)
C
400  CONTINUE
    IF (IWAKE.GT.1) DL0=DL0/COS(ALPHR)
    WTDC=WTDC*WT00
    IF (DL0.GE.0.5) DL0=0.5
    BETAO=BETAO*100./PI
    RETURN
C END OF SUBROUTINE WAKE1
END
C----- WAKE2 -----
C SUBROUTINE TO CALCULATE TANGENTIAL WAKE PROFILE
C SUBROUTINE WAKE2 (IWAKE,ISHAPE,DT,PP)
C
C PI=4.0*ATAN(1.)
C GO TO (100,200,300), IWAKE
C LINEAR RATIONAL FUNCTION FOR ROTOR WAKE PROFILE
C
100  CONTINUE
    GO TO (110,120), ISHAP

```

ORIGINAL PAGE IS
OF POOR QUALITY

```

-DUB0:[CHARLOTTE]RWTVW.FOR:6
110      PP=2.^(EXP(1.3169579*DT)+EXP(-1.3169579*DT))
120      GO TO 400
120      PP=EXP(-0.6931472*DT*DT)
120      GO TO 400
C
C      SILVERSTEIN/KEMP & SEARS WAKE PROFILE
C
200      CONTINUE
        GO TO (210,220),ISHAPE
210      PP=2.^(EXP(1.3169579*DT)+EXP(-1.3169579*DT))
        GO TO 400
        PP=EXP(-PI*DT*DT/4.)
        GO TO 400
C
C      MUGRIDGE & MORFEE WAKE PROFILE
C
300      CONTINUE
        GO TO (310,320),ISHAPE
310      PP=2.^(EXP(1.3169579*DT)+EXP(-1.3169579*DT))
        GO TO 400
        PP=EXP(-PI*DT*DT/4.)
320      CONTINUE
        IF (PP.LT.1.E-20) PP=1.E-20
        RETURN
C
C      END OF SUBROUTINE WAKE2
        END
C----- HRNNIC -----
C
C      SUBROUTINE HRNNIC COMPUTES HARMONIC CONTENT OF ROTOR
C      WAKE/VORTEX FLOW AT 1/4 CHORD POINT OF SATOR
C
C      SUBROUTINE HRNNIC (ISTR,N,NWHM,VREF,VWHEEL)
C
C      COMMON/PRINTD/ IPR,IPR
C      COMMON /HMONIC/ ST(300),VPN(300),FCA(21),FCB(21),FCDB(21)
C
C      COMPLEX CSUM,CPWR,CERC
C
C      PI=4.*ATAN(1.)
        RN=FLOAT(N)
        NS=(N+1)/2
        NF=NS+N-1
C
        DO 100 I=NS,NF
          ST(I)=ST(I)-0.5
        CONTINUE
C
        IF (IPR.EQ.1) THEN
          WRITE (16,1000)
          WRITE (16,1020)
        END IF
C
        DO 220 NH=1,NWHM
          RNH=FLOAT(NH)
          CSUM=CMPLX(0.0,0.0)

```

```

HD3=(ST(NF)-ST(NS))/(3.* (RN-1.))
ICH=1

```

```
C NUMERICAL INTEGRATION - SIMPSON'S RULE
```

```

C DO 210 I=NS,NF
ICH=ICH+(-1)
CPOE=RNH*PI*ST(I)/0.5
CPWR=CMPLX(0.0,CPOE)
CERC=CEXP(CPWR)

C IF (I.EQ.NS.OR.I.EQ.NF) GO TO 200
CSUM=CSUM+VPN(I)*CERC*(3+ICH)
GO TO 210
CSUM=CSUM+VPN(I)*CERC
CONTINUE
C
CSUM=CSUM*HD3

C CMOD=CABS(CSUM)
ARPC=REAL(CSUM)
BIPC=AIMAG(CSUM)
PHASE=ATAN(BIPC/ARPC)      !TO SUM OVER +VE & -VE NH
FCA(NH)=2.*CMOD
FCB(NH)=PHASE
FCDB(NH)=20.0* ALOG10(ABS(FCA(NH)))
FCDB(NH)=FCDB(NH)+20.0* ALOG10(VWHEEL/VREF)

C IF(IPR.EQ.1) WRITE (16,1030) NH,FCA(NH),FCB(NH),FCDB(NH)
CONTINUE
220
C
C RESCALE INTEGRATION INTERVAL
C DO 300 I=NS,NF
ST(I)=ST(I)+0.5
CONTINUE
300
C
C FORMAT STATEMENTS
C
1000  FORMAT (//2X,'HARMONIC CONTENT OF ROTOR WAKE/VORTEX FLOW')
1020  FORMAT ('/8X,'NH',3X,'CMOD',4X,'PHASE',4X,
1   '20*LOG(2*CMOD)',DB')
1030  FORMAT (7X,I3,F10.6,F14.2)
C
RETURN
C
C END OF SUBROUTINE HARMNIC
END

C----- VORTX1 -----
C
C SUBROUTINE VORTX1 COMPUTES VORTEX STRENGTH AND RADIUS OF
C TIP AND HUB VORTICES
C
SUBROUTINE VORTX1(SIG1,SEMAT,STHETAT,SEMTT)
```

```

C COMMON /ANVTX/ NSTR,SSIGR(51),SSEMA(51),SSSTHET(51),SSEMT(51)
COMMON /VTEX1/ ITPTVTX,INBVTX,TAU,ALPHR,CHORD,WTOOT,B1
COMMON /VTEX2/ SAODS(2),SCIRC0(2),SO0(2),SVSDV0(2),SCL(2),
1 SFRL(2)
COMMON /VTEXA/ CLAV,CAV,WTOOT,ABR(51),CI,TVTI
COMMON PRINTD/IPRT,IPR

C PI=4.0*ATAN(1.)
FNBLAD=FLOAT(NBLADE)
IF (ITPTVTX.EQ.0) GO TO 100

C SIGR=SIGT
SEMA=SEMAT
STHETA=STHETAT
SEMT=SEMTT
BETA0=ATAN((1.-STHETA)*SEMT/SEMA)
ALPHR=BETA0
CHORD=SIGR
WTOOT=SEMA/(SEMT*COS(BETA0))
SEMR=SEMA/COS(ALPHR)
VTHEMO=0.5586*WT00T*SQRT(CLAV)
AODST=0.0014*CAV*SQRT(CLAV)*B1/PI
CIRCO=2.0*PI*VTHEMO*AODST
O0T=CIRCO/(AODST*2.*PI)
VSVDV0T=0.0
SAODS(1)=AODST
SCIRC0(1)=CIRCO
SO0(1)=OOT
SVSDV0(1)=VSVDV0T
SCL(1)=CLT
SFRL(1)=FRLT
GO TO 200
C
100
SAODS(1)=0.0
SCIRC0(1)=0.0
SO0(1)=0.0
SVSDV0(1)=0.0
SCL(1)=0.0
SFRL(1)=0.0
IF (IPR.EQ.1) WRITE (16,1000)
200
IF (INBVTX.EQ.0) GO TO 300
SIGR=SSIGR(NSTR)
SEMA=SSEMA(NSTR)
STHETA=SSSTHET(NSTR)
SEMT=SSEMT(NSTR)
BETA0=ATAN((1.-STHETA)*SEMT/SEMA)
ALPHR=BETA0
CHORD=SIGR
WTOOT=SEMA/(SEMT*COS(BETA0))
FRLH=0.2
SEMR=SEMA/COS(ALPHR)
CLH=2.0*SEMT*STHETA/(SEMR*SIGR)
AODSH=0.2*SIGR
CIRCOH=FRLH*CLH/2.*CHORD*WT00T
O0H=CIRCOH/(AODSH*2.*PI)
VSVDV0H=0.2

```

**ORIGINAL PAGE IS
OF POOR QUALITY**

```

SAODS(2)=AODSH
SCIRCO(2)=CIRCOH
SOO(2)=OOH
SVSDVO(2)=VSDV0H
SCL(2)=CLH
SFRL(2)=FRLH
GO TO 400

C
300   SAODS(2)=0.0
      SCIRCO(2)=0.0
      SOO(2)=0.0
      SVSDVO(2)=0.0
      SCL(2)=0.0
      SFRL(2)=0.0
      IF(IPR.EQ.1) WRITE(16,1100)
C
400   CONTINUE
C
C FORMAT STATEMENTS
C
1000  FORMAT(//5X,'NO TIP VORTEX')
1100  FORMAT(//5X,'NO HUB VORTEX')
C
RETURN

C END OF SUBROUTINE VORTX1
END
C----- VORTX2 -----
C
C SUBROUTINE VORTX2 COMPUTES THE VELOCITY FIELD INDUCED BY
C TIP AND HUB VORTICES AT ALL RADIAL LOCATIONS
C
C
SUBROUTINE VORTX2 (IS,N,SIGIT,SEMAT,STHETAT,SEMT,SEMT,SIG1)
COMMON /FANUTY/ NSTR,SSIGR(51),SSEMA(51),SSPHET(51),SSEM1(51)
COMMON /VTEX1/ ITPVTX,IHBVTX,TAU,ALPHR,CHORD,WTO0,B1
COMMON /VTEX2/ SAODS(2),SCIRCO(2),SOO(2),SVSDVO(2),SCL(2),
1 SFRL(2)
COMMON /VTEX3/ SBN(2),SBR(2),SDIST,RAWDS,R,VINRVT(300,2),
1 VISRVT(300,2),HTR,VINRV(300),VISRV(300)
COMMON /VTEX4/ CLAVCAV,WTOOT,ABR(51),CI,TVTI
COMMON/PRINTD/ IPRT,IPR
C
DIMENSION ANL(300),SYO(2)
C
PI=4.0*ATAN(1.0)
FNBLAD=B1
C
IF (ITPVVTX.EQ.0.OR.IHBVVTX.EQ.0) GO TO 100
NVORTX=2
SYO(1)=0.0
FNBLAD=FLOAT(NBLADE)
SYO(2)=RAWDS-HTR*B1/(2.*PI)
GO TO 200
C
100  NVORTX=1
IF (ITPVVTX.EQ.0) GO TO 110
SYO(1)=0.0

```

```

SYO(2)=0.0
GO TO 200
C
SYO(1)=RAWDS-HTR*B1/(2.*PI)
SAODS(1)=SAODS(2)
SCIRCO(1)=SCIRCO(2)
SO0(1)=SO0(2)
VSVDVO(1)=VSVDVO(2)
SCL(1)=SCL(2)
SFRL(1)=SFRL(2)
SBN(1)=SBN(2)

CONTINUE
DO 500 IVORTX=1,NVORTX
AODS=SAODS(IVORTX)
CIRCO=SCIRCO(IVORTX)
OO=SO0(IVORTX)
VSVDVO=VSVDVO(IVORTX)
CL=SCL(IVORTX)
FRL=SFRL(IVORTX)
BN=SBN(IVORTX)
YO=SYO(IVORTX)
SDISTV=SDIST*CHORD/(CAV*B1/PI)
A=(0.0184*SDISTV+0.0014)/(0.184*SDISTV+1.0)*
1 CAV*SQRT(CLAV)*B1/PI
VTHEM=(0.024*SDISTV+0.5586)/(0.0504*SDISTV+1.0)*
1 WTAUT*SQRT(CLAV)
CIRC=2.0*PI*VTHEM*A
CIRC=C1*CIRC
CIRC=CIRC/(1.+SDISTV)**0.25
VSVDV=VSVDVO

IF (ITPVTX.EQ.1.AND.IHBVTX.EQ.1) GO TO 220
IF (ITPVTX.EQ.0) GO TO 210
ZQRT=SDIST*GOS(ALPHR)*R*SIG1*2.*PI/B1
BRRT=TVT1*ZQRT/(16.0*ZQRT+1.0)
BR=BRRT*B1/L2.*PI)
BR=BR+TAU*SIGHT
SBR(1)=BR
IF (IPR.EQ.1) WRITE (16,1000)
GO TO 250
C
210
BR=YO-A
SBR(1)=BR
IF (IPR.EQ.1) WRITE (16,1010)
GO TO 250
C
220
IF (IVORTX.EQ.1) GO TO 230
BR=YO-A
SBR(2)=BR
IF (IPR.EQ.1) WRITE (16,1010)
GO TO 250
C
230
BR=A+TAU*SIGHT
SBR(1)=BR
IF (IPR.EQ.1) WRITE (16,1000)
C

```

DUBO:[CHARLOTTE]RWTV.M.FOR;6

```

250      CONTINUE
C       CIRC=CIRCO
C       VSDV=VSDDV0
C       IF (IPR.EQ.1) THEN
        WRITE (16,1130) AODS
        WRITE (16,1140) A
        WRITE (16,1150) VSDDV0
        WRITE (16,1160) VSDDV
        WRITE (16,1170) CIRCO
        WRITE (16,1180) CIRC
        WRITE (16,1190) BN
        WRITE (16,1200) BN
        WRITE (16,1210) BRRT
END IF

C       RN=FLOAT(N)
RN1=RN-1.0
SANL=1./RN1
ANL(1)=0.0
DO 300 I=2,N
ANL(I)=ANL(I-1)+SANL
CONTINUE

300      ARL=RWD$*(1.-R)
ARL=ARL+TAU*SIGHT
DO 420 I=1,N
FORCED OR FREE VORTEX?

C       RNVL=BN-ANL(I)
RRVL=BR-ARL
RAL=(RNVL**2+RRVL**2)**0.5
IF (RAL.LT.A) GO TO 400

C       FREE VORTEX NORMAL VELOCITY CALCULATION

C       VM=2.*PI*(ARL-YO-BR)
VNN=2.*PI*(ARL-YO+BR)
XN=2.*PI*(ANL(I)-BN)
D1=COSH(VM)-COS(XN)
D2=COSH(VNN)-COS(XN)
VINRVT(I,IVORTX)=CIRC/2.0*(SINH(VM)/D1-SINH(VNN)/D2)
VINRVT(I,IVORTX)=VINRVT(I,IVORTX)*SEMT/SEMT
GO TO 410

C       FORCED VORTEX NORMAL VELOCITY CALCULATION

C       IF (RNVL.GT.RAL) RNVL=RAL
THETAV=ACOS(RNVL/RAL)
X0=A*COS(THETAV)
Y0=A*SIN(THETAV)
IF (ARL.GT.BR) Y1=Y0+BR
IF (ARL.LE.BR) Y1=BR-Y0
X1=BN-X0

C       VM=2.*PI*(Y1-YO-BR)
VNN=2.*PI*(Y1-YO+BR)
XN=2.*PI*(X1-BN)
D1=COSH(VM)-COS(XN)

```

**ORIGINAL PAGE IS
OF POOR QUALITY**

```

D2=COSH(VNN)-COS(XN)
VINPRF=-CIRC/2.0*(SINH(VM)/D1-SINH(VNN)/D2)
VINRVT(I,IVORTX)=(RAL/A)*VINPRF
VINRVT(I,IVORTX)=VINRVT(I,IVORTX)*SEMTT/SEMT

C VORTEX STREAMWISE VELOCITY CALCULATION
C
C
C CONTINUE
110  CONTINUE
      PP=-0.693*(RAL/A)**2
      IF (PP.LT.-40.) PP=-40.
      VISRVT(I,IVORTX)=-VSDF*EXP(PP)
      VISRVT(I,IVORTX)=VISRVT(I,IVORTX)*SEMTT/SEMT

C
C CONTINUE
420  CONTINUE
500  CONTINUE
C
      DO 510 I=1,N
      DO 510 IVORTX=1,IVORTX
      VINRV(I)=VINRV(I)+VINRVT(I,IVORTX)
      VISRV(I)=VISRV(I)+VISRVT(I,IVORTX)
510  CONTINUE

C
C FORMAT STATEMENTS
C
      FORMAT (//,2X,'TIP VORTEX PARAMETERS')
1010  FORMAT (//,2X,'HUB VORTEX PARAMETERS')
1130  FORMAT (5X,'A0/S',8X,'=',F8.4)
1140  FORMAT (5X,'A/S',9X,'=',F8.4)
1150  FORMAT (5X,'VSDF0/U',5X,'=',F8.4)
1160  FORMAT (5X,'VSDF/U',6X,'=',F8.4)
1170  FORMAT (5X,'CIRCO/(S*U)',1X,'=',F8.4)
1180  FORMAT (5X,'CIR/(S*U)',3X,'=',F8.4)
1200  FORMAT (5X,'BN',10X,'=',F8.4)
1210  FORMAT (5X,'BRRT',10X,'=',F8.4)
C
      RETURN

C END OF SUBROUTINE VORTX2
END

C
C-----* SUBROUTINE GAMCAL -----
C-----* SPECIFIC HEAT RATIO CALCULATION FOR AIR AT LOW PRESSURES
C-----* FROM KEENAN AND KAYE GAS TABLES
C
C
SUBROUTINE GAMCAL(TAMB,GAMMA)
C
      TC=-25.0
      GAMMA=1.402
      IF (TAMB.LT.TC) RETURN
      IF (TAMB.GT.200.0) GO TO 1
      GAMMA=1.402 - 0.00001778*(TAMB+25.0)
      RETURN
1    CONTINUE
      GAMMA=1.398 - 0.000043333*(TAMB - 200.0)
      RETURN

```

```

C-----* SUBROUTINE PITCH1 -----
C
C   CALCULATE BLADE COORDINATE CHANGES DUE TO
C   PITCH ANGLE CHANGE RELATIVE TO 'DESIGN' SETTING
C   --- ALSO CALCULATE FACE ALIGNMENT (FA) AND MID-CHORD
C   ALIGNMENT (MCA) ---
C
C   SUBROUTINE PITCH1
C
C   COMMON /COM12/ NZ,DTR,RD,VO,CO,SXOCH(51)
C   COMMON /BLADE1/ THETA1(51), SIGR1(51) , DPINT1(51),
C   1  CHORD1(51) , TMOC1(51) , ALPHAI(51),
C   1  Z1(51) , ZMC1(51) , YMCI(51),
C   1  BETAP1(51) , MCA1(51) , FA1(51),
C   1  BETPP1(51) , DELBPI , SCD1(51),
C   1  ENTI , NB1
C
C   REAL MCA1
C
C   PI=3.1415926
C   DELBPI=R*DTR*DELBPI
C
C   DO 10 I=1,NZ
C
C   D2=0.5*CHORD1(I)*SIN(DTR*BETAP1(I))
C   DY=0.5*CHORD1(I)*COS(DTR*BETAP1(I))
C   ZLE=2*MC1(I)-D2
C   ZTE=2*MC1(I)+D2
C   YLE=MC1(I)-DY
C  YTE=MC1(I)+DY
C
C   RLE=SQRT(ZLE*ZLE+YLE*YLE)
C   RMC=SQRT(ZMC1(I)**2+YMCI(I)**2)
C   RTE=SQRT(ZTE*ZTE+YTE*YTE)
C
C   IF (ZMC1(I).EQ.0.0) GO TO 20
C   PMC=ATAN2(YMC1(I),ZMC1(I))
C   GO TO 30
C   CONTINUE
C
C   PMC=0.0
C   IF (YMC1(I).LT.0.0) PMC=-0.5*PI
C   IF (YMC1(I).GT.0.0) PMC= 0.5*PI
C   CONTINUE
C   IF (ZLE.EQ.0.0) GO TO 40
C   PLE=ATAN2(YLE,ZLE)
C   GO TO 50
C   CONTINUE
C   PLE=0.0
C   IF (YLE.LT.0.0) PLE=-0.5*PI
C   IF (YLE.GT.0.0) PLE= 0.5*PI
C   CONTINUE
C   IF (ZTE.EQ.0.0) GO TO 60
C
      20
      30
      40
      50

```

ORIGINAL PAGE IS
OF POOR QUALITY

```

PTE=ATAN2(YTE,ZTE)
GO TO 70
CONTINUE
PTE=0.0
IF (YTE .LT. 0.0) PTE=-0.5*PI
IF (YTE.GT.0.0) PTE= 0.5*PI
CONTINUE
PPMC=PMC-DELBPIR
PPLC=PPLC-DELBPIR
PPTE=PPTE-DELBPIR
PPTE=PPTE-DELBPIR

      C
YMCY=RMC*SIN(PPMC)
YLEP=RLE*SIN(PPLE)
YTEP=RTE*SIN(PPTE)

      C
ZMCP=RMC*COS(PPMC)
ZLEP=RLE*COS(PPLE)
ZTEP=RTE*COS(PPTE)

      C
TOP = ZTEP - ZLEP
BOT = YTEP-YLEP
IF (BOT.EQ.0.0) GO TO 80
BETPP1(I)=ATAN2(TOP,BOT)
GO TO 90
CONTINUE
BETPP1(I)=0.0
IF (TOP.LT.0.0) BETPP1(I)=-0.5*PI
IF (TOP.GT.0.0) BETPP1(I)= 0.5*PI
CONTINUE
90
      C
COSBPP=COS(BETPP1(I))
SINBPP=SIN(BETPP1(I))
FA1(I) = ZMCP*COSBPP - YMCP*SINBPP
MC1(I) = YMCP*SINBPP + YMCP*COSBPP
BETPP1(I)=RTD*BETPP1(I)
CONTINUE
80
CONTINUE
RETURN
END

      C-----* SUBROUTINE PITCH2 -----
      C
      C-----* CALCULATE BLADE COORDINATE CHANGES DUE TO
      C-----* PITCH ANGLE CHANGE RELATIVE TO 'DESIGN' SETTING
      C-----* ALSO CALCULATE FACE ALIGNMENT (PA) AND MID-CHORD
      C-----* ALIGNMENT (MCA) -----
      C
      C-----* SUBROUTINE PITCH2 -----
      C
      C-----* COMMON/COM12/ NZ,DTR,RTD,VO,CO,SXOCH(51)
      C-----* COMMON/BLADE2/ THETA2(51), SIGR2(51) , DPINT2(51),
      C-----* CHORD2(51),TMOC2(51) ,ALPHA2(51),
      C-----* Z2(51) , ZMC2(51) , YMCA2(51) ,
      C-----* BETAP2(51) , MCA2(51) , FA2(51) ,
      C-----* BETPP2(51) , DELBPI2 , SCD2(51),
      C-----* EMT2 , NB2
      C

```

```

C
C      REAL MC2
C
C      PI=3.1415926
      DELBP2R=DTR*DELBP2
C
C      DO 10 I=1,NZ
C
C      DZ=0.5*CHORD2(I)*SIN(DTR*BETAP2(I))
      DY=0.5*CHORD2(I)*COS(DTR*BETAP2(I))
      ZLE=ZMC2(I)-DZ
      ZTE=2MC2(I)+DZ
      YLE=YMC2(I)-DY
     YTE=YMC2(I)+DY
C
      RLE=SQRT(ZLE*ZLE+YLE*YLE)
      RMC=SQRT(ZMC2(I)**2+YMC2(I)**2)
      RTE=SQRT(ZTE*ZTE+YTE*YTE)
C
      IF(ZMC2(I).EQ.0.0) GO TO 20
      PMC=ATAN2(YMC2(I),ZMC2(I))
      GO TO 30
C
      CONTINUE
      PMC=0.0
      IF(YMC2(I).LT.0.0) PMC=-0.5*PI
      IF(YMC2(I).GT.0.0) PMC= 0.5*PI
      CONTINUE
      IF(ZLE.EQ.0.0) GO TO 40
      PLE=ATAN2(YLE,ZLE)
      GO TO 50
C
      CONTINUE
      PLE=0.0
      IF(YLE.LT.0.0) PLE=-0.5*PI
      IF(YLE.GT.0.0) PLE= 0.5*PI
      CONTINUE
      IF(ZTE.EQ.0.0) GO TO 60
      PTE=ATAN2(YTE,ZTE)
      GO TO 70
C
      CONTINUE
      PTE=0.0
      IF(YTE.LT.0.0) PTE=-0.5*PI
      IF(YTE.GT.0.0) PTE= 0.5*PI
      CONTINUE
      PPMC=PMC-DELBP2R
      PPLE=PLE-DELBP2R
      PPTE=PTE-DELBP2R
C
      YMCP=RMC*SIN(PPMC)
      YLEP=RLE*SIN(PPLE)
      YTEP=RTE*SIN(PPTE)
C
      ZMCP=RMC*COS(PPMC)
      ZLEP=RLE*COS(PPLE)
      ZTEP=RTE*COS(PPTE)
C

```

```

TOP = ZSTEP - ZLEP
BOT = YSTEP-YLEP
IF (BOT.EQ.0.0) GO TO 80
BETPP2(I)=ATAN2(TOP,BOT)
GO TO 90
CONTINUE
80
BETPP2(I)=0.0
IF (TOP.LT.0.0) BETPP2(I)=-0.5*PI
IF (TOP.GT.0.0) BETPP2(I)= 0.5*PI
CONTINUE
C
COSBPP=COS(BETPP2(I))
SINBPP=SIN(BETPP2(I))
FA2(I) = 2*MCPP*COSBPP - YMCP*SINBPP
HCA2(I) = 2*MCPP*SINBPP + YMCP*COSBPP
BETPP2(I)=RTD*BETPP2(I)
C
10
CONTINUE
RETURN
END
C
C-----* SUBROUTINE LSPFIT -----
C
C INTEGRATE OR INTERPOLATE USING A PARABOLA WHICH PASSED THROUGH THE ITH
C AND (I+1) POINTS BUT MISSES THE (I-1) AND (I+2) POINTS (IF THEY BOTH
C EXIST) SUCH THAT THE SQUARE OF THE DEVIATION IS A MINIMUM. NOTE
C THAT I IS GENERALLY SELECTED SUCH THAT
X(I) .LE. XC .LT. X(I+1)
THE EQUATION FOR THE PARABOLA IS
Y-Y(I) = B*(X-X(I)) + C*(X-X(I))**2
C
SUBROUTINE LSPFIT(X,Y,NPTS,XC,YC,NXC,ND,AAA)
DIMENSION AAA(10)
DIMENSION X(10),Y(10),XC(10),YC(10)
NOTE. THE DIMENSION Q10# DOES NOT NEED TO AGREE WITH THE CALLING PROGRAM
C
INPUT-
X, Y          PTS. ON CURVE
NPTS          NO. OF X
XC            LIST OF X AT WHICH CALC TO BE DONE
YC(1)          INTEGRATION CONSTANT IF ND=-1
NXC          NO. OF XC
ND            =0 TO GET COORD, =1 TO GET 1ST DERIVATIVE,
              =-1 FOR INTEGRATION
C
OUTPUT
YC            COORDINATE OR DERIVATIVE AT XC OR
YC(IC)= INTEGRAL(Y*DX) FROM XC(1) TO XC(IC) WHERE IC=2, NXC
C
C NOTES-
C   XC@ MAY BE IN EITHER ASCENDING OR DESCENDING ORDER.
C   FOR INTEGRATION @X@ MUST BE IN THE SAME ORDER AS @Y@. FOR INTERPOLATION
C   NO SPECIAL ORDER IS REQUIRED.
C
COMMON /CLSPFF/ I
LOGICAL WITHIN
C
94

```

```

N      = NPTS-1
I      = MAX0(1,MIN0(I,N))
IF(ND.EQ.(-1)) I=1
ISAVE = 0
SIGN = SIGN(1.,X(N+1)-X(1))

C BEGIN INTERPOLATION LOOP FOR XC(IC)  IC=1,NC
C   IC = 1
C LOCATE APPROPRIATE INTERVAL
C   WITHIN=.FALSE.
100   NCOUNT= N
      IF(NCOUNT) 119,103,103
103   NCOUNT= NCOUNT-1
      XI = X(I)
      XD = XC(IC)-XI
      IF(N) 104,120,104
      IF(SGN.XD) 105,107,110
104   F LT.0. (F IS THE FRACTIONAL POSITION IN THE INTERVAL)
C   F.GT.0. IF(X(I+1).NE.XI) GO TO 120
105   IF(SGN*(XC(IC)-X(I+1))) 120,112,114
110   F.GT.0.
      IF(SGN*(XC(IC)-X(I+1))) 120,112,114
      F.EQ.1.0. CHECK FOR INTEGRATION AND DOUBLE POINT BEFORE INCREMENTING
C   IF((ND.EQ.(-1)) .OR. (I.NE.N .AND. X(I+1).EQ.X(I+2))) GO TO 120
112

C   F.GT.1.0
114   IF(I.LE.N) GO TO 120
      IF(ND.EQ.(-1)) GO TO 122
      I = I+1
116   GO TO 102
CONTINUE

C PRELIMINARY CALCULATIONS FOR INTERPOLATION OR INTEGRATION
C   WITHIN=.TRUE.
120   IF(I-ISAVE) 124,129,124
122   ISAVE = I
124   YI = X(I)
      X3 = X(I+1)-XI
      Y3 = Y(I+1)-YI
      C = 0.
      TOP = 0.
      BOT = 0.
      IF(I.LE.1) GO TO 127
      X1 = X(I-1)-XI
      X13 = X(I-1)-X(I+1)
      TOP = X1*(Y3*X1-(Y(I-1)-YI)*X3)*X13
      BOT = X1*X13*X13*X3
      IF(I.GE.N .OR. (XD.EQ.0. .AND. BOT.NE.0.)) GO TO 128
      X4 = X(I+2)-XI

```

**ORIGINAL PAGE IS
OF POOR QUALITY**

```

X43 = X(I+2)-X(I+1)
TOP = TOP + X4*(Y3*X4-(Y(I+2)-YI)*X3)*X43
BOT = BOT + X4*X4*X43*X43*X3
128 IF(BOT.NE.0.) C = -TOP/BOT
B = 0.
IF(N.GT.0 .AND. X3.NE.0.) B = (Y(I+1)-YI)/X3 - C*X3
IF(ND) 130,140,141

C ND=-1, INTEGRATE
130 IF(.NOT.WITHIN) XD=X3
      S1 = (YI+(B/2.+C/3.*XD)*XD)*XD
      IF(WITHIN) GO TO 135
      C  #1# IS BEING INCREMENTED TO FIND APPROPRIATE INTERVAL. HENCE,
      C CUMULATE THE INTEGRAL OF THE ITH INTERVAL.
      SA = SA + S1
      GO TO 116
      APPROPRIATE INTERVAL FOUND. X(I)-XC(IC)-X(I+1)
135 IF(IC.EQ.1) SA=YC(IC)-S1
      IF(IC.NE.1) YC(IC)=SA+S1
      GO TO 150

C ND=0, INTERPOLATE FOR COORDINATES
140 YC(IC)= YI + (B + C*XD)*XD
      GO TO 150

C ND=1, FIRST DERIVATIVE
141 YC(IC)= B + 2.*C*XD
      GO TO 150
      IC = IC+1
      AKA(IC-1)=2.*C
      IF(NXC-IC) 900,160,160
      IF(ND.NE.(-1).AND.XC(IC).EQ.XC(IC-1)) I=I+1
      GO TO 100
      RETURN
      END

```

C. Definition of Input/Output Parameters

This section of the appendix defines all input and output parameters of the Rotor Wake/Tip Vortex Model (RWTVM) computer program. The input is read into the computer program in terms of two input files, one for each rotor.

Input Parameters

Input parameters are grouped under:

- a. Blade geometry
- b. Blade aerodynamic performance and ambient conditions
- c. Wake parameters (for forward rotor only)
- d. Tip vortex parameters (for forward rotor only)

a. Blade Geometry Input Parameters

BETAP - Design or reference blade section pitch angle, degree; input one value for each streamline.

BETA34 - Pitch angle at 3/4 radius ratio (R/R_{tip}) of the blade for a particular operating condition.

CHORD - Blade chord normalized by tip diameter, input one value for each streamline.

DELBP - Pitch angle change from design, degree

DT - Tip diameter, feet

HTR - Hub-to-tip radius ratio

NB - Number of rotor blades

NP - Number of propellers

NZ - Number of spanwise stations
Maximum value = 10 = default value

Note: Streamline Number 1 should be the tip streamline.

PCTCL - Percent span clipped (applies to aft rotor with clipped tip)

TMOC - Maximum blade section thickness normalized by chord.
Input one value for each streamline.

XPCA - Distance between the pitch change axes normalized by front rotor tip diameter

YMC - Tangential location of blade midchord line relative to pitch change axis normalized by tip diameter at design pitch angle. Input one value for each streamline.

Z - Radius normalized by tip radius.
Input one value for each streamline.

ZMC - Axial location of blade midchord line relative to pitch change axis, normalized by tip diameter, at design pitch angle. Input one value for each streamline.

b. Blade Aerodynamic Performance and Ambient Input Parameters

ALPHA - Blade section angle of attack, degrees; input one value for each streamline.

NCASE - Number of cases
Default value = 1

PAMB - Ambient pressure (static pressure) in psi

RPM - RPM of the rotor (physical)

SHP - Shaft horsepower of the rotor (physical)

TAMB - Ambient temperature (static temperature) in ° F

VO - Flight speed, fps

c. Wake Parameters

BETAW - Parameter to account for wake flow angle variation from freestream.
Default value = 0.0.

IPRNTW - Option to print the velocity profiles
IPRNTW = 0 - No
IPRNTW = 1 - Yes
Default value = 0

IRW - Option to compute wake/tip vortex gust field
 IRW = 0 - No
 IRW = 1 - Yes
 Default value = 1

ISHAPE - Wake tangential profile option
 ISHAPE = 1 - Hyperbolic secant profile
 ISHAPE = 2 - Gaussian profile
 Default value = 2

IWAKE - Rotor wake model
 IWAKE = 1 - Linear rational function model
 IWAKE = 2 - Kemp and Sears model
 IWAKE = 3 - Mugridge and Morfey model
 Default value = 2

NSTEP Number of points in the velocity profile across one blade spacing
 Maximum value: NSTEP = 150

NWHM - Number of sequential harmonics required for Fourier analysis.
 Maximum value: NWHM = 21.

SCD - Local section drag coefficient.
 Input one value for each streamline.

VREF - Reference velocity by which the gust upwash velocity harmonic coefficients are normalized, fps
 Default value: VREF = 10.0.

WTIV - Inviscid velocity gradient, normalized by wheel speed.
 Default value: WTIV = 0.0.

d. Tip Vortex Parameters

CI - Circulation index for tip vortex strength (see Eq. 13a).
 Default value: 1.0.

IHBVTX - Option to include hub vortex
 IHBVTX = 0 - No
 IHBVTX = 1 - Yes
 Default value: IHBVTX = 0

ITPVTX - Option to include tip vortex
 ITPVTX = 0 - No
 ITPVTX = 1 - Yes

PCTVTEX - Percent outboard span whose circulation gets rolled up into tip vortex.
 Default value: PCTVTEX = 30.0.

SBN(1) - Tangential distance normalized by tip blade spacing for the tip vortex center (see Figure 2, b_t).

SBN(2) - Tangential distance normalized by hub blade spacing for the hub vortex center.

TAU - Tip clearance normalized by the rotor chord at the tip.
Default value: TAU = 10.0.

TVTI - Tip vortex trajectory index (see Eq. 19).
Default value: TVTI = 2.0.

Output Parameters

Output parameters are grouped under:

- a. Blade parameters
- b. Wake parameters
- c. Tip vortex parameters
- d. Velocity profile parameters
- e. Gust spectral parameters

a. Blade Parameters

BETAP - Pitch angle for the case under study, degrees

CD - Blade section drag coefficient

CHORD - Chord normalized by tip diameter

CL - Blade section lift coefficient

FA - Face alignment normalized by tip diameter

MCA - Midchord alignment normalized by tip diameter

R/RT - Radius normalized by tip radius

SHP/AA - Shaft Horsepower/(Annulus Area)

SHP/D2 - Shaft Horsepower/(Tip Diameter)²

b. Wake Parameters

CD - Blade section drag coefficient

SDIST - Streamwise distance to 1/4 chord point of aft rotor from forward rotor trailing edge normalized by forward rotor chord.

WAKE - Semiwake width normalized by blade spacing
WIDTH

WD/UT - Wake centerline defect normalized by local wheel speed

WFS/UT - Free-stream velocity normalized by local wheel speed

X/C - Axial distance to leading edge of aft rotor from trailing edge of forward rotor normalized by forward rotor chord

c. Tip Vortex Parameters

A/S - Radius of the tip vortex core normalized by forward rotor tip spacing at the 1/4 chord point of the aft rotor.

A0/S - Radius of the tip vortex core normalized by forward rotor tip spacing at the trailing edge of forward rotor tip.

BN - Tangential location of the tip vortex normalized by tip blade spacing.

BRRT - Spanwise location of the tip vortex from the rotor tip normalized by tip radius.

CIR/ (S*U) - Circulation of the tip vortex core at the 1/4 chord of aft rotor normalized by the product of forward rotor tip spacing and tip speed.

CIRCO/ (S*U) - Circulation of the tip vortex core at the trailing edge of forward rotor tip normalized by the product of forward rotor tip spacing and tip speed.

VSDV/U - Streamline velocity defect of tip vortex core at 1/4 chord of aft rotor normalized by blade tip speed.

VSDVO/U - Streamwise velocity defect of tip vortex core at the trailing edge of forward rotor tip normalized by blade tip speed.

d. Velocity Profile Parameters

ALPHA - Flow angle of the velocity vector relative to aft rotor to the axial flow direction, degrees

I - Index for tangential profile

S - Tangential distance from wake centerline divided by blade spacing

THETA - Angular location relative to the wake centerline, degrees

- VN - Normal (upwash) velocity relative to aft rotor divided by forward rotor wheel speed
- VS - Streamwise velocity relative to aft rotor divided by forward rotor wheel speed
- VT - Total (vector sum of VN and VS) velocity relative to aft rotor divided by forward rotor wheel speed
- VPN - Normal (upwash) perturbation velocity from the free stream relative to aft rotor divided by forward rotor wheel speed. Fourier coefficients are evaluated for this profile.
- VPS - Streamwise perturbation velocity from the free stream relative to aft rotor divided by forward rotor wheel speed.
- VPT - Total (vector sum of VPN and VPS) perturbation velocity relative to aft rotor divided by forward rotor wheel speed
- WN - Normal velocity relative to forward rotor divided by forward rotor wheel speed
- WS - Streamwise velocity relative to forward rotor divided by forward rotor wheel speed
- WT - Total (vector sum of WN and WS) velocity relative to forward rotor divided by forward rotor wheel speed

e. Gust Spectral Parameters

AERO PHASE LAG - Phase lag relative to tip streamline, degrees

2*CMOD - 2X amplitude of complex Fourier coefficient of upwash perturbation velocity divided by wheel speed (factor of 2 to take into account both positive and negative gust harmonic numbers)

20*LOG - dB level of the (2*CMOD) of upwash perturbation (2XCMOD) velocity, VREF, defined by:

$$20 \log (2*CMOD*WHEEL SPEED/VREF)$$

NH - Gust harmonic number

PHASE - Phase of the complex Fourier coefficient of upwash perturbation velocity, radian

D. A Sample Input/Output Case

A sample input/output case enclosed in this section pertains to F7-A7 blade geometry at 80% design rpm in a 9x8 configuration at a flight Mach number of 0.25 (Test Point 3704). The axial distance between the pitch change axes equals 0.2408*tip diameter of forward rotor. The spanwise variation is prescribed in terms of geometric and aerodynamic data at ten streamlines.

The input is prescribed in terms of two data files, one for forward rotor and another one for aft rotor.

T F73704V.DAT
\$INPUT
NCASE=2
DT=2.05 HTR=0.428 NB=9
SHR=205.9 RPM=6722 DELBF=-18.529
VO=284.74 TAMB=48.65 PAMB=14.7 NF=1
XPCA=.2408 BETAS4=41.8
NZ/Z=
1. .979 .9576 .9144 .8221 .7184 .594 .5189 .4762 .4279
ZMC=
.05978 .05538 .05012 .04047 .01881 -.00106 -.01271 -.01086
-.00674 .00092
YMC=
.06248 .05609 .04970 .03770 .01654 .00035 -.00568 -.00341
-.00035 .00248
CHORD=
.0327 .0561 .0703 .088 .1058 .1200 .1279 .1278 .1271 .126
TMOC=
.04 .025 .0218 .02 .023 .0299 .0462 .064 .0805 .1025
BETAP=
43.4 46.2 48 50.2 53.8 58.3 64.8 68.7 70.4 70.7
THETA=
.0383 .056 .072 .087 .145 .202 .272 .3325 .381 .44
ALPHA=
10*0.0
ISHAPE=2, BETAW=0.0, NWHM=10
VREF=10.0, NSTEP=101, IRW=1, IWAKE=2
IPRN=0, SCD=10*.015 WTIV=0.0
ITPVTY=1 IHBVTX=0 SBN=.5 0. TAU=10.0 CI=1.0 TVTI=2.0

Input File for the Forward Rotor

ORIGINAL PAGE IS
OF POOR QUALITY

\$ T A73704.DAT
\$ INPUT
NCASE=2
DT=2.00 HTR=0.4159 NB=8
SHR=208.3 RPM=6718 DELBP=-17.428
BETA34=41.4
NZ/Z=
1. .9776 .9554 .9105 .8015 .7105 .5845 .5078 .4644 .4159
ZMC=
.05442 .04931 .04565 .03616 .01351 -.00314 -.01665 -.01454
-.00877 -.00073
YMC=
.06574 .05917 .05340 .04127 .01812 .00365 -.00533 -.00373
-.00095 .00329
CHORD=

Input File for the Aft Rotor

0 **** RWTUM ****

UDF ROTOR GUST PREDICTION PROGRAM

BETAP SURFACE APPROXIMATION MODEL
WAKE/VORTEX MODEL INCLUDED

FORWARD CRUFILE IS F73704V.DAT

AFT CRUFILE IS A73704.DAT

DATE: 6-NOV-87, TIME: 17:21:41

*** ROTOR 1 INPUT PARAMETERS - CASE NO. 1 ***

PROPELLER TIP DIAMETER DT = 2.0500 FT.

NUMBER OF BLADES NB = 9

SHAFT HORSEPOWER SHP = 205.90

ROTATIVE SPEED (RPM) = 6722.0

FLIGHT VELOCITY VO (FPS) = 284.74

AMBIENT TEMPERATURE TAMB = 48.65 DEG. F

AMBIENT PRESSURE PAMB = 14.700 PSIA

NUMBER OF PROPELLERS NP = 1

*** ROTOR 2 INPUT PARAMETERS - CASE NO. 1 ***

PROPELLER TIP DIAMETER DT = 2.0000 FT.

NUMBER OF BLADES NB = 8

SHAFT HORSEPOWER SHP = 208.30

ROTATIVE SPEED (RPM) = 6718.0

FLIGHT VELOCITY VO (FPS) = 284.74

AMBIENT TEMPERATURE TAMB = 48.65 DEG. F

AMBIENT PRESSURE PAMB = 14.700 PSIA

NUMBER OF PROPELLERS NP = 1

XPCA = 0.2408
IRW = 1
IWAKE = 2
TIP SPEED MACH NO. = 0.6527
FLIGHT MACH NO. = 0.2576
HELICAL MACH NO. = 0.7017

TIP SPEED MACH NO. = 0.6364
FLIGHT MACH NO. = 0.2576
HELICAL MACH NO. = 0.6865

TABLE OF BLADE SECTION PROPERTIES - ROTOR 1

SECTION	R/RT	CHORD	TM/C	ALPHA	BETAP	MCA	FA	CL	CD
1	1.0000	0.0327	0.0400	0.00	26.35	0.0865	0.0005	0.9956	0.0150
2	0.9790	0.0561	0.0250	0.00	31.15	0.0788	-0.0022	0.8283	0.0150
3	0.9576	0.0703	0.0218	0.00	32.95	0.0705	-0.0034	0.8287	0.0150
4	0.9144	0.0880	0.0200	0.00	35.15	0.0552	-0.0031	0.8457	0.0150
5	0.8221	0.1058	0.0230	0.00	38.75	0.0249	-0.0022	0.9282	0.0150
6	0.7184	0.1200	0.0299	0.00	43.25	0.0007	-0.0009	0.9686	0.0150
7	0.5940	0.1278	0.0462	0.00	49.75	-0.0139	-0.0003	0.9623	0.0150
8	0.5189	0.1278	0.0640	0.00	53.85	-0.0114	-0.0007	0.9820	0.0150
9	0.4762	0.1271	0.0805	0.00	55.35	-0.0065	-0.0019	1.0044	0.0150
10	0.4279	0.1260	0.1025	0.00	55.65	0.0017	-0.0020	1.0038	0.0150

TABLE OF BLADE SECTION PROPERTIES - ROTOR 2

SECTION	R/RT	CHORD	TM/C	ALPHA	BETAP	MCA	FA	CL
1	1.0000	0.0343	0.0400	0.00	31.92	0.0849	-0.0084	1.1659
2	0.9776	0.0577	0.0250	0.00	34.32	0.0763	-0.0106	0.9693
3	0.9554	0.0738	0.0212	0.00	35.32	0.0695	-0.0100	0.9335
4	0.9105	0.0917	0.0210	0.00	36.92	0.0542	-0.0087	0.9336
5	0.8015	0.1110	0.0238	0.00	39.92	0.0217	-0.0065	0.9468
6	0.7105	0.1235	0.0298	0.00	42.62	-0.0006	-0.0048	0.9807
7	0.5845	0.1315	0.0471	0.00	47.22	-0.0171	-0.0035	0.9268
8	0.5078	0.1314	0.0662	0.00	50.32	-0.0147	-0.0031	0.9113
9	0.4644	0.1300	0.0860	0.00	51.42	-0.0083	-0.0029	0.9125
10	0.4159	0.1286	0.1048	0.00	50.82	0.0008	-0.0033	0.8917

ROTOR 1

EFFECTIVE AERO SHP	=	205.90
ROTOR ANNULUS AREA	=	2.696 SQ FT
DISK LOADING SHP/D2	=	48.99
DISK LOADING SHP/AA	=	76.37

POWER COEFFICIENT CP = 0.917

ROTOR 2

EFFECTIVE AERO SHP	=	208.30
ROTOR ANNULUS AREA	=	2.598 SQ FT
DISK LOADING SHP/D ²	=	52.08
DISK LOADING SHP/AA	=	80.17
POWER COEFFICIENT CP	=	1.051

ROTOR WAKE/VORTEX FLOW PROGRAM

CASE NUMBER

---- STREAMLINE NUMBER 1 ----

CD = 0.0150

108

NO HUB VORTEX	
WFS/UT	= 1.0286
WD/UT	= 0.0082
X/C	= 6.7121
SDIST	= 18.1786
WAKE WIDTH	= 0.0871

TIP VORTEX PARAMETERS

A0/S	= 0.0003
A/S	= 0.0101
VSDVO/U	= 0.0000
VSDV/U	= 0.0000
CIRCO/(S^U)	= 0.0009
CIR/(S^U)	= 0.0186
BN	= 0.5000
BRRT	= 0.1099

HARMONIC CONTENT OF ROTOR WAKE/VORTEX FLOW

NH	2 * CMOD	PHASE	20 * LOG(2 * CMOD), DB
1	0.004165	0.000008	-10.44
2	0.002783	-0.000022	-13.94
3	0.000076	-0.001055	-45.18
4	0.000926	-0.000096	-23.50
5	0.000437	-0.000192	-30.03

CD =	0.0150
WFS/UT	= 1.0106
A/S	= 0.0003
WD/UT	= 0.0148
X/C	= 3.6512
SDIST	= 9.8043
WAKE WIDTH	= 0.1081
BN	= 0.5000
BRRT	= 0.1094

CASE NUMBER
109

ROTOR WAKE/VORTEX FLOW PROGRAM

--- STREAMLINE NUMBER 2 ---

CD =	0.0150
A0/S	= 0.0003
A/S	= 0.0076
VSDV0/U	= 0.0000
VSDV/U	= 0.0000
CIRCO/(S*U)	= 0.0009
CIR/(S*U)	= 0.0164
BN	= 0.5000
BRRT	= 0.1094

TIP VORTEX PARAMETERS

NH	2*CMOD	PHASE	20*LOG(2*CMOD), DB
1	0.008634	0.000002	-4.30
2	0.006287	0.000006	-7.05
3	0.000296	0.000127	-33.58
4	0.001974	0.000026	-17.11
5	0.000531	-0.000056	-28.51
6	0.000715	0.000038	-25.93
7	0.000296	0.000035	-33.61
8	0.000232	-0.000066	-35.71
9	0.000099	0.0000208	-43.14
10	0.000060	-0.0000792	-47.44

HARMONIC CONTENT OF ROTOR WAKE/VORTEX FLOW

NH	2*CMOD	PHASE	20*LOG(2*CMOD), DB
1	0.008634	0.000002	-4.30
2	0.006287	0.000006	-7.05
3	0.000296	0.000127	-33.58
4	0.001974	0.000026	-17.11
5	0.000531	-0.000056	-28.51
6	0.000715	0.000038	-25.93
7	0.000296	0.000035	-33.61
8	0.000232	-0.000066	-35.71
9	0.000099	0.0000208	-43.14
10	0.000060	-0.0000792	-47.44

ROTOR WAKE/VORTEX FLOW PROGRAM

CASE NUMBER

--- STREAMLINE NUMBER 3 ---

CD = 0.0150	
WFS/UT =	0.9951
WD/UT =	0.0192
X/C =	2.7973
SDIST =	7.3895
WAKE WIDTH =	0.1161

TIP VORTEX PARAMETERS

A0/S	= 0.0003
A/S	= 0.0065
VSDVO/U	= 0.0000
VSDV/U	= 0.0000
CIRCO/(S*U)	= 0.0009
CIR/(S*U)	= 0.0149
BN	= 0.5000
BRRT	= 0.1091

HARMONIC CONTENT OF ROTOR WAKE/VORTEX FLOW

NH	2*CMOD	PHASE	20*LOG(2*CMOD), DB
1	0.014223	0.000001	-0.15
2	0.010431	0.000003	-2.84
3	0.001720	0.000019	-18.50
4	0.003338	0.000009	-12.74
5	0.000131	-0.000079	-40.88
6	0.001104	0.000001	-22.35
7	0.000141	0.000212	-40.23
8	0.0000319	-0.000044	-33.14
9	0.000033	-0.000362	-52.81
10	0.000077	-0.000103	-45.51

110

ROTOR WAKE/VORTEX FLOW PROGRAM

CASE NUMBER

--- STREAMLINE NUMBER 4 ---

CD = 0.0150	
WFS/UT =	0.9739
WD/UT =	0.0257
X/C =	2.0945
SDIST =	5.3166
WAKE WIDTH =	0.1211

TIP VORTEX PARAMETERS

A0/S	=	0.0003
A/S	=	0.0053
VSDVO/U	=	0.0000
VSDV'/U	=	0.0000
CIRCO/(S*U)	=	0.0009
CIR/(S*U)	=	0.0130
BN	=	0.5000
BRRT	=	0.1086

HARMONIC CONTENT OF ROTOR WAKE/VORTEX FLOW

NH	2*CMOD	PHASE	20*LOG(2*CMOD), DB
1	0.021909	0.000001	3.20
2	0.018422	0.000004	1.69
3	0.006762	0.000005	-7.01
4	0.008444	0.000008	-5.08
5	0.003373	-0.000006	-13.05
6	0.004304	0.000015	-10.93
7	0.002292	-0.000023	-16.41
8	0.002359	0.000028	-16.16
9	0.001606	0.000045	-19.48
10	0.001410	0.000025	-20.63

ROTOR WAKE/VORTEX FLOW PROGRAM

CASE NUMBER

--- STREAMLINE NUMBER 5 ---

CD =	0.0150	=	0.0003
WFS/UT	=	0.9417	
WD/UT	=	0.0354	
X/C	=	1.5860	
SDIST	=	3.6393	
WAKE WIDTH	=	0.1173	

TIP VORTEX PARAMETERS

A0/S	=	0.0003
A/S	=	0.0041
VSDVO/U	=	0.0000
VSDV'/U	=	0.0000
CIRCO/(S*U)	=	0.0009
CIR/(S*U)	=	0.0107
BN	=	0.5000
BRRT	=	0.1078

HARMONIC CONTENT OF ROTOR WAKE/VORTEX FLOW

NH	2^*CMOD	PHASE	$20 \cdot \log(2^*CMOD)$, DB
1	0.012393	0.000002	-2.67
2	0.016077	0.000000	-0.41
3	0.002908	0.000013	-15.26
4	0.008159	-0.000001	-6.30
5	0.001673	0.000004	-20.07
6	0.004238	-0.000001	-11.99
7	0.001564	-0.000022	-20.65
8	0.002238	0.000020	-17.54
9	0.001298	0.000033	-22.27
10	0.001282	0.000049	-22.38

ROTOR WAKE/VORTEX FLOW PROGRAM

CASE NUMBER

--- STREAMLINE NUMBER 6 ---

CD =	0.0150	
WFS/UT	=	0.9161
WD/UT	=	0.0467
X/C	=	1.3019
SDIST	=	2.6103
WAKE WIDTH	=	0.1107

TIP VORTEX PARAMETERS

A0/S	=	0.0003	
A/S	=	0.0032	
VSDVO/U	=	0.0000	
VSDV/U	=	0.0000	
CIRCO/(S*U)	=	0.0009	
CIR/(S*U)	=	0.0088	
BN	=	0.5000	
BRRT	=	0.1071	

HARMONIC CONTENT OF ROTOR WAKE/VORTEX FLOW

NH	2^*CMOD	PHASE	$20 \cdot \log(2^*CMOD)$, DB
1	0.005206	0.000001	-11.38
2	0.016019	0.000000	-1.62
3	0.000405	-0.000013	-33.56
4	0.008804	0.000002	-6.81
5	0.000241	0.000047	-38.06
6	0.004564	0.000008	-12.52
7	0.000566	-0.000051	-30.65

DUB01: {CHARLOTTE.NASA.CRUDFAN}73704V.PRN: 1

6-NOV-1987 11:21

Page 8

8	0	0.02248	0.000011	-18.67
9	0	0.00826	0.000062	-27.37
10	0	0.001164	-0.000003	-24.39

ROTOR WAKE/VORTEX FLOW PROGRAM

CASE NUMBER

--- STREAMLINE NUMBER 7 ---

CD = 0.0150	
WFS/UT	= 0.9252
WD/UT	= 0.0623
X/C	= 1.1045
SDIST	= 1.9022
WAKE WIDTH	= 0.1024

TIP VORTEX PARAMETERS

A0/S	= 0.0003
A/S	= 0.0025
VSDVO/U	= 0.0000
VSDV/U	= 0.0000
CIRCO/(S*U)	= 0.0009
CIR/(S*U)	= 0.0072
BN	= 0.5000
BRRT	= 0.1060

HARMONIC CONTENT OF ROTOR WAKE/VORTEX FLOW

NH	2*CMOD	PHASE	20*LOG(2*CMOD), DB
1	0.003537	0.000001	-16.39
2	0.015798	0.000002	-3.39
3	0.005395	0.000002	-12.72
4	0.009626	0.000004	-7.69
5	0.003374	0.000003	-16.80
6	0.005142	0.000007	-13.14
7	0.001229	0.000007	-25.57
8	0.002388	0.000006	-19.80
9	0.000086	-0.000027	-48.63
10	0.001049	-0.000002	-26.95

ROTOR WAKE/VORTEX FLOW PROGRAM

CASE NUMBER

--- STREAMLINE NUMBER 8 ---

CD =	0 . 0150
WFS/UT	= 0 . 9473
WD/UT	= 0 . 0717
X/C	= 1 . 0682
SDIST	= 1 . 6577
WAKE WIDTH	= 0 . 0964

TIP VORTEX PARAMETERS

A/5	= 0 . 0003
A/S	= 0 . 0023
VSDVO/U	= 0 . 0000
VSDV/U	= 0 . 0000
CIRCO/(S*U)	= 0 . 0009
CIR/(S*U)	= 0 . 0066
BN	= 0 . 5000
BRRT	= 0 . 1056

HARMONIC CONTENT OF ROTOR WAKE/VORTEX FLOW

NH	2*CMOD	PHASE	20*LOG(2*CMOD), DB
1	0 . 009751	0 . 000002	-8 . 75
2	0 . 014830	0 . 000002	-5 . 11
3	0 . 008920	0 . 000004	-9 . 53
4	0 . 009764	0 . 000005	-8 . 74
5	0 . 005613	0 . 000005	-13 . 55
6	0 . 005358	0 . 000006	-13 . 95
7	0 . 002587	0 . 000007	-20 . 28
8	0 . 002429	0 . 000008	-20 . 83
9	0 . 000832	-0 . 000011	-30 . 14
10	0 . 000951	0 . 000013	-26 . 97

ROTOR WAKE/VORTEX FLOW PROGRAM

CASE NUMBER

--- STREAMLINE NUMBER 9 ---

CD =	0 . 0150
WFS/UT	= 0 . 9685
WD/UT	= 0 . 0768
X/C	= 1 . 0799
SDIST	= 1 . 5685
WAKE WIDTH	= 0 . 0976

TIP VORTEX PARAMETERS

A0/S	=	0.0003
A/S	=	0.0022
VSDV0/U	=	0.0000
VSDV/U	=	0.0000
CIRCO/(S^U)	=	0.0009
CIR/(S^U)	=	0.0064
BN	=	0.5000
BRRT	=	0.1056

HARMONIC CONTENT OF ROTOR WAKE/VORTEX FLOW

NH	2^NCMOD	PHASE	20^LOG(2^CMOD), DB
1	0.013721	0.000001	-6.53
2	0.013838	0.000002	-6.46
3	0.011076	0.000003	-8.39
4	0.009547	0.000004	-9.68
5	0.006895	0.000005	-12.51
6	0.005258	0.000005	-14.86
7	0.003339	0.000008	-18.81
8	0.002306	0.000007	-22.02
9	0.001251	0.000007	-27.33
10	0.000816	0.000012	-31.05

ROTOR WAKE/VORTEX FLOW PROGRAM

CASE NUMBER

--- STREAMLINE NUMBER 10 ---

CD	=	0.0150
WFS/UT	=	1.0151
WD/UT	=	0.0836
X/C	=	1.0992
SDIST	=	1.4986
WAKE WIDTH	=	0.0993

TIP VORTEX PARAMETERS

A0/S	=	0.0003
A/S	=	0.0021
VSDV0/U	=	0.0000
VSDV/U	=	0.0000
CIRCO/(S^U)	=	0.0009
CIR/(S^U)	=	0.0062
BN	=	0.5000
BRRT	=	0.1057

HARMONIC CONTENT OF ROTOR WAKE/VORTEX FLOW

NH	2^*CMOD	PHASE	$20 \cdot \log(2^*CMOD)$, DB
1	0.018663	0.000001	-4.79
2	0.012771	0.000003	-6.08
3	0.013700	0.000003	-7.47
4	0.009182	0.000005	-10.95
5	0.008259	0.000006	-11.87
6	0.004905	0.000007	-16.40
7	0.004017	0.000007	-18.13
8	0.001954	0.000008	-24.39
9	0.001599	0.000013	-26.13
10	0.000538	0.000009	-35.59

HUB-TO-TIP AERODYNAMIC PHASE LAG

STREAMLINE NO.	AERO PHASE LAG, DEG.
1	0.000000
2	-5.232219
3	-9.057590
4	-15.719318
5	-27.892509
6	-38.541042
7	-49.121807
8	-52.943192
9	-53.968653
10	-54.526115

1 Report No NASA CR-185135	2 Government Accession No.	3 Recipient's Catalog No	
4 Title and Subtitle An Investigation of Counterrotating Tip Vortex Interaction		5 Report Date October 1989	
		6 Performing Organization Code	
7 Author(s) R.K. Majjigi, K. Uenishi, and P.R. Grieve		8 Performing Organization Report No.	
9 Performing Organization Name and Address GE Aircraft Engines 1 Neumann Way P.O. Box 156301 Cincinnati, OH 45215-6301		10 Work Unit No 535-03-01	
12 Sponsoring Agency Name and Address National Aeronautics and Space Administration Lewis Research Center Cleveland, Ohio 44135-3191		11 Contract or Grant No NAS3-24080	
		13 Type of Report and Period Covered Contractar Report (Topical)	
'5 Supplementary Notes Project Manager: F. Humenik, Propulsion Systems Division NASA Lewis Research Center		14 Sponsoring Agency Code	
16 Abstract A tip vortex interaction model originally developed for compressors has been extended and adapted for use with counterrotating open rotors. Comparison of available acoustic data with predictions made with and without the tip vortex model included illustrate the importance of this interaction effect. This report documents the analytical modeling, a limited experimental verification, and certain key parametric studies pertaining to the tip vortex as a noise source mechanism for the unsteady loading noise of counterroating propellers.			
17 Key Words (Suggested by Author(s)) Tip vortex, propeller noise, counterrotation noise		18 Distribution Statement Unclassified- Unlimited	
19 Security Classif (of this report) Unclassified	20 Security Classif (of this page) Unclassified	21 No of Pages 122	22 Price



